12-31-2016

Minibrain and Wings Apart Control Organ Growth and Tissue Patterning Through Downregulation of Capicua

Liu Yang
University of Massachusetts Boston

MINIBRAIN AND WINGS APART CONTROL ORGAN GROWTH AND TISSUE PATTERNING THROUGH DOWNREGULATION OF CAPICUA

A Dissertation Presented

by

LIU YANG

Submitted to the Office of Graduate Studies,
University of Massachusetts Boston,
in partial fulfillment of the requirements for the degree of

DOCTOR OF PHILOSOPHY

December 2016

Molecular, Cellular and Organismal Biology Program

MINIBRAIN AND WINGS APART CONTROL ORGAN GROWTH AND TISSUE PATTERNING THROUGH DOWNREGULATION OF CAPICUA

A Dissertation Presented

by

LIU YANG

Approved as to style and content by:

_____
Alexey Veraksa, Associate Professor
Chairperson of Committee

_____
Richard Kesseli, Professor
Member

_____
Linda Huang, Associate Professor
Member

_____
Kellee Siegfried, Assistant Professor
Member

_____
Kristin White, Associate Professor
Harvard Medical School
Member

_____
Linda Huang, Program Director
Biology Department

_____
Richard Kesseli, Chairperson
Biology Department

ABSTRACT

MINIBRAIN AND WINGS APART CONTROL ORGAN GROWTH AND TISSUE PATTERNING THROUGH DOWNREGULATION OF CAPICUA

December 2016

Liu Yang, B.A., Northwest University, Xi'an
M.S., Northwest University, Xi'an
Ph.D., University of Massachusetts Boston

Directed by Associate Professor Alexey Veraksa

The regulation of organ growth is a fundamental aspect of developmental biology. My work uses *Drosophila* as a model system to understand how the various growth regulators are coordinated. The transcriptional repressor Capicua (Cic) controls tissue patterning and restricts organ growth, and has been recently implicated in several cancers and neurodegenerative diseases. Cic has emerged as a primary sensor of signaling downstream of the receptor tyrosine kinase (RTK)/extracellular signal-regulated kinase (ERK) pathway, but how Cic activity is regulated in different cellular contexts remains poorly understood. In order to identify Cic regulators, I have used affinity purification/mass spectrometry (AP-MS) to study the Cic protein interactome in *Drosophila* S2 cells and embryos. I have found that the kinase Minibrain (Mnb, *Drosophila* ortholog of Down syndrome kinase DYRK1A), acting through the adaptor

protein Wings apart (Wap), physically interacts with and phosphorylates the Cic protein. Mnb and Wap inhibit Cic function by limiting its transcriptional repressor activity. Downregulation of Cic by Mnb/Wap is necessary for promoting the growth of multiple organs, including the wings, eyes, and the brain, and for proper tissue patterning in the wing. This work has uncovered a previously unknown mechanism of downregulation of Cic activity by Mnb and Wap, which operates independently from the ERK-mediated control of Cic. Therefore, Cic functions as an integrator of upstream signals that are essential for tissue patterning and organ growth. Finally, since DYRK1A and CIC exhibit, respectively, pro-oncogenic versus tumor suppressor activities in human oligodendroglioma, my results raise the possibility that DYRK1A may also downregulate CIC in human cells.

ACKNOWLEDGEMENTS

First, I would like to thank my advisor, Dr. Alexey Veraksa. You generously gave me the opportunity to work in the Veraksa lab, and encouraged me to do my best in both research and teaching. You have always been there when I needed support, suggestions and scientific tricks. I deeply appreciate your guidance, patience and help.

The work presented here could not have been completed without the help from my collaborators on the Mnb-Cic project. I would like to thank Dr. Lucas G. Dent, Dr. Francesca Froldi, Dr. Kieran Harvey and Dr. Louise Y. Cheng at Peter MacCallum Cancer Centre; Dr. Marta Forés and Dr. Gerardo Jiménez at Institut de Biologia Molecular de Barcelona-CSIC; Dr. Stanislav Y. Shvartsman at Princeton Universtity; and Dr. Shu Kondo at National Institute of Genetics, Japan. I also would like to thank Sayantanee Paul, Kenny Trieu and Kaitlyn Webster at UMass Boston for your experimental help with this project.

I would like to thank my thesis advisory committee members: Dr. Linda Huang, Dr. Rick Kessili, Dr. Kellee Siegfried, and Dr. Kristin White. They provided valuable advice, suggestions and insights throughout my research.

I feel lucky to have so many amazing labmates and friends in the McCormack Building and ISC at UMass Boston. Many thanks to Wenjian Xu, Kasia Piotrowska, Saima Anjum, Niusha Nikkholgh, Christian Slubowski, Scott Paulissen, Jamie Dombach, Karla Schallies, Heya Zhao, Fei Chai, Charlie Puerner, Dang Truong, Melissa Brown, Walter Flores, Ana Ursu, Sarah DeStefano, Michael Pyle, Timothy Musoke. We had so

many memorable events together: birthdays, happy hours, Banshees, White Mountains, graduations and Chinatown luncheons.

Most importantly, I thank my family. My parents, Liqun Chen and Qibin Yang, have made a lot of sacrifices to support my education and dreams. I am also grateful to my wife, Ruyue Zheng. I am feeling so blessed to have her in my life. She has helped me regain confidence after setbacks and restart journerys after detours. This dissertation would be impossible without her encouragement and support.

TABLE OF CONTENTS

LIST OF TABLES

LIST OF FIGURES

FIGURE Page

FIGURE Page

CHAPTER 1

INTRODUCTION

Dysregulation of organ growth results in many human diseases, such as cancers and neurodevelopmental disorders. Understanding how organ size is controlled is a critical and fundamental question in biological research.

Although both intrinsic and extrinsic factors contribute to the regulation of organ growth, our understanding of this question remains incomplete. Organ size is determined by nutritional sources in the environment. For example, nutritional deprivation at the larval stage in *Drosophila* leads to small, but well-proportioned adults, suggesting an organ-extrinsic mechanism. However, organ growth is not only controlled by nutritional status, but also regulated by many extracellular mitogens, such as insulin, insulin-like growth factors (IGF), epidermal growth factors (EGF) and growth hormones. These extracellular molecules initiate a variety of intracellular signaling events to activate cell growth, DNA replication and cell cycle progression (Lloyd, 2013).

Moreover, there must be homeostatic size-control mechanisms in which the organ knows when to stop growing at the appropriate size. These autonomous mechanisms have

been demonstrated in both developmental and regenerative experiments. For example, when the wing imaginal discs from a mid-third instar larvae were transplanted into an adult abdomen, they developed properly and stopped growth at approximately the same size as normal wildtype discs (Bryant and Levinson, 1985). In mammals, the thyroid and the liver retain the potential to regenerate to their full size after removal of part of their mass in adult (Bryant and Simpson, 1984).

In general, organ growth is a consequence of cell proliferation, cell growth and cell death. The overall growth must be coordinated at the level of individual cells. There are several conserved signaling pathways that regulate cell growth, including the Hippo pathway (Xu et al., 1995), the receptor tyrosine kinase (RTK) pathway (Prober and Edgar, 2000), the mechanistic target of rapamycin (mTOR) pathway (Laplante and Sabatini, 2012), the transforming growth factor β (TGFβ) pathway (Massague et al., 2000), and the insulin/IGF signaling pathway (Oldham and Hafen, 2003). In this section, I will focus on the receptor tyrosine kinase (RTK) pathway and the Hippo pathway that were implicated in organ growth control in *Drosophila*.

1.1 *Drosophila* as a model system

The fruit fly, *Drosophila melanogaster*, was first introduced in the biology laboratory by Charles W. Woodworth at Harvard University in the early 1900s, and further used by Thomas Hunt Morgan in his genetic studies of inheritance at Columbia University (Markow, 2015). In March 1910, Morgan discovered the very first *Drosophila*

mutation, *speck*. Two months later, he discovered the famous *white*^{1} allele in one of his wildtype red-eyed fly bottles (Markow, 2015). Since then, *Drosophila* has been used widely as a powerful genetic system. In recent decades, *Drosophila* has emerged as an ideal model organism to study organ growth. This is largely due to the studies carried out in *Drosophila* imaginal discs.

The *Drosophila* imaginal discs

The *Drosophila* imaginal discs are larval epithelial tissues for forming adult epidermal organs including the wings and eyes. They are folded pouches that are comprised of single-layer epithelia. During the first few days of larval life, they grow dramatically in mass but remain undifferentiated until metamorphosis (Postlethwait and Schneiderman, 1973). This feature makes them an attractive model system to study growth regulation. Moreover, many of the known genes that have been implicated in the regulation of organ growth have homologues in mammals, suggesting conserved growth control mechanisms. For example, the core components of the Hippo pathway in *Drosophila* such as Hippo, Yorkie, and Warts have homologs in mammals. In addition, a tremendous amount of genetic techniques are available in *Drosophila* to modulate gene expression during the imaginal discs development. For instance, mitotic recombination clones lacking specific genes can be generated in imaginal discs using the FRT/Flp technique (Theodosiou and Xu, 1998). Similarly, particular genes can also be

overexpressed or downregulated in mitotic clones using the CoinFLP method (Bosch et al., 2015), or in specific regions by using the GAL4 system (Brand and Perrimon, 1993).

The *Drosophila* wing imaginal disc is likely the most extensively studied model for growth control. Most of our understanding of organ growth control has been derived from the studies of the wing imaginal discs. The *Drosophila* wing imaginal disc derives from a cluster of approximately 30 cells that invaginate from the embryonic epithelium (Hariharan, 2015). These cells undergo 9-11 rounds of cell division and grow to a cluster of 30,000-50,000 cells at the end of the larval stage (Hariharan, 2015; Martin et al., 2009; Worley et al., 2013). The arrangement of the *Drosophila* wing imaginal discs (Fig. 1.1) is

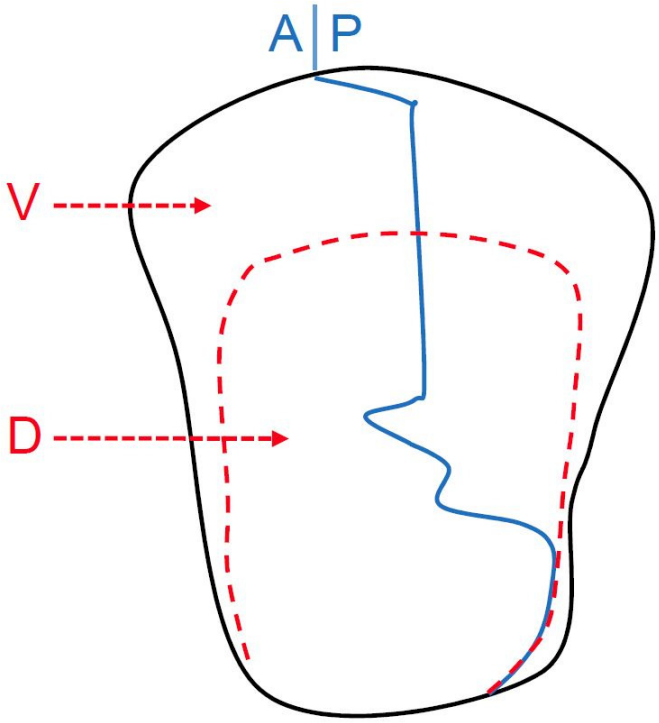

Figure 1.1. Schematic of the *Drosophila* wing imaginal disc. The boundary between anterior (A) and posterior (P) compartments is shown as a blue line, and the boundary between ventral (V) and dorsal (D) is shown as a dotted red line.

subdivided into anterior and posterior compartments, and then into dorsal and ventral compartments at the second-instar larval stage (Irvine and Harvey, 2015). The wing discs from late third-instar larvae consist of two apposed sheets: the thick folded disc epithelium and the thin peripodial membrane. During the prepupal and pupal development, the disc epithelium folds back to form the apposed dorsal and ventral compartments of the wing blade (Fig. 1.1).

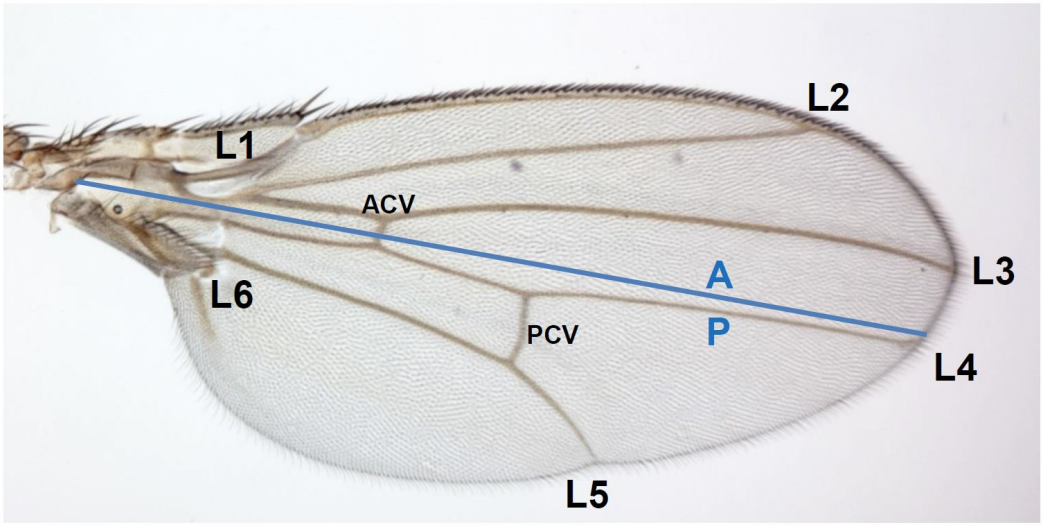

Figure 1.2. The wildtype *Drosophila* adult wing. The locations of the longitudinal veins (L1-L5) and the incomplete vein (L6) are indicated. The crossveins are indicated as ACV and PCV. The boundary between anterior (A) and posterior (P) compartments are shown as a blue line.

The vein pattern of the *Drosophila* adult wing.

In the *Drosophila* wing, there are five longitudinal veins (L1-L5) which span the wing proximodistally. There are also two crossveins, the anterior and posterior crossveins (ACV and PCV), which connect the longitudinal L3-L4 and L4-L5, respectively (Fig. 1.2). In addition, there is an incomplete longitudinal vein, L6, in the posterior compartment. The adult wing consists of two apposed surfaces, dorsal and ventral. Therefore, the veins are sometimes referred to as dorsal or ventral veins. The adult wing veins can be traced back to their primordia in the wing discs.

1.2 The Hippo signaling pathway

In the past two decades, it has been established that the Hippo signaling pathway functions as a key regulator in organ size control (Hariharan, 2015; Irvine and Harvey, 2015). In 1995, the Hippo signaling pathway was first discovered in mosaic genetic screens for *Drosophila* tumor suppressor genes. Loss-of-function alleles of *warts* (*wts*) result in an overgrowth of multiple tissues, which include the eyes, wings, legs, and the central nervous system (Justice et al., 1995; Xu et al., 1995). Subsequently, a flurry of studies identified additional key pathway regulators, including the WW domain-containing protein Salvador (Sav) (Kango-Singh et al., 2002; Tapon et al., 2002), the Ste20-like protein kinase Hippo (Hpo) (Harvey et al., 2003; Pantalacci et al., 2003; Udan et al., 2003; Wu et al., 2003), and the adaptor Mob as tumor suppressor (Mats) (Lai et al., 2005). Lost-of-function mutants for any of these four proteins phenocopy tissue

overgrowth in *Drosophila* caused by *wts* alles. In 2005, the transcriptional coactivator Yorkie (Yki) was identified as a component of the Hippo pathway in a yeast two-hybrid screen for Wts-interacting proteins (Huang et al., 2005). Thus, these five proteins (Wts, Hpo, Sav, Mats and Yki) form the core of the Hippo signaling pathway.

The Hippo pathway is evolutionarily conserved from *Drosophila* to humans. The core five members of the Hippo pathway have direct mammalian orthologs. They have conserved roles in growth control, differentiation and morphogenesis. Recently, more than 40 proteins have been implicated in both *Drosophila* and mammalian Hippo pathway (Irvine and Harvey, 2015; Pan, 2010). These Hippo pathway components can be subdivided into three groups: the core kinase cassette, the upstream regulatory proteins and the downstream transcriptional regulatory proteins (Irvine and Harvey, 2015).

The core kinase cassette of the Hippo pathway

The core kinase cassette proteins include Hpo, Wts, Sav, Mats and Yki, of which Hpo and Wts function as kinases. Sav serves as a scaffold protein for the phosphorylation and activation of Wts by Hpo. Similarly, Yki is phosphorylated by Wts and its adaptor, Mats. Yki is the key effector of the Hippo pathway, and functions as a transcriptional coactivator. In *Drosophila*, Yki requires another transcriptional co-activator, Scalloped (Sd), to regulate gene expression, which facilitates tissue growth (Goulev et al., 2008; Wu et al., 2008; Zhang et al., 2008; Zhao et al., 2008b). Yki functions downstream of Hpo, Sav, and Wts since epistasis experiments have shown that depletion of Yki

suppresses the overgrowth phenotype associated with Hpo, Sav and Wts mutants, whereas overexpression of Yki phenocopies the Hpo, Sav and Wts mutants (Huang et al., 2005). Yki functions as an oncogene and promotes the transcription of genes controlling cell proliferation and the inhibition of apoptosis. When Yki is present in the nucleus, it can activate a variety of factors that promote tissue growth. Activation of Hippo signaling results in the phosphorylation and inactivation of Yki by Wts, followed by nuclear export and cytoplasmic accumulation (Oh and Irvine, 2008; Pan, 2010; Yu and Guan, 2013). Recently, Misshapen (Msn) has been identified as another kinase that phosphorylates Wts, which negatively regulates the Yki activity (Li et al., 2014).

The downstream transcriptional regulatory proteins of the Hippo pathway

The Yki target genes can be classified into three groups (Pan, 2010). The first class of genes includes the cell-autonomous growth promoting targets of Yki, such as the microRNA *bantam*, *Myc*, *CyclinE*, *E2F1*, and the apoptosis inhibitor *diap1* (Goulev et al., 2008; Nolo et al., 2006; Thompson and Cohen, 2006; Wu et al., 2003). The second class of Yki targets includes Kibra, Merlin (Mer), Expanded (Ex) and Four-jointed (Fj), as Yki upregulates their expression. Interestingly, Kibra, Mer and Ex can serve as upstream signals for the Hippo pathway, suggesting a negative feedback mechanism (Cho et al., 2006; Genevet et al., 2010; Hamaratoglu et al., 2006; Yu et al., 2010). The third class of Yki targets contains signaling molecules that are also implicated in pathway crosstalk. These proteins include the Notch ligand Serrate, the EGFR ligand Vein, Wingless, E-

Cadherin, and Dally and Dally-like (Baena-Lopez et al., 2008; Cho et al., 2006; Genevet et al., 2009; Zhang et al., 2009).

The upstream regulatory proteins of the Hippo pathway

Unlike ligand-receptor driven signaling pathways, the upstream signals for the Hippo pathway are not yet fully understood. It has been shown that the Hippo signaling pathway is regulated by cell polarity, cell adhesion, the actin cytoskeleton, cell contact and mechanical force (Sun and Irvine, 2016).

Three cell-cortex localized proteins, Kibra, Mer and Ex, were reported as scaffold proteins for the core kinase cassette to activate the Hippo pathway, as their loss-of-function mutants have similar tissue overgrowth phenotype. In contrast, overexpression of Kibra, Mer and Ex was found to promote the activity of Hpo and Wts (Baumgartner et al., 2010; Genevet et al., 2010; Yu et al., 2010). Additionally, Kibra, Mer and Ex might activate the Hippo pathway through the Tao-1 kinase, which phosphorylates and activates Hpo (Boggiano et al., 2011; Poon et al., 2011).

Cell adhesion and cell polarity proteins can also regulate Hippo signaling. For example, the cell adhesion protein, Echinoid (Ed) was found to function as a tumor suppressor since it binds to and stabilizes Sav, which activates Hpo (Yue et al., 2012). In addition, many proteins that regulate apicobasal polarity of the epithelial cells have been implicated in controlling the Hippo pathway activity. These proteins include Lethal giant

larvae (Lgl), Scribble (Scrib), Discs Large (Dlg) and Crumbs (Crb) (Chen et al., 2010; Ling et al., 2010; Robinson et al., 2010; Zhao et al., 2008a).

The Hippo pathway is also controlled by the actin cytoskeleton. Modulating the expression of actin regulators, including capping proteins and Diaphanous, can affect Yki activity and tissue growth (Fernandez et al., 2011; Sansores-Garcia et al., 2011). In *Drosophila* wing disc, increased cytoskeletal tension can suppress Yki activity by inducing the apical localization of Ajuba/LIM protein Jub, which is a negative regulator of Warts (Rauskolb et al., 2014). Recently, it has been shown that disruption of the Spectrin proteins network leads to tissue overgrowth by activating Yki-mediated gene expression (Deng et al., 2015; Fletcher et al., 2015).

In addition, the atypical cadherins, Fat (Ft) and Dachsous (Ds), play important roles in regulating the Hippo pathway (Bennett and Harvey, 2006; Matakatsu and Blair, 2006). Ds and Ft function as a ligand-receptor pair to affect the localization of each other (Ma et al., 2003). The interaction between Ft and Ds is mediated by the kinase Fj, as it phosphorylates Ft and Ds on their extracellular regions (Ishikawa et al., 2008). Ft and Ds can affect the subcellular localization of the atypical myosin, Dachs, and thereby influence the protein level and/or cellular distribution of Wts and Ex (Bennett and Harvey, 2006; Cho et al., 2006; Silva et al., 2006; Willecke et al., 2006). This mechanism is likely independent of Wts phosphorylation by Hpo. More recently, it has been shown that the Wts activity is regulated by an allosteric mechanism, in which a *Drosophila* Mps1 one binder (Mob) protein, Mats, converts Wts from an inactive to active state. This

transition can be inhibited or reversed by Ft and Ds signaling via Dachs (Vrabioiu and Struhl, 2015).

We and our collaborators have identified another downstream branch of Ft and Ds signaling that regulates the Hippo signaling (Degoutin et al., 2013). In this study, we identified the WD40 repeat protein, Wings apart (Wap), also known as Riquiqui, as a Ds-interacting protein. Wap functions together with the Minibrain kinase (Mnb) to interact with and phosphorylate Wts, which in turn inhibits Wts-mediated phosphorylation of Yki, resulting in Yki derepression. This branch of signaling downstream of Ds regulates Wts and Yki independently of Dachs (Degoutin et al., 2013).

The Mnb Kinase

In addition to its role in Hippo signaling, Mnb and its mammalian homolog, DYRK1A, functions as key regulator of neuronal development. The role of Mnb in neurodevelopment was first elucidated by the analysis of *mnb* mutants of *Drosophila* (Tejedor et al., 1995). The *mnb* mutant alleles display a remarkable reduction in the size of the adult brain, particularly in the optic lobes (OL). However, the overall neuronal architecture is preserved. The reduction in the size of the central brain occurs mainly in the dorsal-ventral (DV) and anterior-posterior (AP) directions (Tejedor et al., 1995). However, the sizes of other organs, such as the body and sensory organs, appear almost indistinguishable from wildtype. This neuronal specific phenotype is caused by altered proliferation in the neuroepithelial primordia of the larval CNS, as axon bundles between

the lobula complex and the optic stalk are thinner, and the anterior optic tract fibers and cervical connective fibers are reduced. In addition, the mutant animals display behavioral abnormalities, such as reduced locomotor activity and impaired odor discrimination (Tejedor et al., 1995).

In *Drosophila* embryos, Mnb proteins are expressed predominately in the central nervous system (CNS) (Tejedor et al., 1995). *Drosophila* embryos and pupae contain more Mnb proteins than adults. In late embryos, Mnb is expressed in the supraesophageal ganglion and the ventral nerve cord, but is absent in the peripheral nervous system. In third instar larval brain, Mnb is expressed prominently in the mushroom body neuropil and OL. However, Mnb expression is relatively low in the adult OL and central brain (CB), suggesting that Mnb is critical for the development of the OL and CB, but not for the maintenance of neurons in these structures (Tejedor et al., 1995). More recently, Mnb has been found to be expressed in a subset of symmetrically located neurons, posterior to the antennal lobe in the adult brain (Hong et al., 2012).

Mnb is an evolutionarily conserved kinase. Its mammalian ortholog, DYRK1A, plays critical roles in neurogenesis, proliferation, neuronal differentiation, survival, apoptosis and synaptic plasticity. DYRK1A belongs to the dual-specificity tyrosine–regulated kinase (DYRK) family. The human *DYRK1A* gene is located on chromosome 21 (Guimera et al., 1997). *DYRK1A* in trisomy produces multiple cognitive deficits associated with Down syndrome (DS) (Becker et al., 2014; Duchon and Herault, 2016; Hammerle et al., 2003; Smith et al., 1997). In addition, elevated DYRK1A activation has

been implicated in Alzheimer's disease and Pick disease (Ferrer et al., 2005; Kimura et al., 2007). Recently, DYRK1A has been associated with autism spectrum disorders (ASDs) (O'Roak et al., 2014; Willsey and State, 2015).

DYRK1A is a dose-sensitive gene, as both overexpression and reduction of DYRK1A protein in transgenic mice results in growth defects and DS related phenotypes, including locomotor activity, coordination, and cognition defects (Altafaj et al., 2001; Arque et al., 2008; Benavides-Piccione et al., 2005; Branchi et al., 2004; Dierssen, 2013; Dierssen and de Lagran, 2006; Ferrer et al., 2005; Fotaki et al., 2002; Fotaki et al., 2004; Martinez de Lagran et al., 2004). Homozygous null *DYRK1A* mutation causes lethality in the mouse in utero and results in delayed general growth and size reductions in multiple organs including the developing brain in the embryo. Mice heterozygous for the *DYRK1A* allele survive to adulthood, but display decreased neonatal viability and reduction in brain size, as well as behavioral defects (Fotaki et al., 2002; Fotaki et al., 2004). Moreover, patients with heterozygous mutations in *DYRK1A* exhibit developmental delays and mental retardation associated with microcephaly, seizures, facial dysmorphisms and cardiac hypertrophy (Bronicki et al., 2015; Fernandez-Martinez et al., 2015; Ruaud et al., 2015; van Bon et al., 2016). Disruptive or loss-of-function mutations of *DYRK1A* have been implicated in many neurodevelopmental disorders, including autosomal dominant mental retardation 7 (MRD7), autism spectrum disorder (ASD) and intellectual disability (ID) (Bronicki et al., 2015; Duchon and Herault, 2016; Moller et al., 2008; van Bon et al., 2016).

The overexpression of *DYRK1A* in mouse models is sufficient to induce phenotypes similar to DS patients (Dierssen and de Lagran, 2006; Dierssen et al., 2006; Dierssen et al., 2009; Guedj et al., 2012). In contrast, reducing the expression of *DYRK1A* in DS mouse models by shRNA injection results in a persistent increase in synaptic strength, reduced motor alteration and restored memory performance (Altafaj et al., 2013; Ortiz-Abalia et al., 2008). As a result, DYRK1A inhibitors, such as harmine and epigallocatechin-3-gallate (EGCG), have been developed for the treatment of DS (Bain et al., 2003; De la Torre et al., 2014; Gockler et al., 2009; Laguna et al., 2008; Noll et al., 2012).

1.3 The receptor tyrosine kinase (RTK) pathway

The receptor tyrosine kinase (RTK) pathway is a critical pathway that regulates growth and survival since the RTK receptors mediate the transduction of proliferation signal from growth factors, including EGF, Platelet-derived growth factor (PDGF), fibroblast growth factor (FGF), vascular endothelial growth factor (VEGF) and hepatocyte growth factor (HGF) (Lemmon and Schlessinger, 2010). It is well known that the RTK pathway serves not only as a critical regulator of normal cellular responses, but also as a key element in development and progression of human cancers (Kratchmarova et al., 2005; Meloche and Pouyssegur, 2007). Dysregulation of RTK pathways is frequently implicated in human cancers and hyper-proliferative diseases (Dhillon et al., 2007).

Overview of RTK signaling

The receptor tyrosine kinase (RTK) signaling pathway has been intensively studied for the past three decades. It controls numerous critical cellular responses, which include proliferation, differentiation, development, metabolism, cell migration and cell survival (Dhillon et al., 2007; Lemmon and Schlessinger, 2010; Marshall, 1995; Simon, 2000). The key regulatory mechanisms of RTK signaling are highly conserved from *C. elegans* to humans. Dysregulation of the RTK pathway leads to numerous human diseases, such as cancers, diabetes and inflammation. In addition, cancer driver mutations are frequently found in RTK pathway components (Cai et al., 2013; Li and Hristova, 2006; Robertson et al., 2000).

Human RTKs include 20 subfamilies of proteins with similar overall structures: they contain a single transmembrane domain that separates the extracellular region from the intracellular tyrosine kinase region. Typically, binding of the extracellular ligands to the cell surface RTK receptors induces conformation change and RTK dimerization, which leads to RTK autophosphorylation on tyrosine residues as well as a series of phosphorylations on other signaling molecules. This in turn initiates a number of intracellular signaling cascades including the mitogen-activated protein kinase (MAPK) pathway, the phosphatidyl-inositol-3-kinase (PI3K) pathway and phospholipase Cγ (PLCγ) pathways (Lemmon and Schlessinger, 2010). The most well characterized pathway downstream of RTKs is the MAPK pathway.

Most RTKs activate the small GTPase Ras, which stimulates the MAPK cascade by a series of phosphorylation events (Schlessinger, 2000). The sequential activation of the MAPK cascade includes activation of Raf (MAPKKK), MEK (MAPKK) and ultimately ERK (MAPK), and is a conserved mechanism. Activated MAPK phosphorylates more than 200 substrates in the cytoplasm, nucleus and cell membrane (Futran et al., 2015). Previous studies showed that Ets-domain transcription factors are key effectors of RTK signaling (Hollenhorst et al., 2011; Jacobs et al., 1998; Murphy et al., 2002). For example, two ETS factors, Pointed-P2 and Yan, are thought to be downstream effectors of all RTKs in *Drosophila* (Rebay and Rubin, 1995). Pointed-P2 and Yan are both direct targets of MAPK in response to RTK signaling. MAPK dependent phosphorylation activates Pointed-P2, which serves as a transcriptional activator to activate the downstream target genes that are required for eye development. Conversely, Yan functions as a transcriptional repressor, which is inhibited by MAPK dependent phosphorylation. Phosphorylated Yan is exported from the nucleus to the cytoplasm for degradation, which leads to the expression of the RTK target genes (Brunner et al., 1994; Gabay et al., 1996; Rebay and Rubin, 1995; Schlessinger, 2000).

The RTK pathway and growth control

Considerable evidence suggests that the activation of the RTK pathway is required for organ growth. Loss-of-function mutations in the core components of the RTK pathway result in many growth defects in *Drosophila*. For example, *raf* mutant

larvae lack imaginal discs except the underdeveloped eye imaginal discs, and reduction of organ size is also observed in brain lobes, lymph glands, testes and ovaries (Nishida et al., 1988). *rl* (ERK) null mutation leads to larval lethality and a significant reduction in the size of imaginal discs (Biggs et al., 1994). Moreover, mitotic clones expressing a dominant negative form of Ras exhibit decreased cell and clone sizes, whereas gain-of-function mutations in Ras result in increased cell and clone sizes (Prober and Edgar, 2000).

In humans, it has been shown that the deregulation of the RTK pathway can lead to increased signaling activity. This results in a variety of diseases including cancers. For example, gene amplification and overexpression of HER2 is implicated in a variety of human cancers, particularly in human breast and ovarian cancer (Slamon et al., 2001). In addition, the overexpression of EGFR is frequently found in squamous-cell carcinomas of the head and neck in non-small-cell lung, kidney, pancreatic, ovarian, cervical, and bladder cancer (Rocha-Lima et al., 2007). Furthermore, the aberrations in RTK activation have been implicated in other hyperproliferative diseases such as psoriasis (Zwick et al., 2002). However, the mechanisms how RTK pathway regulates growth are not well understood.

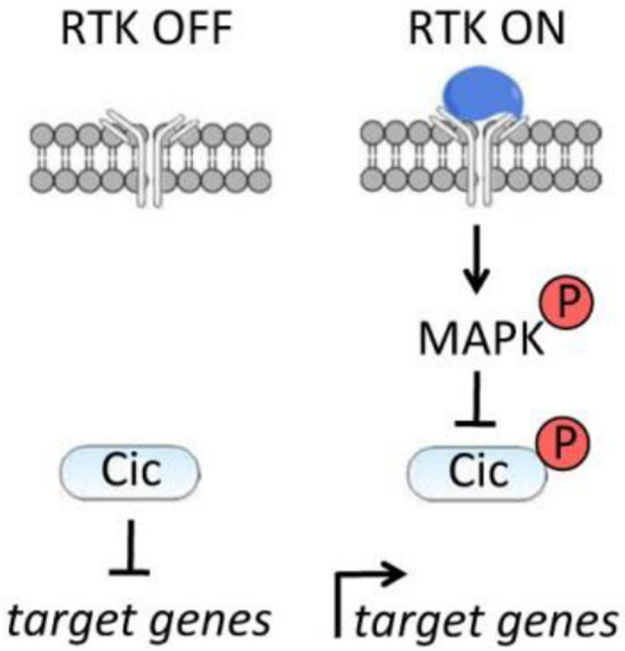

Figure 1.3. Schematic of RTK-dependent Control of gene expression by Cic.

1.4 The Capicua transcriptional repressor

Recently, the High Mobility Group (HMG)-box protein Capicua (Cic) has been identified as a general downstream sensor of RTK activation (Jimenez et al., 2000). Cic was first identified as a repressor of RTK Torso target genes, which control the development of the terminal regions of the embryo. Therefore, it was named "Capicua", which means "head and tail" in Catalan (Jimenez et al., 2000). It was demonstrated that Cic mediates the expression of multiple RTK target genes downstream of Torso and the epidermal growth factor receptor (EGFR) pathways (Ajuria et al., 2011; Goff et al., 2001;

Jimenez et al., 2000; Jimenez et al., 2012; Roch et al., 2002). As shown in Fig. 1.3, in the absence of RTK activation, Cic represses the transcription of RTK target genes. When RTK signaling is activated, active MAPK (ERK) phosphorylates Cic, which relieves the Cic-mediated repression of RTK target genes.

Cic is conserved from worms to mammals. Three conserved domains have been identified in the Cic proteins. One is the HMG box region which is responsible for recognition and binding to the octameric T(G/C)AATG(A/G)A DNA sites in target genes (Ajuria et al., 2011). The other motif that has a repressor function, C1, is located at the carboxy-terminal end of the Cic protein (Astigarraga et al., 2007; Jimenez et al., 2000). The third motif is amino-terminal to the HMG-box and includes a binding interface for the Ataxin-1 (ATXN1) protein. The *Drosophila* Cic protein also contains the C2 domain which was identified as the MAPK-docking motif (Astigarraga et al., 2007). There are two main CIC isoforms (CIC-L and CIC-S) expressed in *Drosophila* (Fig. 1.4). Cic-S has been intensively studied in recent years while little is known about the amino-terminal extension in Cic-L (Jimenez et al., 2012).

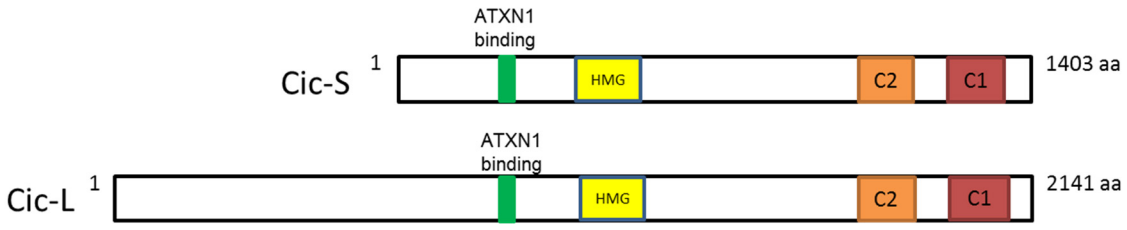

Figure 1.4. Schematic of the two main isoforms of Cic proteins in *Drosophila*.

MAPK-dependent regulation of Cic

MAPK dependent phosphorylation of Cic is a well-characterized mechanism in *Drosophila*. For example, RTK Torso activation induces the phosphorylation of the *Drosophila* MAPK ERK homologue, Rolled (Rl), in the pole regions of the early embryo. Activated MAPK phosphorylates and downregulates Cic in the same regions (Coppey et al., 2008; Jimenez et al., 2000). This phosphorylation is dependent on the interaction between the Cic C2 motif and Rl since mutations in the Cic C2 motif are insensitive to Torso or EGFR inactivation. The resulting phenotype is similar to the effects of Torso or EGFR loss-of-function (Astigarraga et al., 2007). Torso signaling not only induces Cic phosphorylation but also reduces the Cic protein level. For example, activation of Ras in the wing imaginal disc results in reduction of Cic levels (Roch et al., 2002). Phosphorylation of Cic also changes the rate of its nucleocytoplasmic shuttling (Grimm et al., 2012). A recent study showed that MAPK dependent relief of Cic repression is a two-tier process: phosphorylated Cic rapidly loses its repressor activity which is followed by a slower export from the nucleus, ultimately resulting in the reduction of protein level (Lim et al., 2013).

Studies in mammalian cells also provide evidence for RTK/MAPK dependent phosphorylation of Cic, which indicates that this is a conserved mechanism. A global phosphoproteomic analysis in HeLa cells revealed that Cic becomes phosphorylated within 10 minutes after stimulating the cells with EGF (Olsen et al., 2006). Another study showed that EGF stimulation of HEK293T cells induces phosphorylation of Cic,

which prevents its binding with importin α4/karyopherin α3 (KPNA3) (Dissanayake et al., 2011). This is consistent with the *Drosophila* study that showed that RTK activation affects nucleocytoplasmic shuttling of Cic (Grimm et al., 2012). In addition, the study in HEK293T cells showed that p90 ribosome S6 kinase ($p90^{RSK}$) phosphorylates Ser^{173} of Cic, which promotes its interaction with 14-3-3 proteins (Dissanayake et al., 2011).

Cic and its targets in RTK signaling

Cic was first identified as a repressor of the RTK Torso target genes such as *tailless* (*tll*) and *huckebein* (*hkb*) in *Drosophila* (de las Heras and Casanova, 2006; Jimenez et al., 2000; Li, 2005). The Torso receptor is ubiquitously expressed in the plasma membrane of the early *Drosophila* syncytial embryo, but its activation only happens in the anterior and posterior poles of the embryo. This is due to the restricted proteolytic processing of its ligand, Trunk (Trk), that only takes place at the poles of the oocyte, producing the C terminal part of Trk as an active ligand (Furriols and Casanova, 2003). Then the Torso-Ras-MAPK pathway is activated at the poles. As a result, Cic is downregulated in the same regions, which allows for the expression of the target genes *tll* and *hkb.*

In addition, Cic functions as a repressor of *Drosophila* wing vein-specific genes downstream of the EGFR pathway. One of these genes is *argos* (*aos*), which encodes a secreted factor involved in negative feedback control of EGFR signaling (Freeman and Gurdon, 2002). In wing vein cells, *aos* expression is autonomously repressed by Cic.

Similarly, EGFR activation downregulates Cic level and induces the expression of *aos* in vein cells, which is required for vein patterning (Ajuria et al., 2011; Blair, 2007; Roch et al., 2002). Moreover, Cic acts in a similar way to repress the expression of the *intermediate neuroblasts defective* (*ind*) in embryonic neuroectoderm, and *mirror* (*mirr*) in ventral cells (Ajuria et al., 2011; Atkey et al., 2006; Roch et al., 2002).

In humans, few Cic targets have been identified. A study in HEK293T cells reported that the RNAi depletion of Cic results in elevated mRNA levels of the PEA3 subfamily of ETS transcription factors, including ETV1, ETV4 and ETV5 (Dissanayake et al., 2011). This finding suggests that Cic is required for transcriptional repression of these genes, which are overexpressed in several breast and prostate cancer cases (Carver et al., 2009; Hermans et al., 2008; Jane-Valbuena et al., 2010). This is consistent with the study in Ewing's sarcoma cases, as *CIC-DUX4* fusions were found in both two Ewing's sarcoma cases and the CIC-DUX4 chimera results in a significant upregulation of *ERM/ETV5* and *ETV1* genes (Kawamura-Saito et al., 2006).

Cic and EGFR signaling

The role of the EGFR-Ras-MAPK pathway in promoting proliferation of imaginal discs is well characterized in *Drosophila* (Hariharan and Bilder, 2006). For example, loss-of-function mutations in Ras/MAPK pathway components result in small imaginal discs, whereas gain of function mutations such as Ras^{V12} are sufficient to drive ectopic cell proliferation and tissue growth (Karim and Rubin, 1998; Prober and Edgar, 2000).

Considerable evidence suggests that Cic negatively regulates proliferation downstream of the EGFR-Ras-MAPK pathway. The role of Cic as a negative regulator of growth was first described by the Hariharan lab. Loss-of-function mutations of Cic were shown to promote tissue growth in eye imaginal discs, which indicated that the normal function of Cic is to inhibit cell growth (Tseng et al., 2007). In the same study, Cic protein level was elevated in the loss-of-function clones of EGFR or Ras, whereas Ras^{V12} clones had reduced level of Cic. In addition, loss-of-function mutations of Cic bypassed the requirement of Ras in cell proliferation. These data support the role of Cic in regulating proliferation downstream of EGFR-Ras-MAPK.

Moreover, Cic restricts the growth of stem cells, as studies in *Drosophila* showed that RNAi depletion of Cic induced the ectopic proliferation of intestinal stem cells (ISCs) (Jiang et al., 2011; Jin et al., 2015). The activation of EGFR pathway results in ISC growth as well as regeneration in the midgut epithelial cells (Buchon et al., 2010; Jiang and Edgar, 2009; Jiang et al., 2011). Cic functions downstream of the EGFR pathway to regulate ISC proliferation (Jin et al., 2015). A genome-wide mapping of Cic target genes in ISC has identified cell cycle genes, *string (stg*, *Cdc25)* and *Cyclin E (CycE),* as RNAi depletion of Cic leads to elevated mRNA levels of these genes (Jin et al., 2015). Cic was found to regulate the ETS family transcription factors, *pnt* and *Ets21C* through direct binding to the TGAATGAA motif (Jin et al., 2015).

Cic and the Hippo signaling pathway

It has been shown that Cic is regulated by the Hippo pathway. One of the Yki-target genes is microRNA *bantam*. Yki activates expression of *bantam* microRNA, and *bantam* is necessary for Yki-induced overproliferation (Thompson and Cohen, 2006). Interestingly, it was found that *bantam* expression was repressed by Cic (Herranz et al., 2012). Herranz et al. also showed that *bantam* is subject to regulation by the EGFR pathway via relief of Cic repression, suggesting that *bantam* serves as a common target of the EGFR and Hippo pathways. Conversely, *bantam* represses the expression of Cic through a negative feedback loop mechanism. In addition, the same study showed that Yki could activate the EGFR pathway but EGFR was not required for Yki to activate *bantam* (Herranz et al., 2012). Overall, cross-regulatory relationships between the Hippo and EGFR pathways appear to be rather complex, suggesting that there might be two parallel signaling inputs from Yki to Cic: EGFR-dependent and *bantam* dependent.

Cic and neurodegeneration

Cic has been implicated in several human diseases, such as spinocerebellar ataxia type1 (SCA1) neurodegeneration, which is caused by the expansion of the polyglutamine region of the disease protein, Ataxin-1 (ATXN1) (Watase et al., 2002). The normal ATXN1 protein contains up to 39 copies of glutamine, whereas the polyglutamine-expanded mutant contains 40 or more copies (Lasagna-Reeves et al., 2015).

It has been reported that both Cic isoforms (Cic-L and Cic-S) form a native nuclear complex with ATXN1 in the wildtype mouse cerebellum (Lim et al., 2006). Polyglutamine-expanded ATXN1 interacts less efficiently with Cic, which indicates that ATXN1 might function as a co-repressor and loss of repressor activity may contribute to SCA1 neurodegeneration (Crespo-Barreto et al., 2010). This is consistent with the finding that Cic target genes such as *ETV5* are upregulated in mice expressing polyglutamine-expanded ATXN1 (Lam et al., 2006; Lim et al., 2008). However, another study reported that polyglutamine-expanded ATXN1 promotes the binding of Cic to the promoters of specific genes causing hyper-repression of these genes, whereas reducing the binding of Cic to other specific genes leading to derepression effects (Fryer et al., 2011). As a result, genetic reduction of Cic levels by 50% resulted in a partial rescue of SCA1 mouse, improving motor functions and survival rate (Fryer et al., 2011; Zoghbi and Orr, 2009). More recently, a study proposed that Cic does not discern between wildtype ATXN1 and polyglutamine-expanded ATXN1. Cic interacts with wildtype ATXN1, and forms a natural transcriptional repressor complex with ATXN1. Cic binds equally well to polyglutamine-expanded ATXN1, but assembles and stabilizes a dysfunctional oligomeric complex. This dysfunctional complex assembles into toxic aggregates, driving pathogenesis (Lasagna-Reeves et al., 2015).

Cic and human tumors

Recently, mutations in CIC have been implicated as potential markers for certain human brain tumors (Alentorn et al., 2012; Chan et al., 2014). As shown in Table 1.1,

CIC mutations were frequently found in human brain tumor samples, especially oligodendrogliomas (OD), which is the second most common malignant brain tumor in adults. Most of the mutations are located in the HMG-box region, which indicates that the mutations result in loss of CIC activity as a transcriptional repressor and suggests that CIC may act as a tumor suppressor (Bettegowda et al., 2011). In addition, CIC-DUX4 fusion proteins resulting from chromosomal translocations were identified in Ewing-like sarcoma cases. The CIC-DUX4 fusion functions as a transcription activator rather than a repressor, which results in the overexpression of the downstream genes, including the PEA3 subfamily of ETS transcription factors (Arvand and Denny, 2001; Kawamura-Saito et al., 2006). Moreover, CIC mutations have been implicated in other cancers, including breast cancer (Sjoblom et al., 2006), and colon cancer (Seshagiri et al., 2012). More recently, a study showed that CIC negatively regulates prostate cancer progression (Choi et al., 2015).

In summary, it is obvious that Cic plays a critical role in controlling tissue growth, and is implicated in several neurodegenerative diseases and human cancers. There is evidence that Cic activity is under the control of the RTK pathway as well as possibly the Hippo pathway. However, the molecular details of how Cic activity is regulated by signaling pathways is not well understood. My research started from a proteomic approach to study Cic-interacting proteins, with the goal of uncovering how Cic is regulated and how it contributes to organ growth and tissue patterning.

Tumor Types	Positive/ Total	References
Oligodendrogliomas	6/7	(Bettegowda et al., 2011)
Oligodendrogliomas	22/47	(Chan et al., 2014)
Oligodendrogliomas	15/18	(Sahm et al., 2012)
Oligodendrogliomas	23/50	(Jiao et al., 2012)
Oligodendrogliomas	14/42	(Sahm et al., 2012)
Oligodendrogliomas	20/29	(Yip et al., 2012)
Astrocytomas	3/10	(Sahm et al., 2012)
Oligodendrogliomas	60/127	(Gleize et al., 2015)
Breast cancer	3/11	(Sjoblom et al., 2006)
Colon cancer	6/72	(Seshagiri et al., 2012)

Table 1.1 Cic mutations found in tumor samples.

CHAPTER 2

MINIBRAIN AND WINGS APART CONTROL ORGAN GROWTH AND TISSUE PATTERNING THROUGH DOWNREGULATION OF CAPICUA

This chapter was adapted from Yang, L., Paul, S., Trieu, K.G., Dent, L.G., Froldi, F., Forés, M., Webster, K., Siegfried, K.R., Kondo, S., Harvey, K., Cheng, L., Jiménez, G., Shvartsman, S.Y. and Veraksa, A. (2016). Minibrain and Wings apart control organ growth and tissue patterning through down-regulation of Capicua. *Proc Natl Acad Sci USA* 113(38), 10583-10588. The analysis of mnb^{d419} mutant phenotypes in larva and pupal brains were performed by Dr. Francesca Froldi. Dr. Marta Forés generated the cic^{3} allele, recombined cic^{3} allele with mnb^{RNAi}, and performed the analysis of the wing phenotypes involving this mutation. I performed all other experiments discussed in this chapter.

2.1 Introduction

The High Mobility Group (HMG)-box transcriptional repressor protein Capicua (Cic) has been identified as a key regulator of tissue patterning and organ growth in multiple developmental contexts (Jimenez et al., 2000; Jimenez et al., 2012). In *Drosophila*, Cic controls anteroposterior and dorsoventral embryonic polarity, the subdivision of the lateral ectoderm, and pattern formation in several tissues (Ajuria et al., 2011; Astigarraga et al., 2007; Goff et al., 2001; Jimenez et al., 2000; Roch et al., 2002). In addition, Cic negatively regulates the growth of imaginal discs and the midgut (Jin et

al., 2015; Tseng et al., 2007). In humans, a single Cic ortholog (CIC) has been implicated in the neurodegenerative disease spinocerebellar ataxia 1 (SCA1) (Lam et al., 2006), and recently mutations in Cic have been found in the majority of oligodendroglioma cases, suggesting that CIC is a tumor suppressor (Bettegowda et al., 2011; Sahm et al., 2012; Wesseling et al., 2015).

In both *Drosophila* and mammals, Cic functions as a primary sensor of signaling downstream of the receptor tyrosine kinase (RTK)/extracellular signal-regulated kinase (ERK) pathway (Ajuria et al., 2011; Astigarraga et al., 2007; Dissanayake et al., 2011; Grimm et al., 2012; Jimenez et al., 2012; Jin et al., 2015; Kim et al., 2010b; Kim et al., 2011; Tseng et al., 2007). According to the current model, activation of RTK signaling results in the accumulation of doubly-phosphorylated activated ERK, which directly binds to and phosphorylates Cic (Astigarraga et al., 2007). ERK-mediated Cic phosphorylation leads to a rapid relief of repression of Cic target genes, followed by a slower export from the nucleus and eventual cytoplasmic degradation (Grimm et al., 2012; Lim et al., 2013). The molecular details of these processes are unknown, though apparently each of them contributes to the overall downregulation of Cic activity. Cic is also involved in a mutual regulatory relationship with the Hippo pathway, though regulation of Cic in this context appears to take place at the RNA level (Herranz et al., 2012).

In this chapter, I present the identification of the kinase Minibrain (Mnb) (Degoutin et al., 2013; Tejedor et al., 1995) and an adaptor protein, Wings Apart (Wap) (Degoutin et al., 2013; Morriss et al., 2013), as novel Cic regulators that cooperate to

phosphorylate Cic and restrict its repressor activity. I show that Mnb/Wap and ERK target different regions of the Cic protein for phosphorylation, and that inhibition of Cic activity by Mnb and Wap is required for the growth of several organs and for correct patterning of the wing. These data suggest that Mnb/Wap-dependent downregulation of Cic occurs in parallel to the RTK/ERK and Hippo signaling pathways. I propose that Cic functions as an integrator of upstream developmental signals which together tightly control its activity. This mechanism is necessary for the proper execution of tissue patterning and regulation of organ growth.

2.2 Results

Characterization of Cic interactomes

In order to identify Cic regulators, I used affinity purification/mass spectrometry (AP-MS) (Veraksa, 2013) to study the Cic protein interactome in *Drosophila* S2 cells and embryos (Fig. 2.1A). SBP tagged Cic protein was expressed in *Drosophila* S2 Cells. Embryonic *cic-Venus* was expressed at endogenous levels as part of a genomic rescue construct (Grimm et al., 2012) (Fig. 2.1B). The tagged protein and associated interactors were purified by affinity purification, and protein complexes were analyzed by liquid chromatography-tandem mass spectrometry (LC-MS/MS).

The identified Cic-interacting proteins were analyzed with the SAINT program (Choi et al., 2011), which is designed to assign probability scores for *bona fide* protein-protein interactions. Probability scores above 0.8 are considered highly significant. The

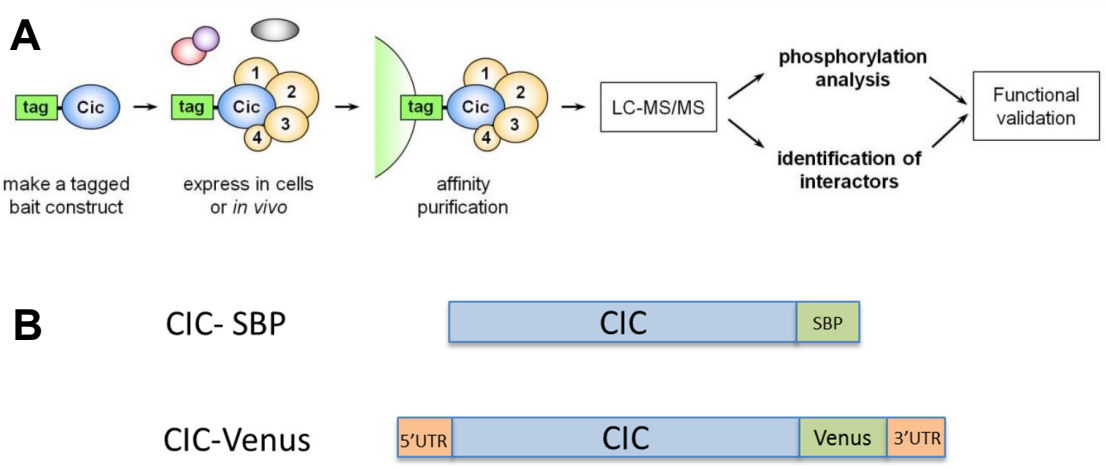

Figure 2.1. Affinity purification mass spectrometry (AP-MS) method. (A) AP-MS work flow. (B) Schematic of Cic-SBP and Cic-Venus constructs used for protein expression in *Drosophila* S2 cells and embryos, repectively.

top 20 Cic interacting proteins identified in S2 cells and embryos are shown in Table 2.1 and Table 2.2, repectively. From the S2 cells, I successfully recovered the known Cic interactor MAPK rl (Astigarraga et al., 2007), and also identified 14-3-3 proteins, which were previously found to interact with human Cic in HEK293T cells (Dissanayake et al., 2011). Rolled (rl) was also identified as a top interactor in the embryo data. Interestingly, the SCA1 disease protein, Ataxin-1 (Atx-1), was identified with a high SAINT score of 0.9487. The human homolog of Atx-1 was previously shown to interact with human CIC (Lam et al., 2006), and my data suggest that this interaction is conserved in *Drosophila*. In conclusion, I successfully recovered most of the known interactors of Cic, including *Drosophila* ERK ortholog Rolled, Ataxin-1 and 14-3-3 proteins (proteins marked in red, Fig. 2.2A).

Protein	Pep. Num. in exp.	Pep. Num. in ctrl.	SAINT Probability
cic	81|89	0|0|0|0|0	1
rl	10|22	3|0|0|0|0	1
Wap	8|11	0|0|0|0|0	0.9995
Hsp70Aa	11|7	1|1|0|0|0	0.9985
14-3-3epsilon	10|19	8|0|0|0|1	0.9965
Ranbp9	8|8	3|0|0|1|0	0.994
Hsp68	8|8	4|2|0|0|0	0.9785
Ef1alpha100E	6|11	0|0|0|0|5	0.974
RpS14b	4|6	0|0|0|0|0	0.965
Hsc70-2	5|4	1|0|0|0|0	0.9605
CG30382	4|5	0|0|0|0|0	0.949
RpS27A	4|3	0|0|0|0|0	0.901
sesB	3|3	1|0|0|0|0	0.8965
14-3-3zeta	7|13	7|1|0|0|2	0.8745
Thiolase	4|6	3|0|0|0|2	0.8715
RagC-D	2|6	0|0|0|0|0	0.8605
CtBP	3|16	3|0|0|0|0	0.7965
CG8230	2|4	2|0|0|0|0	0.7755
Roe1	4|2	1|0|0|0|0	0.77
CaBP1	3|3	4|0|0|0|0	0.737
Rab6	2|4	3|0|0|0|0	0.7355
ms(3)72Dt	2|2	0|0|0|0|0	0.6945

Table 2.1. Statistical analysis of Cic interactome from S2 cells expressing Cic-SBP.

Protein	Pep. Num. in exp.	Pep. Num. in ctrl.	SANIT Probability
cic	49|68|63	0|0|0|0|0	1
rl	5|8|5	0|0|0|0|0	0.9967
Atx-1	3|4|4	0|0|0|0|0	0.9487
cin	2|5|6	0|1|0|0|0	0.888
Klp61F	4|3|7	0|1|2|0|0	0.8613
Wap	2|4|2	0|0|0|0|0	0.8593
Nup358	35|30|32	0|16|17|0|21	0.83
CG1677	7|3|5	0|1|2|0|1	0.8263
CG1091	2|2|3	0|0|0|0|0	0.823
Nup50	4|5|6	1|3|1|1|0	0.7923
CG8108	2|2|4	0|0|1|0|1	0.7257
Top2	13|8|14	1|2|9|1|4	0.718
Hsc70-5	17|11|12	0|6|8|0|7	0.7143
Pgi	3|7|5	0|0|4|0|2	0.6983
RanGAP	9|7|10	1|4|3|1|5	0.6957
Hsp23	4|4|3	0|2|1|0|1	0.684
CG6453	5|5|7	0|3|2|0|3	0.6777
Rrp1	1|5|5	0|0|0|0|2	0.6737
wech	5|3|4	0|2|0|0|3	0.6733
tacc	2|2|3	0|1|0|0|1	0.666
CG1218	3|2|3	0|1|2|0|0	0.665
Hcf	1|4|3	0|0|0|0|1	0.6507

Table 2.2. Statistical analysis of Cic interactome from *Drosophila* embryos expressing Cic-Venus.

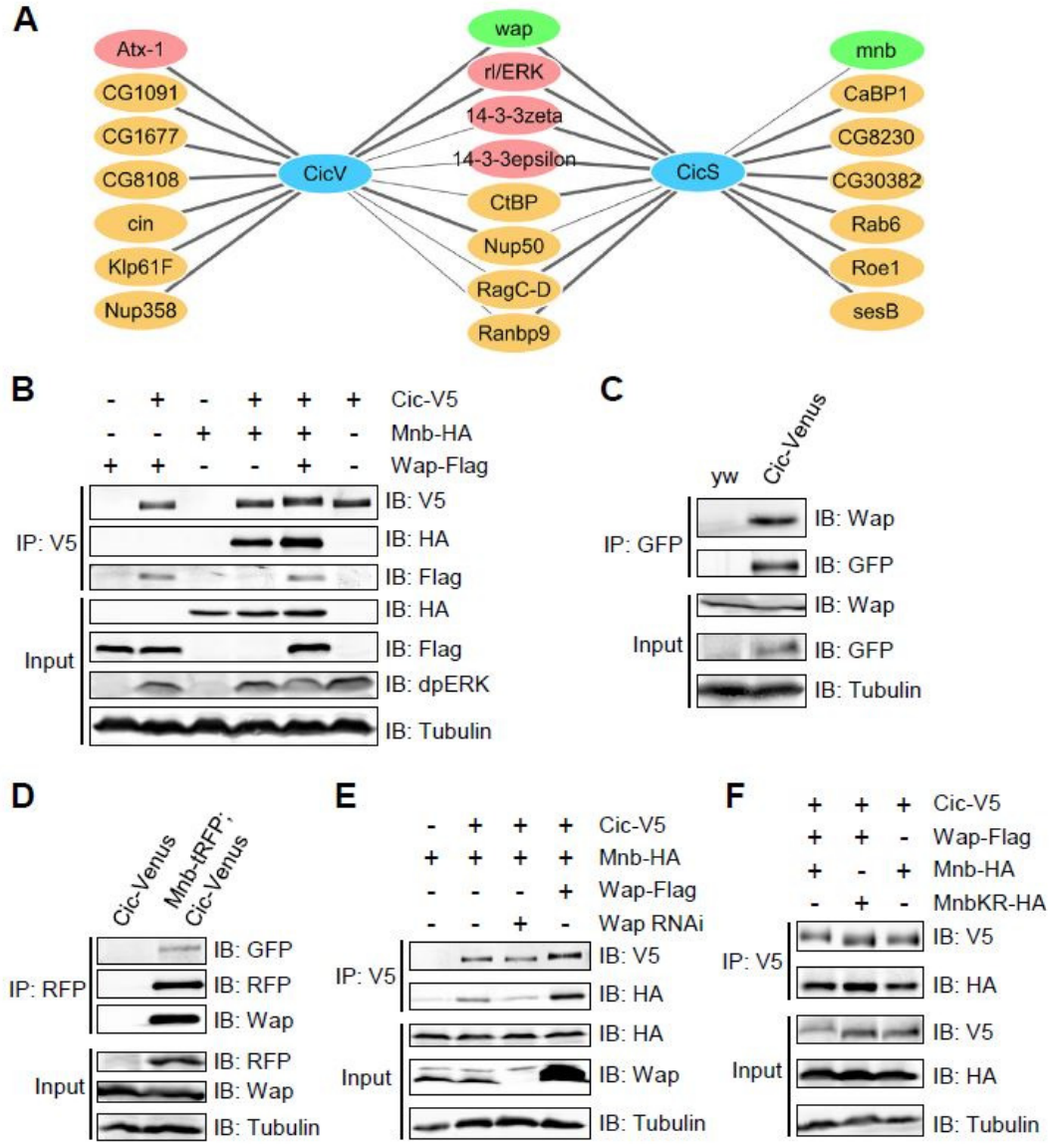

Figure 2.2. Mnb and Wap physically interact with Cic, and Wap promotes the binding of Mnb to Cic. (A) The Cic protein interactome identified in *Drosophila* S2 cells (CicS) and embryos (CicV). Thick lines, highly significant interactions. (B) Western blots showing co-immunoprecipitation of Cic, Mnb and Wap in S2 cells. Endogenous dpERK is stabilized by Cic expression. (C-D) Co-immunoprecipitation of Cic, Mnb, and Wap *in vivo* using embryo lysates from *yw* (control), *cic-Venus*, or *cic-Venus* crossed with *mnb-tRFP*. (E) Wap is required and sufficient to bridge Cic and Mnb. (F) Cic mobility was changed when Cic was co-expressed with Wap and wildtype Mnb, but not kinase-dead Mnb (MnbKR).

Wap and Mnb interact with Cic

I hypothesized that the interactors found from both *in vitro* and *in vivo* data would be the strongest candidates to be true Cic-interacting proteins. Cytoscape was used to incorporate the interactome data into Fig. 2.2A for visualization. I found two hits that were common between the cell culture and embryo data: rl and Wap. Wap is a WD40 repeat domain containing protein, which was previously reported to regulate neuromuscular development and tissue growth (Degoutin et al., 2013; Morriss et al., 2013). Wap is a highly conserved protein and its mammalian orthologue, DDB1 and CUL4 associated factor 7 (DCAF7), is expressed in vertebrate muscle and the nervous system. Wap mutant flies failed to properly form a jump muscle (Degoutin et al., 2013; Morriss et al., 2013). Wap functions together with the kinase Minibrain (Mnb) to regulate wing and leg tissue growth through the Hippo pathway downstream of Dachsous (Degoutin et al., 2013). Wap interacts with both Mnb and Wts, and serves as an adaptor to promote the Mnb-dependent phosphorylation and inhibition of Wts. The interaction between Wap and Mnb is conserved in mammals, as the Wap ortholog DCAF7 forms a stable complex with the dual-specificity tyrosine phosphorylation-regulated kinase 1A (DYRK1A), which is the mammalian ortholog of Mnb (Skurat and Dietrich, 2004). The AP-MS experiments also identified four peptides of Mnb in the Cic-SBP pulldown in S2 cells (Fig. 2.2A), suggesting that Wap, Mnb and Cic form a protein complex. Co-immunoprecipitation in S2 cells using overexpressed proteins confirmed that Cic binds to both Wap and Mnb (Fig. 2.2B).

To study the interactions between proteins expressed at endogenous levels *in vivo*, I used tagged *mnb-tagRFP-T* (*mnb-tRFP*) and *wap-Venus* alleles that were generated in Dr. Shu Kondo's laboratory by CRISPR/Cas9-mediated homologous recombination. Endogenous Wap was detected in the Cic-Venus complex using an anti-DCAF7 antibody (Fig. 2.2C), and both Wap and Cic-Venus were present in Mnb-tRFP complexes isolated from embryos expressing both Mnb-tRFP and Cic-Venus (Fig. 2.2D). Next I asked whether Wap could serve as a bridge for the interaction between Mnb and Cic. RNAi depletion of *wap* in S2 cells led to a reduction in the binding of Cic to Mnb, whereas overexpression of Wap promoted the interaction (Fig. 2.2E). Collectively, these data suggest that Wap, Mnb and Cic form a protein complex, with Wap likely serving as a bridging adaptor between Cic and Mnb.

Mnb phosphorylates the amino-terminal third of Cic in S2 cells.

Given that Mnb/DYRK1A is a kinase (Degoutin et al., 2013; Tejedor et al., 1995), I asked whether Mnb could phosphorylate Cic. Cic mobility on an SDS-PAGE was reduced when Cic, Mnb, and Wap were co-expressed (Fig. 2.2B, E, and F). Notably, the levels of activated ERK (dpERK) did not increase in this condition (Fig. 2.2B). In contrast, a kinase-dead mutant of Mnb (MnbKR) (Degoutin et al., 2013) failed to reduce Cic mobility (Fig. 2.2F), suggesting that the kinase activity of Mnb is required to reduce Cic mobility and that this modification is likely to be phosphorylation.

To determine which region of Cic was phosphorylated by Mnb, three Cic fragments (Cic1-3, Fig. 2.3A) were coexpressed with Wap in the presence or absence of

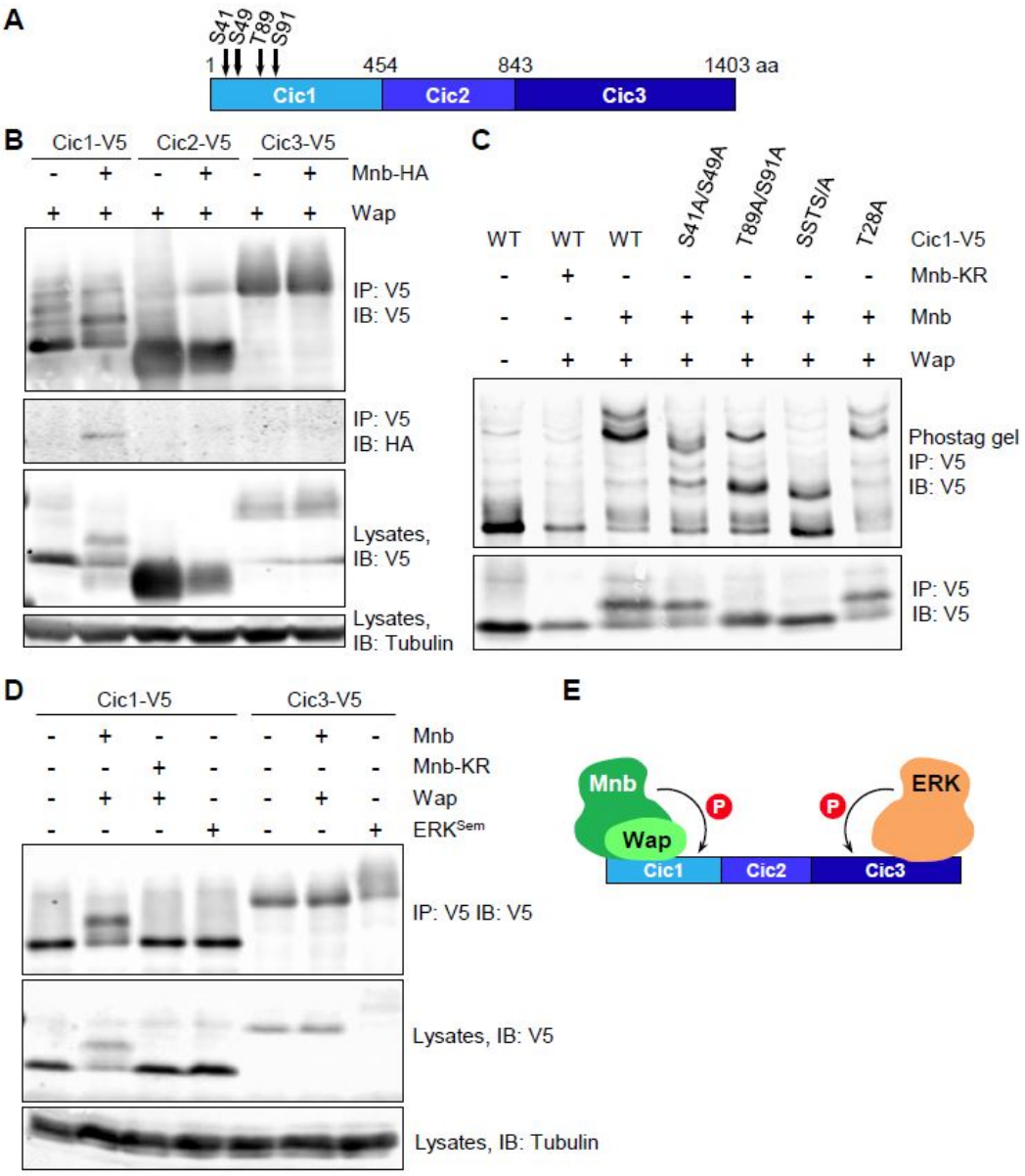

Figure 2.3. Mnb and ERK target different regions of Cic for phosphorylation. (A) Schematic diagram of the three Cic fragments (Cic1, Cic2 and Cic3) with locations of phosphorylation sites. (B) Mnb interacts with and phosphorylates only the amino terminal Cic fragment, Cic1. (C) Phos-tag^{TM} gel analysis of Cic1 phosphorylation. Bottom panel: regular SDS-PAGE. (D) Mnb phosphorylates region Cic1, whereas activated ERK (ERK^{Sem}) phosphorylates region Cic3. (E) Summary of Cic binding and phosphorylation data.

Mnb in S2 cells. Only the amino-terminal fragment of Cic (Cic1, representing amino acids 1-453) was found to interact with Mnb (Fig. 2.3B). In addition, Mnb decreased the electrophoretic mobility of Cic1, but not Cic2 or Cic3 (Fig. 2.3B). Phos-tag^{TM} gel analysis confirmed phosphorylation of Cic1 by wildtype but not kinase-dead Mnb (Fig. 2.3C). Next I asked which residue(s) in Cic1 are phosphorylated by Mnb. Threonine 28 is part of a motif in Cic1 (RSATP) that closely matches the DYRK1A phosphorylation consensus RP(X)(S/T)P (Himpel et al., 2000). Surprisingly, mutation of this residue (T28A) did not alter the phosphorylation pattern of Cic1 (Fig. 2.3C). To identify Cic residues that are phosphorylated by Mnb, Cic1 and Wap were coexpressed in S2 cells either with Mnb or MnbKR, Cic1 was purified, and its phosphorylation was analyzed by mass spectrometry. Four Cic1 residues (S41, S49, T89, and S91) were more highly phosphorylated by Mnb compared to MnbKR, with T89 and S91 phosphorylations found exclusively in the wildtype Mnb sample (Figs. 2.3A and 2.4). The S41 and S49 residues were also found to be phosphorylated in an unbiased global phosphoproteomic study in *Drosophila* embryos (Zhai et al., 2008). Alanine substitutions of the four residues resulted in a reduction of phosphorylation of Cic1, with the most pronounced effect observed for a quadruple mutant, Cic-SSTS/A (Fig. 2.3C).

Previous studies showed that region Cic3 includes an ERK docking site and is subject to ERK-mediated phosphorylation (Astigarraga et al., 2007; Futran et al., 2015; Kim et al., 2010b). To compare the activities of Mnb and ERK, I co-expressed Cic1 or Cic3 with Mnb or a constitutively active *Drosophila* ERK, ERK^{Sem} (Brunner et al., 1994). Mnb could only reduce the electrophoretic mobility of Cic1 but not Cic3, whereas

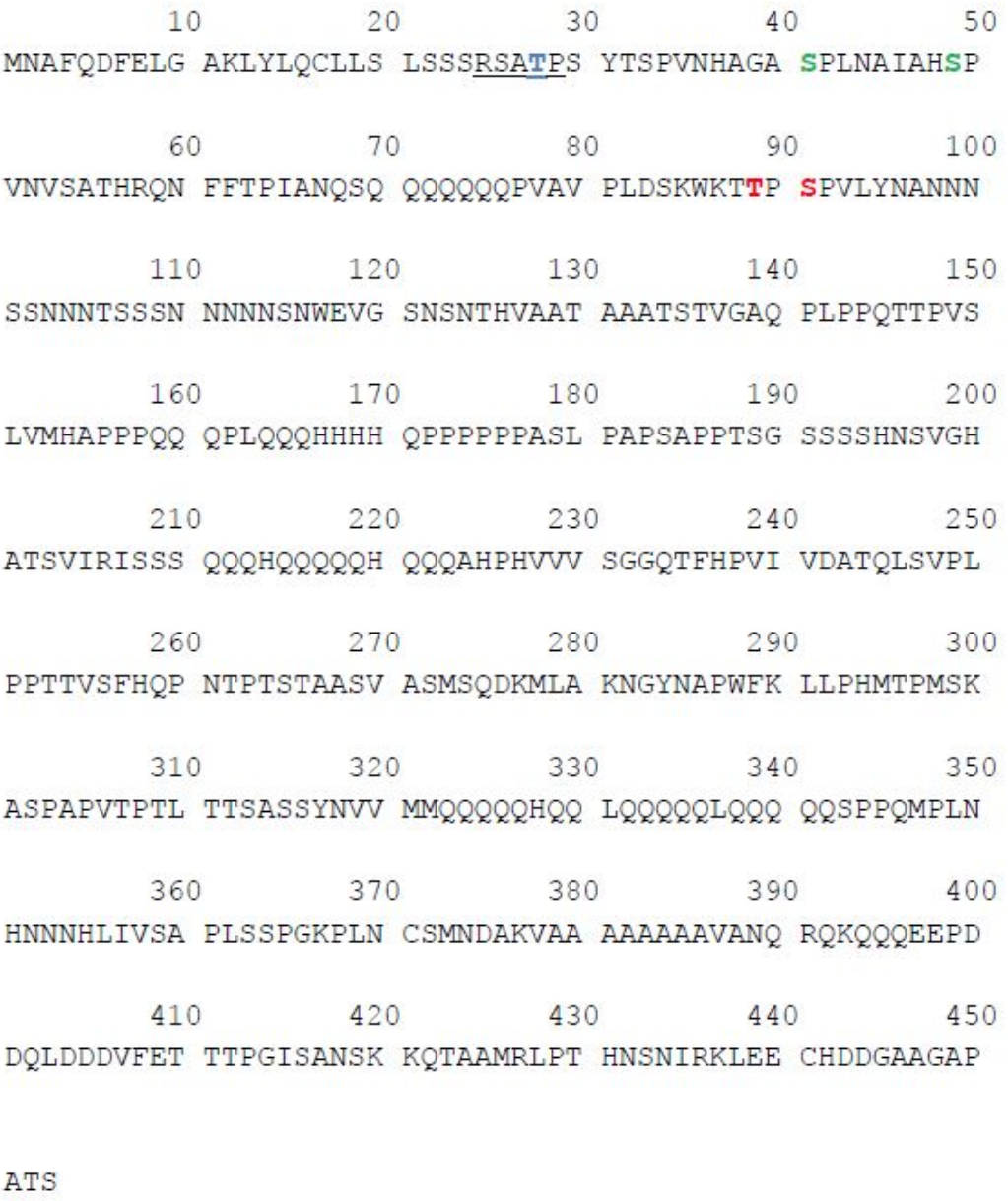

Figure 2.4. Locations of Cic phosphorylation sites identified by mass spectrometry. A Cic1 region is shown (amino acids 1-453). The putative DYRK1A consensus is underlined, and the corresponding residue (T28) is highlighted in blue. T28 phosphorylation was not detected by mass spectrometry. S41 and S49 (green) were more highly phosphorylated in wildtype Mnb samples compared to MnbKR. T89 and S91 phosphorylations (red) were found exclusively in the wildtype Mnb samples.

ERK^{Sem} only reduced the electrophoretic mobility of Cic3 but not Cic1 (Fig. 2.3D). Collectively, these results suggest that Mnb and ERK target different regions of Cic for phosphorylation: Wap facilitates Mnb-dependent phosphorylation of the amino-terminal third of Cic, whereas ERK targets the carboxy-terminal region (Fig. 2.3E).

Mnb and Wap reduce Cic repressor activity

Previous studies have shown that phosphorylation of Cic by ERK can result in downregulation of Cic by lowering its repressor activity, protein level, or nuclear localization (Ajuria et al., 2011; Astigarraga et al., 2007; Lim et al., 2013). I hypothesized that Mnb may exert similar effects. First, I used the CoinFLP-GAL4 system (Bosch et al., 2015) to generate RNAi-depletion clones in the eye imaginal discs (Fig. 2.5A). As expected, I observed reduced levels of Cic protein in *UAS-cic-RNAi* clones (Fig. 2.5B). However, no obvious increase in Cic protein level or change in subcellular localization was found in CoinFLP-generated *UAS-mnb-RNAi* clones (Fig. 2.5C). Therefore, Mnb is unlikely to control Cic at the level of protein turnover or nuclear access.

It has been shown that the relief of Cic repressor function by ERK does not necessarily require reduction in Cic protein levels (Lim et al., 2013). To assess whether Mnb could similarly affect Cic repressor activity, I used a reporter, *CUASC-lacZ*, which contains five GAL4 binding sites flanked on either side by two Cic binding motifs (Fig. 2.6A) (Ajuria et al., 2011). This reporter is only responsive to GAL4 in areas where Cic activity is inhibited, e.g. by RTK signaling (Fig. 2.6B). Uniform induction of GAL4

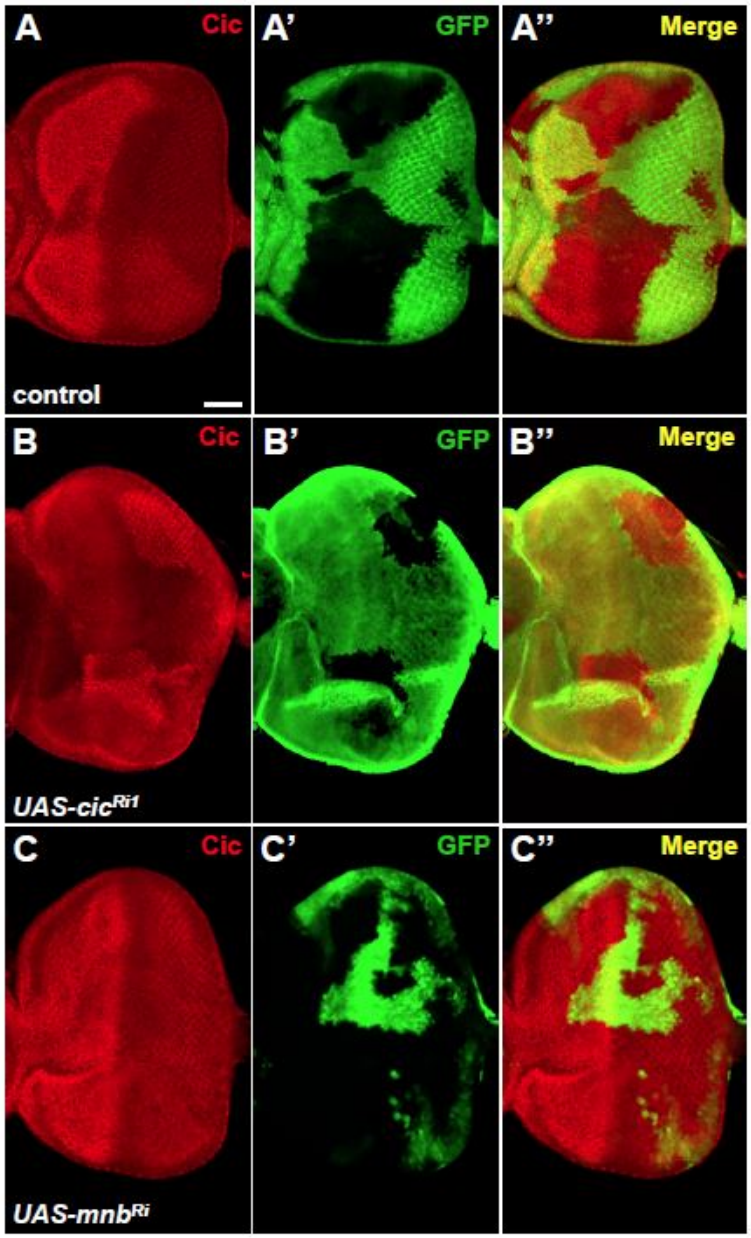

Figure 2.5. RNAi depletion of Mnb does not increase Cic levels in imaginal eye discs. (A-C'') Mosaic eye discs of the indicated genotypes generated using CoinFLP-GAL4 and stained with anti-Cic antibody (red). GAL4-positive cells are marked with *UAS-GFP* (green). (A-A'') Control clones do not affect Cic protein levels. (B-B'') Knockdown of *cic* reduces Cic protein levels. (C-C'') Knockdown of *mnb* does not increase Cic protein level or change Cic subcellular localization. Scale bar, 50 μm.

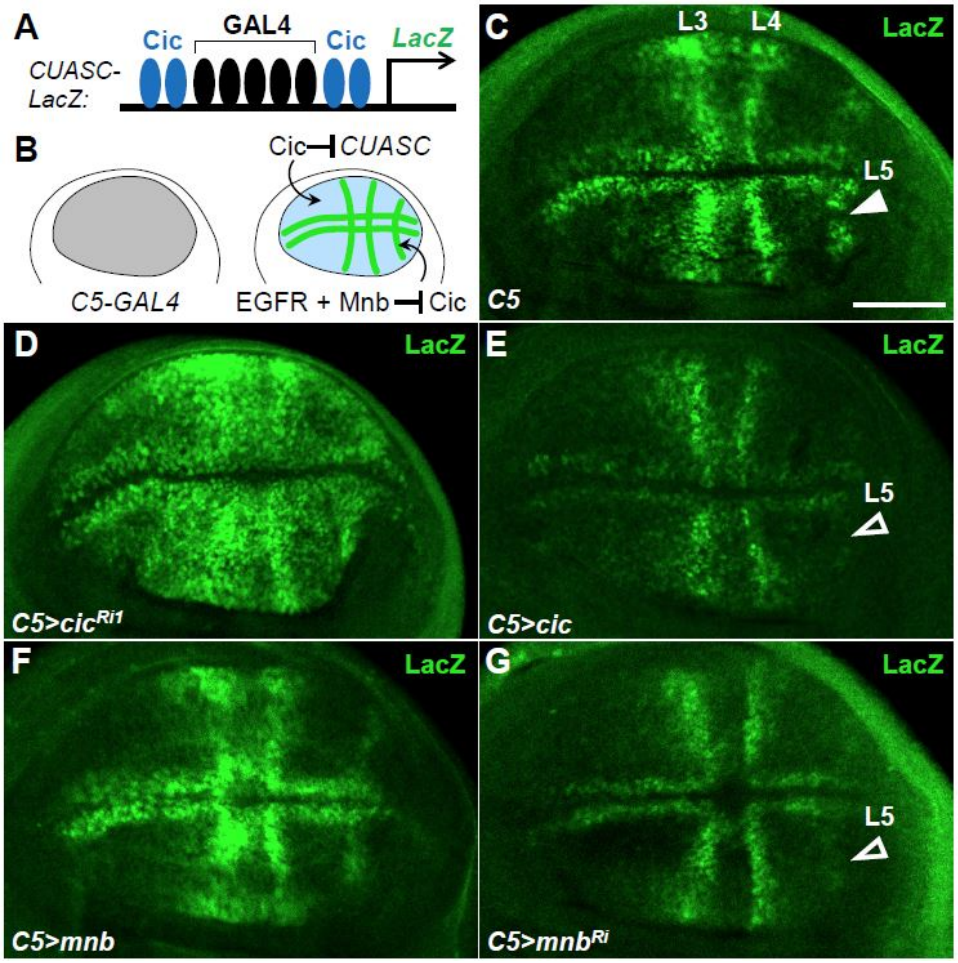

Figure 2.6. Mnb reduces Cic repressor activity. (A) Diagram of the *CUASC-lacZ* reporter. (B) Summary diagram of expression patterns. (C-G) LacZ expression pattern resulting from *C5-GAL4*-directed activation of *CUASC-lacZ* in wing discs from control (C), *UAS-cic*^{RNAi1} (D), *UAS-cic* (E), *UAS-mnb* (F), and *UAS-mnb*^{RNAi} (G) larvae. Scale bar, (C-G), 50 μm.

expression in the wing pouch under the control of the *C5-GAL4* driver (Yeh et al., 1995) resulted in a localized activation of LacZ expression in prospective veins (Fig. 2.6C). This pattern results from Epidermal Growth Factor Receptor (EGFR)/ERK-mediated inactivation of Cic in these regions (Fig. 2.6B) (Ajuria et al., 2011). RNAi depletion of *cic* or overexpression of ERK^{Sem} throughout the wing pouch led to a much broader expression of LacZ (Figs. 2.6D and 2.7B), confirming that the normal restriction of the expression pattern of *CUASC-lacZ* to prospective veins is Cic dependent. In contrast, overexpression of Cic resulted in the loss of LacZ expression in the vein L5 region (Fig. 2.6E, open arrowhead). Overexpression of Mnb or Wap induced a broader LacZ expression in the wing pouch (Figs. 2.6F and 2.7C). Conversely, RNAi depletion of *mnb* or *wap* under the control of *C5-GAL4* resulted in reduced LacZ expression, particularly in vein L5 (Figs. 2.6G and 2.7D). These data suggest that Mnb and Wap limit Cic repressor function in the wing disc. This contribution likely complements the regulation by ERK, which appears to be insufficient on its own, at least for vein L5 (Fig. 2.6B).

Mnb and Wap have been shown to phosphorylate and inhibit Warts, which results in elevated Yki activity (Degoutin et al., 2013). To test whether *CUASC-lacZ* expression was affected by Hippo signaling, I depleted the levels of the Yki-interacting transcription factor Scalloped (Sd), which is required for the activation of Yki targets (Zhang et al., 2008). I observed that knockdown of *sd* using RNAi had no obvious effect on the expression of *CUASC-lacZ* (Fig. 2.7E), suggesting that Hippo signaling is not involved in the regulation of Cic repressor activity in this context. To further assess whether Mnb and

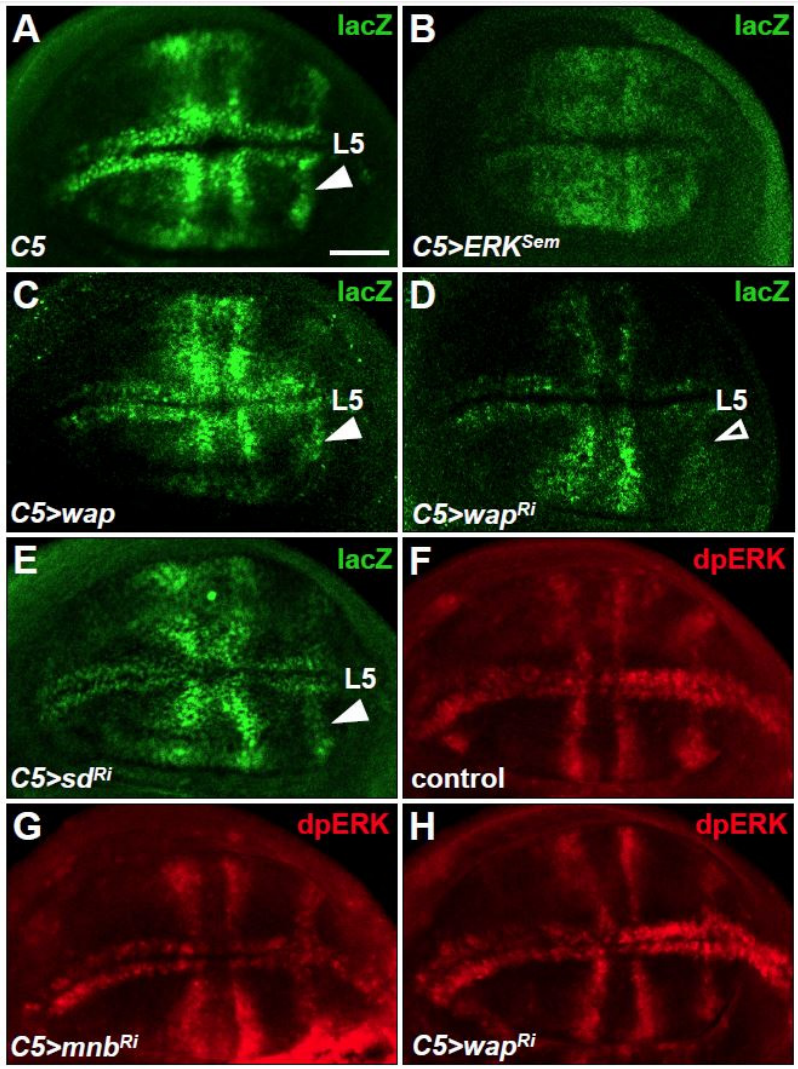

Figure 2.7. Modulation of Cic repressor activity by Mnb and Wap does not require Sd and does not affect activity of ERK. (A-E) LacZ expression pattern resulting from *C5-GAL4*-directed activation of *CUASC-lacZ* in wing imaginal discs from control (A), *UAS-ERK*^{Sem} (B), *UAS-wap* (C), *UAS-wap*^{RNAi} (D), and *UAS-sd*^{RNAi} (E) larvae. Expression of ERK^{Sem} and Wap led to a broader activation of the reporter (B, C), whereas knockdown of *wap* resulted in lower LacZ expession, particularly in presumptive vein L5 (D). Knockdown of *sd* did not alter the normal pattern of expression in presumptive veins. (F-H) dpERK expression pattern in wing discs from control (F), *C5-GAL4>UAS-mnb*^{RNAi} (G), and *C5-GAL4>UAS-wap*^{RNAi} (H) larvae. Scale bar, 50 μm.

Wap engage RTK/ERK signaling to control Cic, I analyzed dpERK levels in wing pouches expressing *mnb-RNAi* or *wap-RNAi*. I found that RNAi depletion of *wap* or *mnb* did not alter the dpERK pattern in wing discs (Figs. 2.7F-H). This result is in agreement with the observation that overexpression of Mnb did not increase dpERK levels in S2 cells (Fig. 2.2B). I conclude that Mnb and Wap downregulate Cic repressor activity independently from the RTK/ERK and the Hippo pathways.

To directly address how Mnb and Wap affect Cic function as a transcriptional repressor, I studied the activity of a reporter, *CUASC-Luc*, which is controlled by GAL4 and Cic, in S2 cells (Fig. 2.8A). Transfection of GAL4 activated this reporter ~10-fold, and this activation was repressed by co-expression of Cic in a dose-dependent manner (Fig. 2.8B). Depletion of endogenous *mnb*, *wap*, or *rl* (ERK) by RNAi resulted in a reduction of reporter activity (Fig. 2.8C), suggesting that Mnb, Wap and ERK are required to limit the activity of Cic. I next tested whether Mnb and Wap could reduce the capacity of Cic to repress *CUASC-Luc* expression, and found that co-transfection of Cic with Mnb and Wap partially relieved Cic-mediated repression of this reporter (Fig. 2.8D). Whereas the Cic-SSTS/A mutant repressed the reporter gene expression to a similar level as wildtype Cic, co-expression of this mutant with Mnb and Wap did not affect its ability to repress *CUASC-Luc* (Fig. 2.8D). Collectively, these results indicate that Mnb and Wap reduce the activity of Cic as a transcriptional repressor, likely via Mnb-mediated phosphorylation of residues located in the amino terminus of the Cic protein.

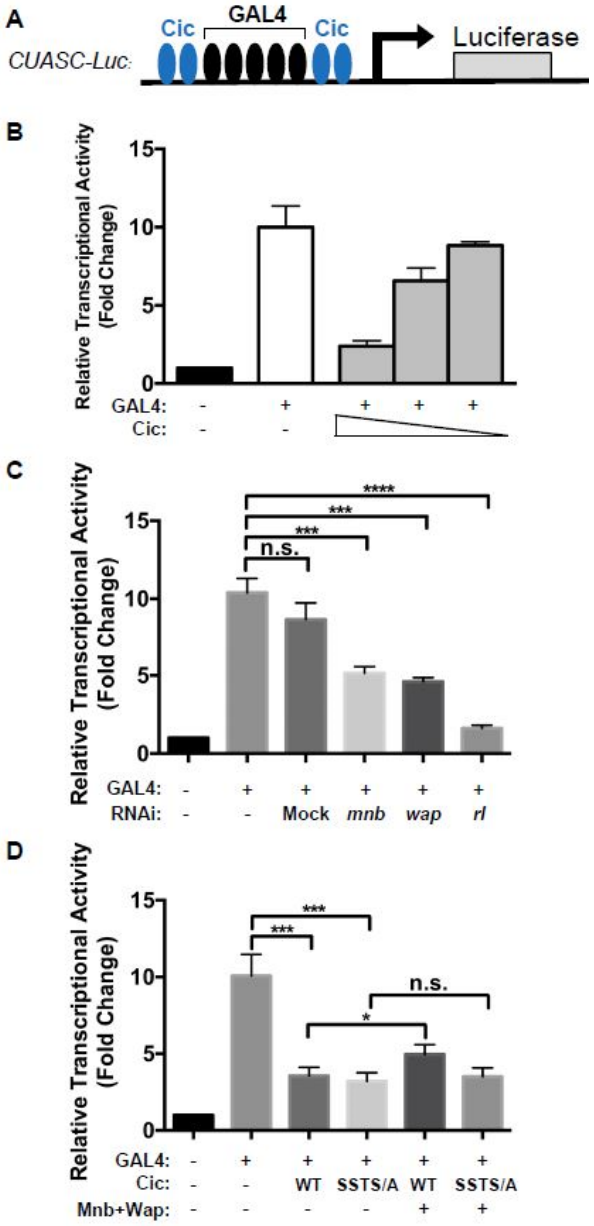

Figure 2.8. Mnb and Wap reduce Cic repressor activity in Luciferase assay. (A) Schematic diagram of the *CUASC-Luc* reporter construct. (B) Dose-dependent repression of *CUASC-Luc* expression by Cic. S2 cells were co-transfected with the reporter *CUASC-Luc*, pMT-GAL4 and decreasing amounts of Cic expressing plasmid (500 ng, 250 ng, 125 ng). The values shown are fold changes over the negative control set at 1. (C) *mnb*, *wap*, and *rl* (ERK) are required to limit the activity of Cic. (D) Mnb and Wap reduce transcriptional repressor activity of wildtype Cic, but not of the phosphorylation site mutant, Cic-SSTS/A. n.s., not significant, * $p<0.05$, ** $p<0.01$, *** $p<0.001$, Statistical significance was analyzed using unpaired Student's *t* test. Error bars represent standard deviation.

Mnb opposes Cic function in controlling wing and eye growth.

I next investigated whether the inhibitory effects of Mnb/Wap on Cic were involved in the control of organ growth. Overexpression of Mnb using the wing pouch *MS1096-GAL4* driver (Capdevila and Guerrero, 1994) promoted wing growth (Figs. 2.9B and G). Conversely, overexpression of Cic or the Cic-SSTS/A mutant resulted in a reduction of wing size (Figs.2.9C, E and G). Whereas coexpression of Mnb with Cic suppressed the smaller wing size associated with Cic overexpression (Figs. 2.9C, D, and G), coexpression of Mnb with Cic-SSTS/A did not modify this phenotype (Figs. 4E, F, and G). These data suggest that Mnb regulates Cic function at least in part through the phosphorylation of the SSTS residues. I also asked whether *mnb* and *cic* would display opposing effects on growth in a reduction-of-function context. RNAi depletion of *cic* using the *MS1096-GAL4* driver caused a severe defect in wing development. I thus used a weaker driver, *C96-GAL4*, which is expressed primarily around the wing margin (Helms et al., 1999), to study the effects of reduced levels of *mnb* and *cic*. Knockdown of *cic* caused wing overgrowth (Figs. 2.9I, L), and RNAi depletion of *mnb* resulted in an opposite effect (Figs. 2.9J, L). Importantly, RNAi depletion of *cic* partially rescued the small wing phenotype induced by expression of *mnb-RNAi* (Figs. 2.9K, J). Mutually antagonistic effects of Mnb and Cic on growth were also observed in the eye (Fig. 2.10). Collectively, I conclude that Mnb and Wap promote wing and eye growth by antagonizing the growth-restricting function of Cic.

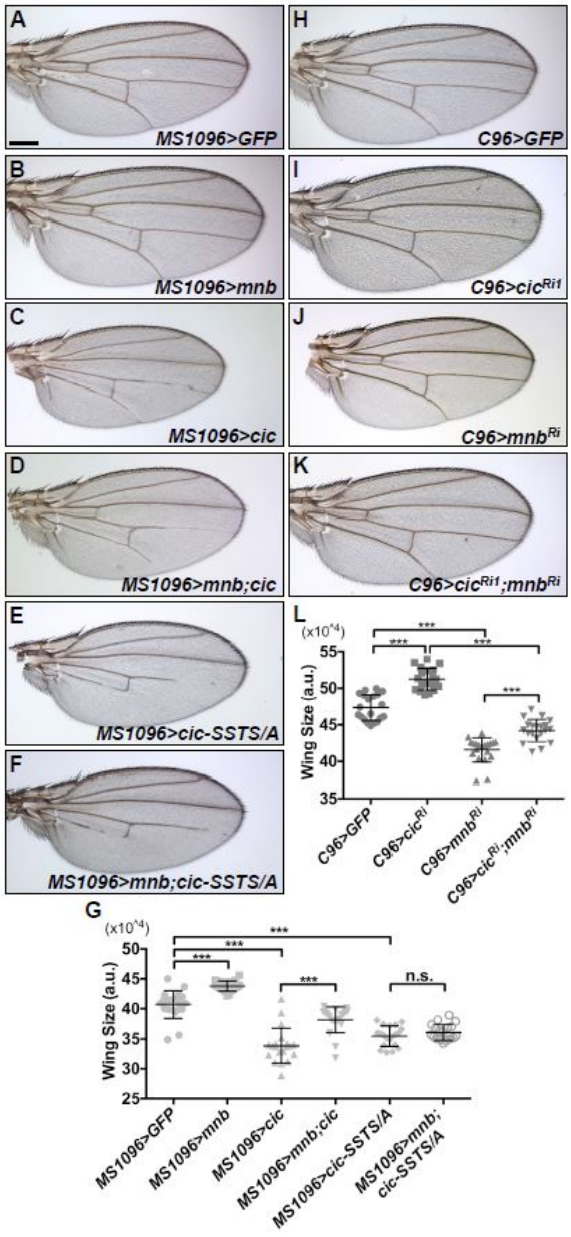

Figure 2.9. Mnb opposes Cic function in controlling wing growth. (A-F) Wings from adult female flies expressing *UAS-GFP* as a control (A), *UAS-mnb* (B), *UAS-cic* (C), *UAS-mnb* together with *UAS-cic* (D), *UAS-cic-SSTS/A* (E), and *UAS-mnb* together with *UAS-cic-SSTS/A* (F) using the *MS1096-GAL4* driver. (G) Quantification of the wing areas for the genotypes shown in (A-F) (n=20 for each genotype). (H-K) Wings from adult female flies expressing *UAS-GFP* as a control (H), *UAS-cic*^{RNAi1} (I), *UAS-mnb*^{RNAi} (J), and *UAS-cic*^{RNAi1} together with *UAS-mnb*^{RNAi} (K) using the *C96-GAL4* driver. (L) Quantification of the wing areas for the genotypes shown in (H-K) (n=20 for each genotype). * p<0.05, ** *p*<0.01, *** *p*<0.001. Statistical significance was analyzed using Student's *t* test. Error bars represent standard deviation. Scale bar, 200 μm.

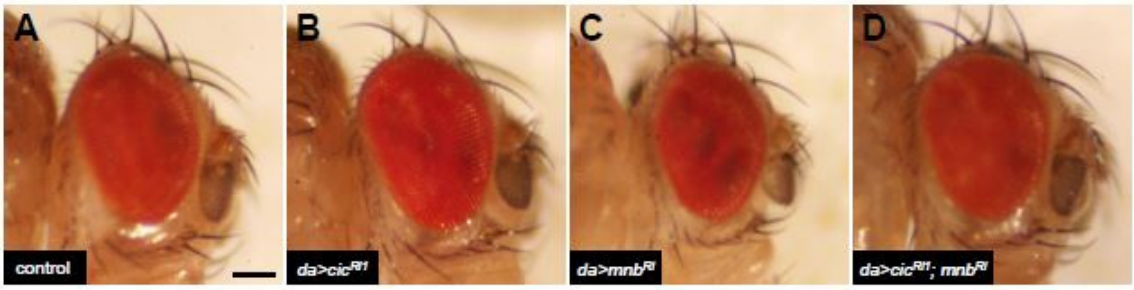

Figure 2.10. Mnb opposes Cic function in controlling eye growth. (A-D) Adult female flies expressing *UAS-GFP* (A), *UAS-cic*^{RNAi1} (B), *UAS-mnb-RNAi* (C), and *UAS-mnb-RNAi* together with *UAS-cic*^{RNAi1} (D) under the control of the *da-GAL4* driver. Knockdown of *mnb* results in a smaller eye (C), which is reversed by a concomitant knockdown of *cic* (D). Scale bar, 100 μm.

Reduction of *cic* level restores adult brain size in *mnb* mutants.

Mnb was originally identified in a genetic screen for mutants with altered brain structure (Tejedor et al., 1995). Mutant *mnb* adult animals have smaller brains, with the optic lobes (OLs) most significantly affected (Tejedor et al., 1995). In *Drosophila* development, the size of the central brain (CB) is determined by the proliferative ability of the neuroblasts (NBs) that are of embryonic origin, whereas the OLs are generated by the neuroepithelium (NE) which gives rise to the OL NBs during the larval stages (Sousa-Nunes et al., 2010). In order to identify the tissue origins of the reduction in adult brain size, the larval and pupal brains from the wildtype and mnb^{d419} animals were analyzed (mnb^{d419} is a null allele, (Hong et al., 2012)). The volumes of the larval and pupal brains in the mnb^{d419} mutants were significantly smaller than controls (Fig. 2.11), suggesting that the effects of loss of *mnb* can be traced to these developmental stages. I asked whether the smaller OLs in *mnb* mutants could result from altered proliferation in the NE and/or NB regions during the larval stages. The widths of both the NB and NE regions in the larval brains from mnb^{d419} animals were significantly reduced, compared to controls (Figs. 2.12A-D, G, H). Conversely, overexpression of Mnb in MARCM clones resulted in an increase of the width of NE specifically in the clone area (Figs. 2.12E and F). These results suggest that Mnb is required for the proper growth of both the NE and NB regions in the OL. Additionally, Mnb may be involved in controlling the timing of NE to NB differentiation (Reddy et al., 2010).

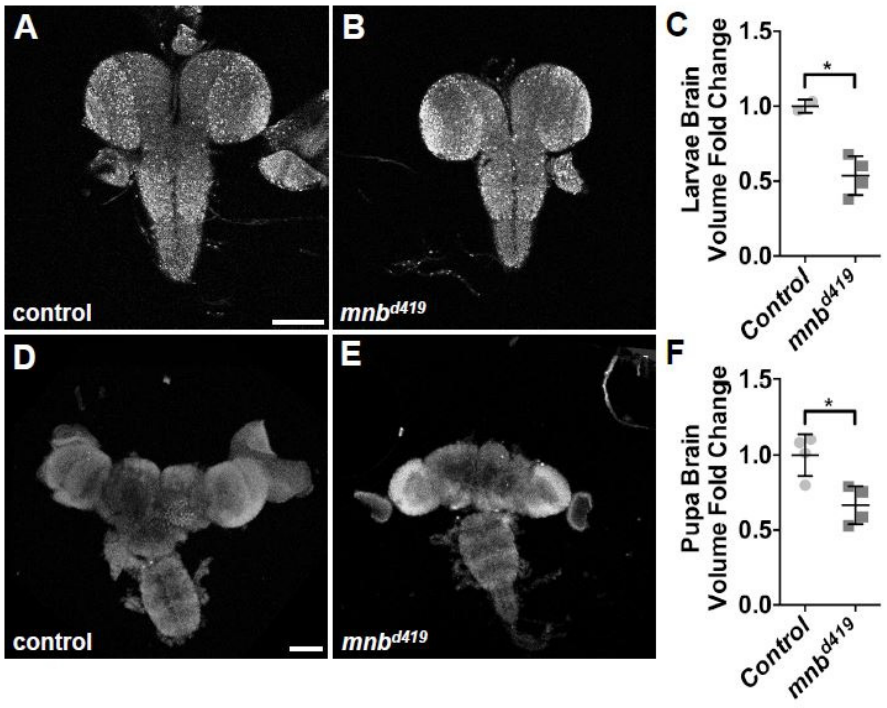

Figure 2.11. Loss of *mnb* leads to smaller brain size in larvae and pupae. (A, B) Third instar larval brains from control (w^{1118}) (A) and mnb^{d419} (B) animals. (C) Quantification of the larval brain volumes in (A, B) (n=2, 4). (D, E) Pupal brains from control (w^{1118}) (D) and mnb^{d419} (E) animals. (F) Quantification of the pupal brain volumes in (D, E) (n=4, 4). * $p<0.05$. Statistical significance was analyzed using Student's *t* test. Scale bars, 100 μm. These data were obtained in collaboration with Francesca Froldi (Cheng Lab).

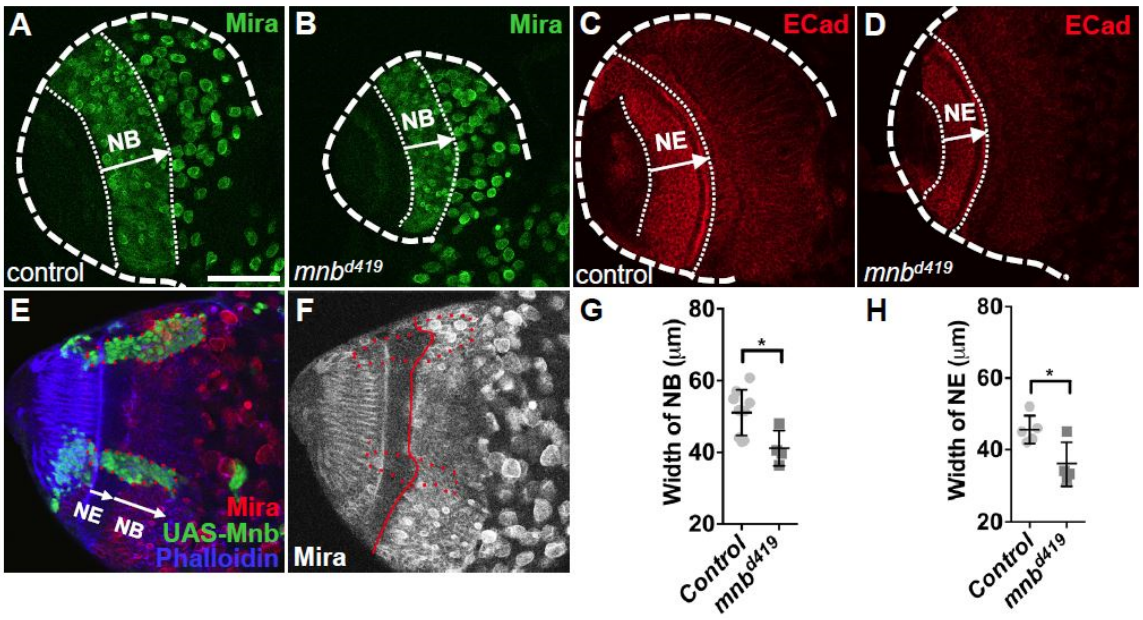

Figure 2.12. Loss of *mnb* leads to thinner Neuroblast (NB) and Neuroepithelium (NE) regions in larvae. (A, B) NB regions (Mira-positive cells) in larval CNS from control (w^{1118}) (A) and mnb^{d419} animals (B). (C, D) NE regions (E-cad positive cells) in larval CNS from control (w^{1118}) (C) and mnb^{d419} animals (D). (E, F) NE region is expanded cell-autonomously in *UAS-mnb* overexpression clones (marked in green in E). Dotted red line: clone areas; solid red line: boundary between NB and NE. (G) Quantification of results in (A, B) (n=9, 4). (H) Quantification of results in (C, D) (n=5, 4). Scale bars: 50 μm $*p<0.05$, $**p<0.01$, $***p<0.001$. Error bars represent standard deviation. Statistical significance was analyzed using Student's *t* test. These data were obtained in collaboration with Francesca Froldi (Cheng Lab).

Next I asked whether interactions between *cic*, *mnb* and *wap* were involved in the control of adult brain size. RNAi knockdown of *mnb* or *wap* with a ubiquitous *da-GAL4* driver (Wodarz et al., 1995) resulted in a smaller adult brain, especially in the optic lobes (Figs. 2.13A, C and G). This result suggests that both Mnb and Wap are required for normal brain growth. Knockdown of *cic* resulted in an increased adult brain size (Figs. 2.13B and G). Strikingly, depletion of *cic* strongly suppressed the small brain phenotype caused by the knockdown of *mnb* (Figs. 2.13C, E and G), suggesting that Mnb promotes brain growth via downregulation of Cic. Similarly, RNAi depletion of *cic* rescued the smaller brain phenotype of *wap-RNAi* (Figs. 2.13D, F and G). Overall, these results implicate Cic, Mnb and Wap in a common pathway controlling organ growth, and suggest that at least some of the growth-promoting functions of Mnb and Wap are mediated via their inhibition of Cic activity.

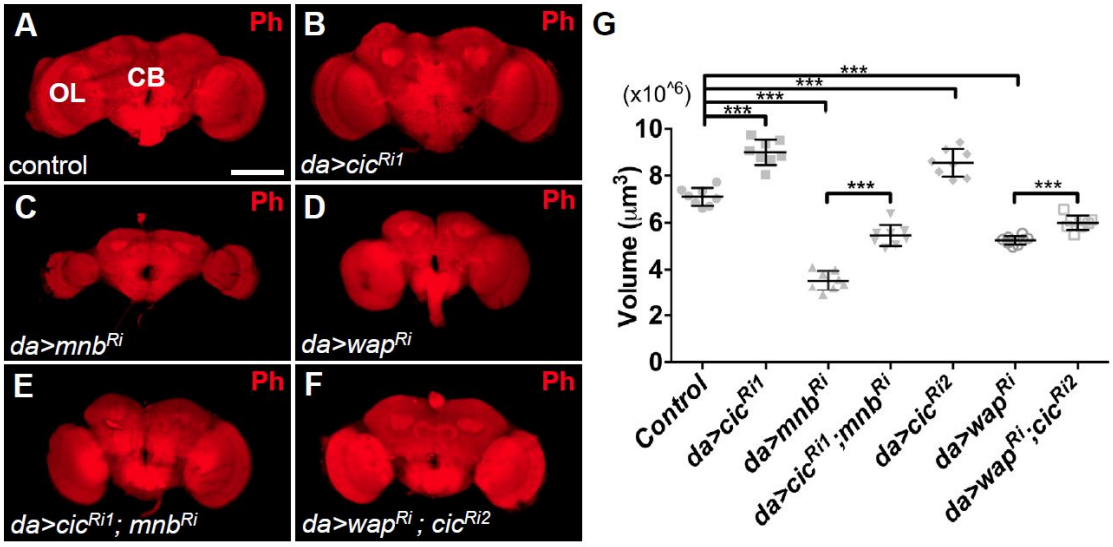

Figure 2.13. Reduction in *cic* level restores adult brain size in mnb mutants. (A-G) Brains from adult female flies with the indicated genotypes. *da-GAL4* driver was used to drive the expression of *UAS-GFP* (A), *UAS-cic*^{RNAi1} (B), *UAS-mnb*^{RNAi} (C), *UAS-wap*^{RNAi} (D), *UAS-cic*^{RNAi1} together with *UAS-mnb*^{RNAi} (E), or *UAS-cic*^{RNAi2} together with *UAS-wap*^{RNAi} (F). Ph, phalloidin stain. (G) Quantification of brain volumes for the genotypes shown in (A-F) (n=8 for each genotype). Scale bars: 100 μm. *p<0.05, *p<0.05, **p<0.01, ***p<0.001. Error bars represent standard deviation. Statistical significance was analyzed using Student's t test.

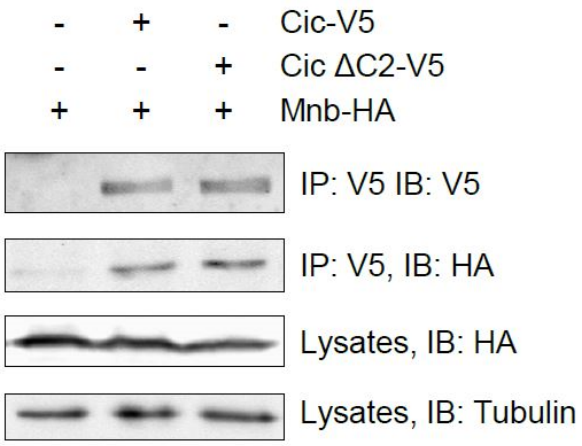

Figure 2.14. Deletion of the C2 motif does not affect the binding between Cic and Mnb. Protein lysates from S2 cells transfected with the indicated plasmids were incubated with anti-V5 beads, and immunocomplexes were analyzed on western blots probed with anti-V5, anti-HA, and anti-tubulin antibodies.

Mnb and ERK have additive effects on Cic activity

This study so far has shown that Mnb is required for inhibiting Cic activity in various tissue contexts, which is also how ERK transmits signals from RTKs to control growth and patterning. Next I asked whether the effects of ERK and Mnb on Cic are additive, by first individually and then simultaneously reducing their ability to inhibit Cic. ERK-mediated downregulation of Cic depends on the conserved C2 motif located in region Cic3, which serves as the ERK docking site (Astigarraga et al., 2007). Deletion of the C2 motif abrogated Cic-ERK interaction (Astigarraga et al., 2007), and a single amino acid substitution, F1054A, in the C2 motif (QQ**F**ILAPTPAQLG) reduced the binding of Cic to ERK (Futran et al., 2015). Importantly, deletion of the C2 domain did not affect the binding of Cic to Mnb (Fig. 2.14).

Using CRSPR/Cas9-mediated mutagenesis, our collaborators from Jiménez laboratory generated an allele (cic^3) lacking residue F1054, which is predicted to specifically disrupt the interaction of Cic with ERK. Most of the cic^3 mutant animals showed normal wing vein pattern (Figs. 2.15A and B), however a partial loss of vein L5 was observed in approximately 30% of adult flies, indicating that this is a gain-of-function mutation. RNAi depletion of *mnb* using *C5-GAL4* resulted in a partial loss of veins L4 and L5 (Fig. 2.15C, arrowheads), which is in agreement with our observation that *CUASC-lacZ* expression was lost in the L5 region in this background (see Fig. 2.6G). I reasoned that if Mnb and ERK had additive effects on Cic activity, reduction of *mnb* level in the cic^3 background would cause a more severe vein loss phenotype, compared to

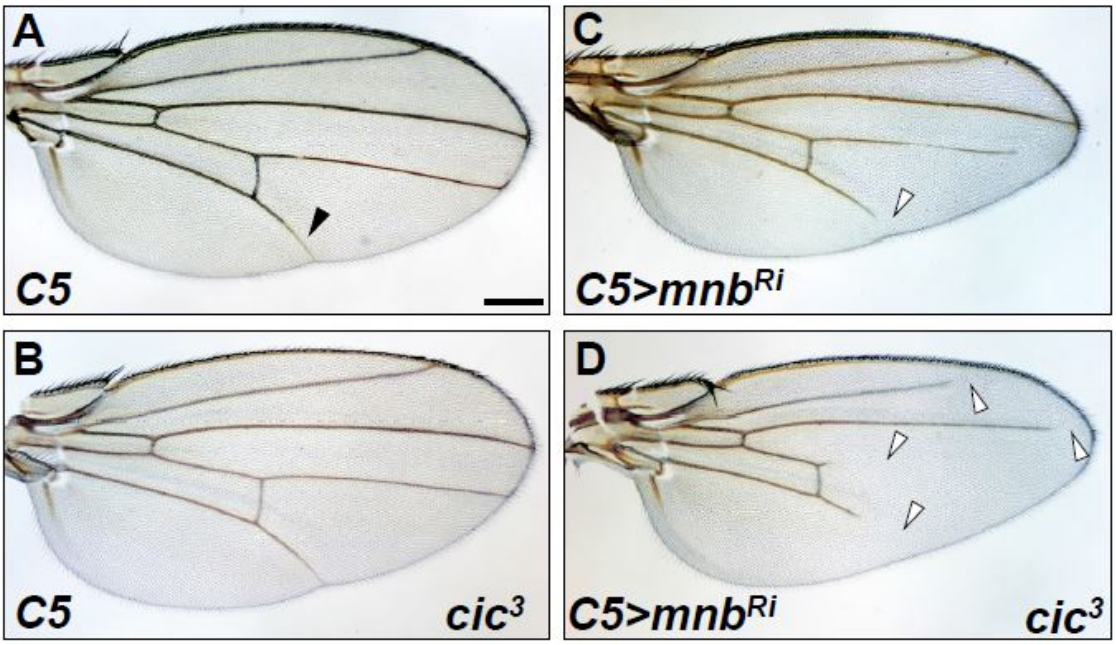

Figure 2.15. Mnb and ERK function additively to inhibit Cic. (A-D) Wings from adult female flies of the following genotypes: *C5-GAL4* (A), *C5-GAL4 cic^3/+* (B), *C5-GAL4/UAS-mnb^{RNAi}* (C), *C5-GAL4 cic^3/UAS-mnb^{RNAi}* (D). Scale bar: 200 μm. These data were obtained in collaboration with Marta Forés (Jiménez Lab).

depletion of *mnb* alone. Indeed, I observed not only a more severe loss of veins L4 and L5, but also partial loss of veins L2 and L3 in the *C5>mnbRi; cic*^{3} animals (Fig. 2.15D). I conclude that Mnb and ERK function additively to regulate wing tissue patterning via inhibition of Cic activity.

2.3 Discussion

Our knowledge of upstream signals controlling Cic activity has been largely limited to its regulation by the RTK/ERK pathway (Jimenez et al., 2012). In this study, I have identified a previously unknown mechanism for the regulation of Cic by the kinase Mnb and its adaptor Wap. Wap facilitates Mnb-dependent phosphorylation of Cic in the amino-terminal region, which is necessary for downregulation of Cic activity. I found that the primary mechanism of Cic downregulation by Mnb is through the relief of Cic-dependent transcriptional repression. Mnb-dependent downregulation of Cic is necessary for the proper growth of multiple organs and correct patterning of tissues.

In this study, I have used AP-MS to identify Mnb and Wap as novel Cic-interacting proteins. Co-immunoprecipitation experiments from 0-16 h *Drosophila* embryos have shown that Mnb, Wap and Cic interact with each other *in vivo*. I have shown that Mnb interacts with and phosphorylates the amino-terminal third of the Cic protein. However, it is still not known how Mnb interacts with Cic. Future studies are required to elucidate the structural basis for the interaction between Mnb and Cic. It may be informative to screen for the inhibitors specifically disrupting the Mnb-Cic interaction.

The Mnb-Cic interaction and phosphorylation is different from the ERK-mediated phosphorylation of Cic, as previous reports showed that ERK interacts with Cic through C2 motif located in the carboxyl-terninal third of Cic (Astigarraga et al., 2007; Futran et al., 2015). This distinct Mnb-mediated phosphorylation of the amino-ternimal third of Cic results in at least 4 phosphorylation sites (S41, S49, T89, and S91), as revealed by a kinase assay. It would be informative to perform an *in vitro* kinase assay to survey the ERK-dependent phosphorylation sites on Cic. This assay will allow us to have a better understaning of the functional outcomes of Cic phosphorylations.

Unlike ERK-mediated phosphorylation, Mnb does not affect Cic protein level or cellular localization. Instead, I found that Mnb only inhibits Cic transcriptional repressor activity. However, the molecular details of this inhibition are still not clear. One possible explanation is that Mnb-mediated phosphorylation of Cic interferes with the binding of the Cic protein to its target DNA sequences, despite the fact that no phosphorylation site in the HMG box region has yet been identified. Therefore, it is worth performing a thorough kinase assay to identify all possible Mnb-dependent phosphorylation sites in full-length Cic. Previous studies showed that the repression of RTK target genes requires co-repressors such as Groucho (Gro) (Astigarraga et al., 2007; Cinnamon et al., 2008). Another possible reason for a reduction in Cic repressor function could be that Mnb-mediated phosphorylation of Cic disrupts its binding to the co-repressors, which in turn reduces its transcriptional repressor activity.

According to the current model (Fig 1.3), the RTK activation results in the phosphorylation of ERK, which in turn phosphorylates and downregulations Cic. This

RTK/ERK mediated regulation of Cic allows the derepression of RTK target genes, which are essential for development, patterning and growth. Therefore, Cic was regarded as a general sensor of RTK signaling (Jimenez et al., 2012). At least two RTKs function as upstream inputs into Cic signaling to regulate multiple cellular responses. Torso signaling functions through Cic to regulate embryo tissue patterning in *Drosophila* (Cinnamon et al., 2004; de las Heras and Casanova, 2006; Jimenez et al., 2000). EGFR signals are transduced through Cic to control patterning, differentiation, and proliferation (Ajuria et al., 2011; Atkey et al., 2006; Blair, 2007; Goff et al., 2001; Jiang et al., 2011; Jin et al., 2015; Roch et al., 2002). However, little is known about the upstream regulatory mechanisms of Mnb and Wap.

Mnb is expressed and required in neuroblast proliferation centers during neurogenesis, but what upstream signals activate Mnb is still unknown (Tejedor et al., 1995). One study revealed that Mnb formed a transitional intermediate during translation, which phosphorylates tyrosine326 in the activation loop of the kinase domain. This autophosphoryaltion is an intramolecular event. Once Mnb is released from the ribosome, tyrosine kinase activity is lost, and the Mnb kinase only functions as a serine/threonine kinase (Lochhead et al., 2005). Its mammalian homologue, DYRK1A, also relies on autophosphorylation of the conserved tyrosine321 in the activation loop of the kinase domain. In addition, autophosphorylation is not restricted to tyrosine321. A study showed that DYRK1A also autophosphorylates on serine520 in the PEST domain, which is

important for its interaction with 14-3-3 proteins (Alvarez et al., 2007). Given that the DYRK family kinases autoactivate themselves soon after translation (Becker and Sippl, 2011), it is likely that the effects of Mnb and Wap on Cic are constitutive.

Inhibition of Cic activity by Mnb/Wap has two developmentally important consequences (Fig. 2.16). First, this regulation is important for the proper growth of several organs, such as the wings, eyes, and the brain. Second, downregulation of Cic activity by Mnb/Wap is required for proper tissue patterning. Given the broad expression patterns of Cic, Mnb, and Wap, the inhibitory mechanism I describe appears to operate in most, if not all, cells. In relation to ERK, the contribution from Mnb and Wap to Cic downregulation depends on the tissue context and includes three possible scenarios: in some cells (e.g. developing vein L5 in the wing), both pathways are required for complete inhibition of Cic and operate additively. In other cells, ERK is the primary inhibitory signal, whereas the contribution of Mnb/Wap is less prominent (e.g. veins L2 and L3). Finally, in yet other cells in which ERK is not active, the function of Mnb and Wap to limit Cic activity would be dominant.

In addition to the RTK/ERK pathway, Cic was also shown to be regulated by Hippo signaling (Herranz et al., 2012), and we have previously implicated Mnb and Wap as Hippo pathway regulators downstream of Dachsous (Degoutin et al., 2013). In this study, I found that knockdown of *sd*, a required component of Hippo signaling, did not affect the pattern of expression of *CUASC-LacZ*, and that knockdown of *mnb* or *wap* did not alter the pattern of ERK activation (Fig. 2.7), suggesting that Mnb and Wap control

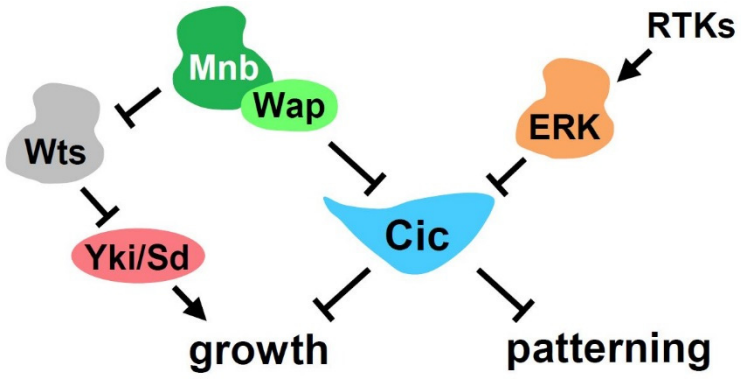

Figure 2.16. Cic integrates upstream signals to control organ growth and tissue patterning.

Cic activity independently from ERK and Hippo signaling. Altogether, current evidence suggests that Cic functions as an integrator of upstream developmental signals that converge on Cic to limit its activity, which is necessary for the proper execution of developmental programs responsible for tissue patterning and organ growth (Fig. 2.16). Cic controls these developmental programs by direct binding to the enhancers of the genes encoding regulators of tissue patterning and cell proliferation in *Drosophila* and mammals (Ajuria et al., 2011; Fores et al., 2015; Jin et al., 2015; Kawamura-Saito et al., 2006).

Interactions between Mnb/Wap and Cic in the brain have interesting parallels in human biology. The majority (>70%) of oligodendrogliomas, which are aggressive brain tumors, have been recently shown to harbor loss-of-function mutations in CIC, suggesting that it functions as a tumor suppressor (Sahm et al., 2012; Wesseling et al., 2015). Higher expression of DYRK1A was also found in a subset of oligodendroglioma patient samples (Pozo et al., 2013), raising a possibility that DYRK1A may suppress Cic activity in human cells, much like Mnb does in *Drosophila*. A connection between DYRK1A and Cic in controlling brain development may extend even deeper, since both proteins have been implicated in neurodegenerative diseases (Guimera et al., 1996; Lam et al., 2006; Moller et al., 2008; Tejedor and Hammerle, 2011).

2.4 Materials and Methods

Drosophila melanogaster Stocks

All *Drosophila* stocks were maintained on standard yeast-cornmeal-agar medium at 25°C or 18°C as indicated. *MS1096-GAL4*, *da-GAL4*, *C96-GAL4*, *en-GAL4 and hh-GAL4 UAS-GFP*, ey-*FLP UAS-dcr2* (#58757), *CoinFLP UAS-GFP* (#58751) were from the Bloomington *Drosophila* Stock Center. *UAS-wap RNAi* (KK 107076), *UAS-mnb RNAi* (GD 28628), *UAS-cic RNAi1* (KK 103012), *UAS-cic RNAi2* (GD 40867), *UAS-sd RNAi* (KK 101497) were from the Vienna *Drosophila* Resource Center (VDRC). *UAS-cic*, *UAS-mnb*, *UAS-wap* were made using standard cloning methods, and transgenic lines were generated by Genetic Services, Inc (Cambridge, MA). *Cic-Venus* is a genomic Cic

rescue construct from (Grimm et al., 2012). Other stocks were *C5-GAL4* and *CUASC-lacZ* (Ajuria et al., 2011), *mnb*^{d419} (Hong et al., 2012), *mnb-tagRFP-T* and *wap-Venus* (Poon et al., 2016). The targeting vectors comprised the tagRFP-T (Shaner et al., 2008) or Venus gene, the 3xP3-RFP gene for transformant selection and 1-kb homology arms. The vectors were designed such that the fluorescent protein gene is inserted immediately in front of the stop codon of the target gene and expressed as a fusion protein. The *cic*^{3} allele was obtained by CRISPR/Cas9-mediated mutagenesis. A guide RNA (gRNA) sequence (5'-GTGGGTGCCAAAATAAACTGC-3') targeting the C2 coding sequence was subcloned in vector *pCFD3* (Port et al., 2014) and inserted at the *attP40* genomic site via PhiC31-based integration. Transgenic gRNA males were crossed to *nanos-cas9* females, and the resulting founder males were then crossed to *TM3*-bearing females for recovery of mutations. Induced alleles were identified by sequencing PCR products amplified from candidate flies.

Immunohistochemistry and Immunoblotting

Primary antibodies were: mouse anti-β-galactosidase (LacZ) 1:100 (Promega), mouse anti-dpERK 1:100 (Sigma), rabbit anti-GFP 1:1,000 (Abcam), mouse anti-V5 1:1,000 (Sigma), rabbit anti-Flag 1:1,000 (Sigma), rabbit anti-HA 1:1,000 (Sigma), guinea pig anti-Cic 1:100 (gift from Iswar Hariharan, University of California, Berkeley), rabbit anti-DCAF7 1:100 (Novus Biologicals), rabbit anti-tRFP 1:1000 (Evrogen), mouse anti-Mira 1:100 (gift from Alex Gould), mouse anti-Ecad 1:50 (Developmental Studies Hybridoma Bank), mouse anti-Engrailed 1:5 (Developmental Studies Hybridoma Bank). Secondary antibodies used were: Alexa Donkey anti Rabbit-647 (Life Technologies),

Alexa Donkey anti-Mouse 488 (Abcam), Alexa Donkey anti-Rabbit 555 (Life Technologies), IRDye 800CW Donkey anti-Rabbit IgG (LI-COR), IRDye 680CW Donkey anti-Guinea pig IgG (LI-COR), IRDye 680CW Donkey anti-Mouse IgG (LI-COR). Dissected imaginal discs were stained as in (Degoutin et al., 2013). Stained tissues were mounted with Prolong Gold anti-fade mounting reagent with DAPI (Life Technologies), and images were acquired with Zeiss LSM 510 or Zeiss LSM 880 confocal microscopes. Tissues from the *Mnb-tRFP, Wap-Venus, Cic-Venus* stocks were mounted in 90 percent glycerol and images were acquired with the Nikon C2 confocal microscope and processed in Fiji.

Quantification of Wing and Brain Size

Wing area from 20 flies was quantified using Adobe Photoshop. For quantification of brain size, flies were raised at 18°C. Brains from 8 ten-days old female flies were dissected in cold 1x PBS, fixed with 4% formaldehyde/PBS and stained with Alexa Fluor 594 Phalloidin (Life Technologies) overnight. Stained brains were mounted with Prolong Gold anti-fade mounting reagent with DAPI (Life Technologies). Brain volume measurements were done from 3D reconstructions of 2.5 µm-spaced confocal Z-stacks acquired with a Zeiss LSM 880 or Leica SP5 confocal microscopes, using a 3D Viewer plugin in Fiji or Volocity software. Significance was calculated with a Student's *t*-test. In all figures, the following indications are used: * $p<0.05$, ** $p<0.01$, *** $p<0.001$.

Expression Plasmids and Cell Culture

For establishing a stable S2 cell line, full-length Cic open reading frame was tagged with streptavidin binding peptide (SBP) at the C terminus and cloned into pMK33 vector (Kyriakakis et al., 2008). Full-length open reading frame and fragments of Cic were cloned into pMT/V5-His A vector (Invitrogen). Full-length Wap was tagged with the Flag tag and cloned into the pMT vector. pMT-Mnb-HA and pMT-MnbKR-HA plasmids were from (Degoutin et al., 2013). The pGL2-CUASC-Luc ("*CUASC-Luc*") reporter was generated by PCR amplification of the promoter regions of pC4PLZ-CUASC vector (Ajuria et al., 2011) with primers CUASC-XhoI-UP1 (5'-ATCGCTCGAGGAATTCCCAGTTTATG-3') and CUASC-XhoI- DN1 (5'-GCTACTCGAGTTATCACCCACGGCTCTGCTC-3'), which was subcloned into pGL2 basic (Promega). Full-length GAL4 was cloned into pMT/V5-His A vector (Invitrogen) to generate pMT-GAL4. pIE4-lacZ was described previously (Frolov et al., 2001). *Drosophila* S2 cells were maintained in standard Schneider's S2 medium with fetal bovine serum (Gibco) at 25°C, and transfections were performed using Effectene transfection reagent (Qiagen). In some instances, cells were treated with 30 μg dsRNA specific for *wap*, *mnb* or *rl* (ERK) for 96 h. After 96 h, cells were transfected with indicated plasmids. $CuSO_4$ was added to culture media at a final concentration of 0.35 mM for inducing expression. Cells were lysed using Default Lysis Buffer (DLB) (50 mM Tris pH 7.5, 125 mM NaCl, 5% glycerol, 0.2% IGEPAL, 1.5 mM $MgCl_2$, 1 mM DTT, 25 mM NaF, 1mM Na_3VO_4, 1mM EDTA and 2x Complete protease inhibitor, Roche). Clear cell lysates were incubated with anti-V5 beads (Sigma), streptavidin beads (Pierce), GFP-

Trap or RFP-Trap resin (ChromoTek) for 2 hrs at 4°C. Beads were washed three times with lysis buffer, and protein complexes were eluted with SDS buffer. To visualize differences in Cic1 mobility, 6% Tris-Glycine gels were used with 50 μM Phos-tag™ (Wako Laboratory Chemicals) and 100 μM $MnCl_2$.

Luciferase Reporter Assays

S2 Cells were co-transfected with the luciferase reporter vector pGL2-CUASC-Luc and with the effector plasmids. pIE4-LacZ was used to normalize transfection efficiencies. Each transfection point was assayed in triplicate, and each experiment was repeated three times. Luciferase and β-galactosidase activities were measured in S2 cell lysates by Luc-Screen® Extended-Glow Luciferase Reporter Gene Assay System (Thermo Fisher) and Galacto-Star™ One-Step beta-Galactosidase Reporter Gene Assay System (Thermo Fisher), respectively. Luminescence signals were acquired on POLARstar Omega multifunction microplate reader (BMG Labtech).

Mass Spectrometry

Cic-interacting proteins were purified from *Drosophila* S2 cells (Cic-SBP) essentially as described in (Kyriakakis et al., 2008), using a modified single-step procedure for SBP-tagged Cic. For expression in S2 cells, pMK33-Cic-SBP construct was transfected using Effectene transfection reagent (Qiagen), and stable cell lines were selected in the presence of 300 μg/mL hygromycin (Sigma). Cic-SBP purifications were performed in 2 biological replicates. To analyze Cic complexes in vivo, 0-16 hr Cic-Venus embryos were collected and the proteins were extracted and purified on GFP-Trap

resin (ChromoTek) as described in (Neumuller et al., 2012). The Cic-Venus construct uses genomic regulatory sequences of the *cic* gene and therefore expresses the Cic-Venus protein at endogenous levels (Grimm et al., 2012). Functionality of this construct was previously confirmed in a rescue assay (Grimm et al., 2012). Cic-Venus purifications were performed in 3 biological replicates. Protein complexes were analyzed by nanoLC-MS/MS as described in (Kyriakakis et al., 2008) at the Taplin Mass Spectrometry Facility at Harvard Medical School. Identified Cic-interacting proteins were analyzed by the SAINT program (Choi et al., 2011). A complete mass spectrometry dataset is shown in Table S1. Interactions with SAINT scores >0.8 were considered significant.

To identify Cic residues that are phosphorylated by Mnb, Cic1-V5 and Wap-Flag were coexpressed in S2 cells either with Mnb-HA or MnbKR-HA, Cic1-V5 was purified on anti-V5 agarose resin, and its phosphorylation was analyzed by nanoLC-MS/MS.

CHAPTER 3

CONCLUSION

The work presented in this dissertation aimed to identify novel regulators that control developmental processes through a critical node, Cic, in a signaling network. This work started with addressing an open question: What are the Cic-interacting proteins? Current proteomic studies of signaling interactomes are limited to cultured cells (Friedman et al., 2011; Kwon et al., 2013). My research used affinity purification-mass spectrometry (AP-MS) to study the Cic interactome in both S2 cells and the developing *Drosophila* embryos. This unbiased approach provided a comprehensive understanding of Cic signaling at a systems level *in vivo*.

I identified the Minibrain kinase (Mnb) and the adaptor protein, Wings apart (Wap), as novel Cic-interacting proteins. Furthermore, I employed various molecular biology tools, including co-immunoprecipitation (CoIP), RNA interference (RNAi), mutagenesis, *in vitro* kinase assay, mass spectrometry (MS), to characterize the interactions between Cic, Wap, and Mnb, and phosphorylation of Cic by Mnb. I found that Mnb interacts with Cic via amino-terminal third of Cic protein, which is distinct from the interaction between ERK and Cic. In addition, I showed that Mnb and ERK

target different regions of Cic protein for phosphorylation. I discovered 4 Mnb-dependent phosphorylation residues (S41, S49, T89, and S91) in the amino-terminal region of Cic. The functional importance of these residues was confirmed in luciferase and in vivo assays.

This study also investigated the consequences of Mnb-mediated phosphorylation of Cic. By using reporter assays, I showed that Mnb inhibits Cic transcriptional repressor activity in *Drosophila* wing imaginal discs and in S2 cells. Alanine substitution of the 4 putative Mnb phosphorylation residues (S41, S49, T89, and S91) resulted in a form of Cic that was resistant to the inhibition by Mnb, suggesting that Mnb and Wap reduce Cic repressor activity via Mnb-mediated phosphorylation of these residues. One question still unanswered is how Mnb-mediated phosphorylation of Cic reduces Cic activity. Answering this question would elucidate how Mnb downregulates Cic.

In this study, I investigated the effects of Mnb on Cic in multiple developmental contexts. Most notably, the downregulation of Cic by Mnb is required for the proper growth of several organs, such as the wings, eyes, and the brain. In addition, I discovered that the downregulation of Cic by Mnb is required for proper tissue patterning. Finally, I showed that Mnb functions additively with ERK to regulate Cic. Altogether, I uncovered a previously unknown mechanism of Cic regulation which acts in parallel to other signaling pathways.

APPENDIX

SINGLE-STEP AFFINITY PURIFICATION OF ERK SIGNALING COMPLEXES USING THE STREPTAVIN-BINDING PEPTIDE (SBP) TAG

This section was adapted from Yang, L. and Veraksa, A. (2016) Single-step affinity purification of ERK signaling complexes using the streptavidin-binding peptide (SBP) tag. *Methods in Molecular Biology* (in press)

Summary

Elucidation of biological functions of signaling proteins is facilitated by studying their protein-protein interaction networks. Affinity purification combined with mass spectrometry (AP-MS) has become a favorite method to study protein complexes. Here I describe a procedure for single-step purification of ERK (Rolled) and associated proteins from *Drosophila* cultured cells. The use of the streptavidin-binding peptide (SBP) tag allows for a highly efficient isolation of native ERK signaling complexes, which are suitable for subsequent analysis by mass spectrometry. Our analysis of the ERK interactome has identified both known and novel signaling components. This method can be easily adapted for SBP-based purification of protein complexes in any expression system.

1. Introduction

Receptor tyrosine kinase (RTK)/extracellular signal-regulated kinase (ERK) signaling controls many cellular processes, including proliferation, differentiation, and apoptosis (Futran et al., 2015; Lemmon and Schlessinger, 2010). Dysregulation of this pathway has been implicated in multiple human diseases, including cancer (Jindal et al., 2015; Lemmon and Schlessinger, 2010; Newbern et al., 2008; Rauen, 2013; Rauen et al., 2011; Tidyman and Rauen, 2009). The development of relevant therapies depends on the knowledge of the structure and dynamics of the ERK signaling network. Genetic analysis of the RTK/ERK pathway in *Drosophila* and other model systems identified its key components, and subsequent biochemical studies revealed key protein-protein associations, such as those involving the core Raf-MEKERK kinase cascade, as well as scaffolding and adaptor proteins (Li, 2005; Shilo, 2014; Sopko and Perrimon, 2013). However emerging evidence suggests that the ERK signaling network is complex and includes dozens of substrates and additional regulatory molecules (Friedman et al., 2011; von Kriegsheim et al., 2009). Affinity purification of protein complexes followed by mass spectrometry-based identification of interacting components has emerged as a powerful method to study signaling networks (Gavin et al., 2011; Veraksa, 2013). Previously our lab applied tandem affinity (TAP) purification to isolate signaling complexes in *Drosophila*, first using the original TAP tag (Rigaut et al., 1999; Veraksa et al., 2005), and more recently using an improved version, the GS-TAP tag (Burckstummer et al., 2006; Kyriakakis et al., 2008). Both of these methods are rather lengthy, as they require two affinity binding steps separated by tobacco etch virus (TEV) protease

cleavage after the first affinity column. Due to inevitable sample loss at every step, they require a large amount of starting material. In order to overcome these limitations, I have developed and present here an efficient single-step purification approach for isolating signaling complexes from *Drosophila* cultured cells, based on the use of streptavidin-binding peptide (SBP). SBP is a 38-amino acid peptide that was artificially selected for high-affinity binding to native streptavidin (Keefe et al., 2001). Compared to other affinity purification methods, the SBP tag offers several advantages. First, the SBP tag is relatively compact and therefore less likely to impair protein function (4 kDa vs. 20 kDa for the TAP or GS-TAP tags). Second, SBP interacts with native streptavidin with high affinity (K_d = 2.5 nM), which results in an efficient association of the tagged protein with the matrix (Keefe et al., 2001). Third, the SBP tag works well when placed either at the amino or carboxy terminus of the protein, or even in the middle. Fourth, SBP-tagged proteins can be eluted with a heterologous compound, biotin, which results in a lower carryover of contaminants compared to other elution methods, such as competition with excess tag peptide. Fifth, streptavidin matrices are less costly than many other affinity resins.

Finally, single-step purification is faster and less labor-intensive than TAP. These properties make SBP tagging an attractive option for affinity purification studies. Usability of this approach has been validated in our studies involving various signaling proteins (Degoutin et al., 2013; Dent et al., 2014; Gilbert et al., 2011; Zhang et al., 2015), and this method has also been used to purify complexes from vertebrate cultured cells (Kim et al., 2010a). In this section I describe a procedure to generate *Drosophila* cultured

cells stably expressing SBP-tagged ERK, followed by purification of ERK protein complexes. The mass spectrometry step is not presented, however I give suggestions for preparing samples for this analysis and for analyzing mass spectrometry data using the SAINT (significance analysis of interactome) program (Choi et al., 2011). Using this workflow, I was able to identify most of the known core components of ERK signaling, including two major ERK phosphatases. In addition, the identified list of ERK interactors includes several proteins that have not been previously associated with ERK signaling. Though the method I describe is for *Drosophila* cultured cells, it can be easily adapted for mammalian cells or any other cell culture system.

2. Materials

A tissue culture facility and a general molecular biology lab with -20°C and -80°C freezers and a 4°C cold room or a refrigeration chamber are needed for carrying out this protocol. Prepare all solutions using ultrapure (18.2 MΩ·cm) water.

2.1. Tissue culture and cell transfection materials and reagents

1. Tissue culture hood with vacuum connection. Cell transfections are performed in the hood.

2. Cell culture incubator at 25°C. Use a dish with ultrapure water at the bottom shelf to maintain humidity in the incubator.

3. Qiagen Maxiprep plasmid purification kit.

4. Qiagen Effectene transfection reagent.

5. *Drosophila* S2 cells (see Note 1).

6. Tissue culture treated sterile 6-well plates, e.g. Corning catalog number 3516.

7. Tissue culture treated vented 25 cm^2 and 75 cm^2 flasks, e.g. Corning catalog number 353109.

8. 15-mL and 50-mL Falcon tubes, sterile and regular Eppendorf tubes.

9. 250-mL and 500-mL sterile disposable filter units for preparing S2 cell media, 0.2 μm pore size.

10. Clinical centrifuge that accommodates 15-mL and 50-mL Falcon tubes, at 4°C.

11. Microcentrifuge, at 4°C.

12. Vortex mixer in or next to the tissue culture hood.

13. Gibco Schneider's *Drosophila* Medium (1x) with L-glutamine (Life Technologies catalog number 21720024). Store at 4°C.

14. Gibco Fetal Bovine Serum (FBS), heat-inactivated (Life Technologies catalog number

10082147). Aliquot by 50 mL in 50-mL Falcon tubes, store at -20°C.

15. Gibco Penicillin-Streptomycin, "Pen/Strep" (5,000 U/mL) (Life Technologies catalog number 15070063). Aliquot by 5 mL in 15-mL Falcon tubes, store at -20°C.

16. Complete S2 cell medium: in the tissue culture hood, combine in a 500-mL filter unit:

500 mL Schneider's *Drosophila* Medium, 50 mL FBS, and 5 mL Pen/Strep, filter using vacuum connection, cap and swirl to mix. Store at 4°C. Warm to room temperature before use.

17. Hygromycin, 300 mg/mL stock solution: dissolve 250 mg hygromycin (Sigma catalog number H3274) in 800 μL sterile PBS or ultrapure water, store at 4°C in the dark.

18. Complete S2 cell medium with 300 μg/mL hygromycin: co-filter 250 mL complete S2 cell medium (item 16) with 250 μL hygromycin stock solution (1:1,000 dilution). Wrap medium with hygromycin with aluminum foil to protect from light and store at 4°C for up to 1 month. A larger (500 mL) batch can be made as needed.

19. Anti-SBP antibody: Santa Cruz Biotechnology sc-101595, anti-SBP Tag (clone SB19-C4). Use 1:1000 for western blotting to check the expression of SBP-tagged proteins.

2.2. Affinity purification reagents

1. 0.07 M $CuSO_4$: dissolve 8.74 g $CuSO_4 \cdot 5H_2O$ in 500 mL water, filter-sterilize, store at room temperature.

2. 1x phosphate buffer saline (PBS). Store at 4°C.

3. 5x lysis buffer: 250 mM Tris pH 7.5, 25% glycerol, 1% IGEPAL, 7.5 mM $MgCl_2$, 625 Mm NaCl, 125 mM NaF, 5 mM Na_3VO_4. To make 200 mL: completely dissolve 1 g NaF powder and 184 mg Na_3VO_4 powder in 71 ml water with constant stirring. Add 50 mL 1

M Tris pH 7.5, 2 mL 100% IGEPAL (Sigma catalog number I8896), 1.5 mL 1 M $MgCl_2$, 25 mL 5 M NaCl, then add 50 mL glycerol (add last) and continue stirring for one hour. Filter-sterilize using 250-mL filter unit (this step can be slow). Aliquot by 10 mL in 50-mL Falcon tubes and store at -80°C.

4. 1 M dithiothreitol (DTT) solution. Store at -20°C.

5. cOmplete™ protease inhibitor cocktail tablets, with EDTA: Roche catalog number 11697498001 (20 tablets). Store at 4°C.

6. Streptavidin beads: Pierce™ Streptavidin Plus UltraLink™ Resin, Pierce catalog number 53117.

7. 10-ml Luer-Lok disposable syringes.

8. Syringe filters, 26 mm diameter, SFCA membrane, 0.45 μm pore size, e.g. Corning catalog number 431220.

9. Dry heating block at 95°C.

10. 4x SDS sample buffer: 8% SDS, 160 mM Tris pH 6.8, 30% glycerol, 1 mg/ml bromophenol blue. To make 100 mL; combine 50 mL water, 8 g SDS powder, 16 mL 1 M Tris pH 6.8, 30 mL glycerol, 100 mg bromophenol blue powder. Dissolve well with constant stirring, filter-sterilize and store at room temperature. Before use, mix 950 μL buffer with 50 μL 1 M DTT (to get 50 mM final DTT concentration), vortex to mix. Buffer with DTT is stored at -20°C.

11. 2x SDS sample buffer: mix equal volumes of 4x SDS sample buffer (with DTT) and water.

12. Rotating wheel with clamps for Falcon tubes and Eppendorf tubes, at 4°C.

13. 200 mM biotin stock solution: in the chemical hood, mix 875 µL water with 125 µL NH_4OH (ammonium hydroxide solution, 28% NH_3 in water), this will make 2 M NH_4OH solution. To this solution, add 50 mg biotin (e.g. Sigma catalog number B4501) and vortex well. Store at -20°C.

14. 2 mM biotin working solution: dilute 200 mM biotin stock solution 1:100 with lysis buffer with DTT and cOmplete™ protease inhibitor, see protocol step 3.2.2 (e.g. 990 µL lysis buffer and 10 µL of 200 mM biotin stock). Make 2 mM biotin working solution right before use and discard unused portion.

15. 100% (w/v) trichloroacetic acid (TCA) solution. To make 100% (w/v) TCA solution, combine 500 g TCA crystals with 350 mL water, mix and store at room temperature.

16. 10% (w/v) TCA solution. Dilute 100% TCA 1:10 with water. Store at 4°C.

17. Acetone at -20°C.

2.3. Reagents for silver-staining gels

1. Molecular weight marker: any unstained marker can be used, but prefer BioRad Precision Plus unstained standards. Dilute 1:10 with 2x SDS sample buffer. Store at -20°C.

2. Gel for silver staining: a regular SDS-PAGE can be used, however I find that commercial gradient gels provide a better coverage of the complete molecular weight range. I use Novex NuPAGE 4-12% Bis-Tris gels, 1.5 mm thick, with 10 wells, Life

Technologies catalog number NP0335. They require a corresponding gel apparatus, such as the XCell SureLock Mini system.

3. Electrophoresis buffer for NuPage Bis-Tris gels: MOPS SDS running buffer, with antioxidant, Life Technologies catalog number NP0001.

4. Silver staining kit: Life Technologies SilverQuest Staining Kit, catalog number LC6070.

5. Dish for silver staining.

3. Methods

3.1. Transfection and establishment of stable S2 cell lines

1. Clone your protein of interest into the pMK33-SBP-N or pMK33-SBP-C vector (Fig. 1A) (see Note 2). For this procedure, I used full-length *Drosophila* ERK (Rolled) cloned into pMK33- SBP-C. Prepare DNA for transfection using Qiagen Maxiprep protocol following manufacturer's recommendations (see Note 3).

2. Dispense 1.5 mL per well of complete S2 cell medium in a 6-well plate. Add 0.5 mL of *Drosophila* S2 cells from dense cultures (4-5 days). Incubate at 25°C overnight (optional) or at least 3 hours to allow cell attachment to the bottom of the well.

3. Use Qiagen Effectene transfection reagent to prepare DNA for transfection into cells (see Note 4). Perform all transfection steps in the hood. Mix in a sterile Eppendorf tube: 150 µL buffer EC, 2 µg DNA, 16 µL Enhancer, and vortex for 5 sec. Incubate at room

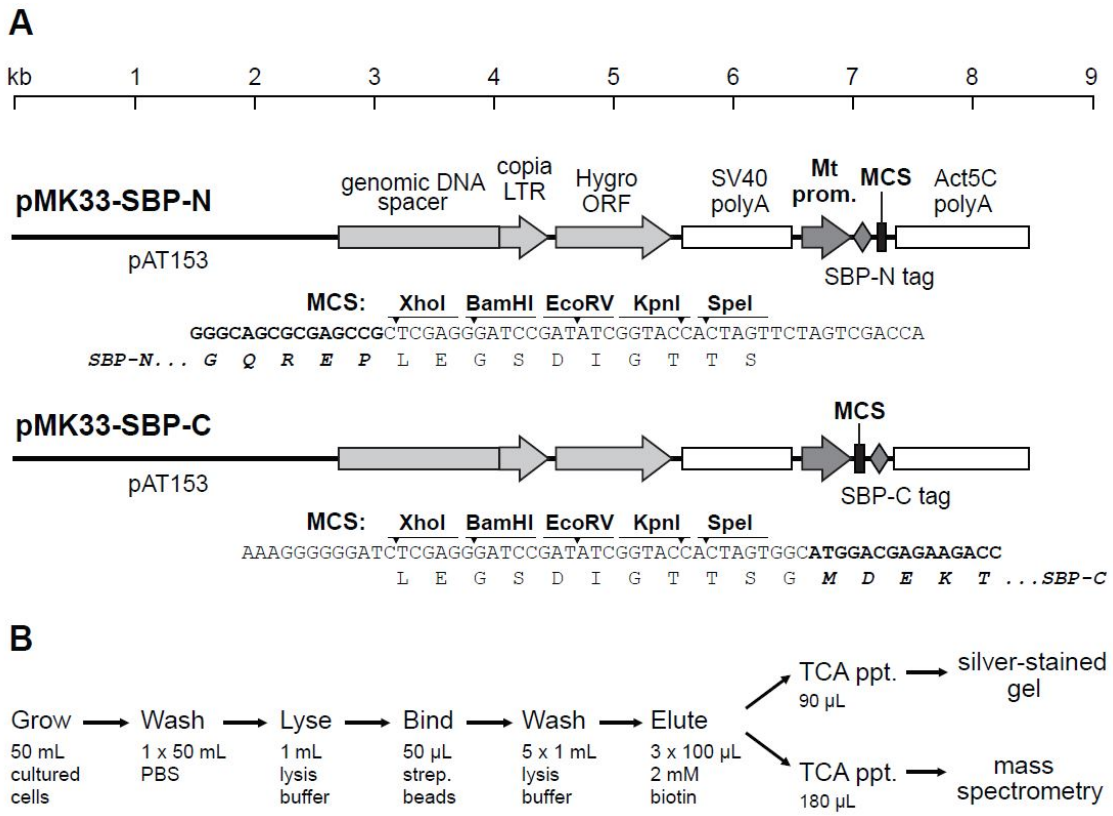

Figure 1 Diagram of the pMK33-SBP vectors and workflow for single-step SBP-based purification. (A) Diagram of the pMK33-SBP vectors. Mt prom.: metallothionein promoter for $CuSO_4$-inducible expression; MCS: multiple cloning site (polylinker). Unique cloning sites in the MCS are shown in bold and underlined. (B) Workflow for single-step SBP-based purification, as described in the protocol.

temperature for 5 min, briefly spin down. Add 21 μL Effectene reagent, immediately vortex for exactly 10 sec, do not spin down. Incubate at room temperature for 15 min.

4. Remove old medium from cells using 1-mL tip. Add 1 mL of fresh complete medium to cells, then add 1 mL of fresh complete medium to the tube with DNA from step 3, gently but thoroughly pipet up and down 4-5 times, add DNA/medium solution dropwise to cells, swirl to mix. Total volume will be 2 mL per well. Incubate plates with transfected cells for 48 hours at 25°C.

5. Resuspend cells in the well, transfer to 15-mL Falcon tube, spin down for 3 min at 500 *g* in a clinical centrifuge, resuspend in 10 mL of complete medium with 300 μg/mL hygromycin, and seed the cells in a 25 cm^2 vented flask.

6. Carry out selection of stable cell lines. Watch the number of cells in the flasks and allow them to reach good density before splitting. During the first 2-3 weeks, significant cell death will be visible, and splitting can be done more rarely and retaining a higher volume of cells (e.g. 1:1 split once a week instead of a normal 1:5 split every 4-5 days). Medium should contain hygromycin during all passages. Cells in a control well (e.g. transfected with actin-GFP) will completely die out after 3-4 weeks, and cells in the experimental well should grow normally after about a month of continuous selection (see Note 5).

3.2. Cell lysis and affinity purification

A general workflow for affinity purification steps is shown in Fig. 1B. Unless indicated otherwise, all cell collection, lysis and affinity purification steps should be performed on ice (see Note 6).

1. Amplify cells in two 75 cm^2 vented flasks, 25 mL in each flask, for a total of 50 mL (see Note 7). Use untransfected S2 cells grown in parallel as a negative control sample for purifications, and follow all of the same steps with that sample. Allow the cells to grow to medium-high density (3-4 days) and induce overnight with 0.07 mM $CuSO_4$ by adding 25 μL of 0.07 M $CuSO_4$ stock solution to 25 mL of cells in a flask (1:1000 dilution). Mix well by swirling and rocking the flask (see Note 8).

2. Prepare lysis buffer: add 40 mL water to 10 mL of 5x concentrated lysis buffer (stored at - 80°C) in a 50-mL Falcon tube. Add 50 μL of 1 M DTT to a final concentration of 1 mM, mix well and separate into two 50-mL Falcon tubes, 25 mL in each. To one of the tubes, add one cOmplete™ protease inhibitor tablet and rotate at 4°C for 30 min (see note 9). At the end, check to make sure the cOmplete™ tablet has fully dissolved. The second tube can be stored at -80°C and will only require addition of the cOmplete™ tablet before the next experiment. 25 mL of lysis buffer is sufficient for up to 4 purification samples.

3. While cOmplete™ tablet is dissolving, resuspend cells in flasks with a 10-mL pipette and collect into a 50 mL Falcon tube on ice.

4. Spin in a clinical centrifuge at 500 g for 3 minutes at 4°C.

5. Remove supernatant by aspiration and wash cells with 50 mL of cold PBS. Mix by inversion.

6. Spin in a clinical centrifuge at 500 g for 5 minutes at 4°C. Remove as much supernatant as possible.

7. Lysis: add 1 mL of cold lysis buffer with cOmplete™ protease inhibitor (from step 2) to cells and pipet up and down 4-5 times to lyse the cells. For more efficient lysis, press the tip against the bottom of the tube to create shearing force. Transfer lysate to a chilled Eppendorf tube and incubate on ice for 15-20 minutes.

8. Prepare streptavidin beads, aiming for 50 µL of packed beads per sample. Take the appropriate amount of 50% bead slurry and add to an Eppendorf tube. Wash beads three times with 1 mL of lysis buffer (see step 2), mixing by inversion. After each wash, centrifuge the tube for 1 min at 500 g at 4 °C. After the last wash, remove supernatant, leaving the volume that is equal to the volume of packed beads (to obtain 50% slurry after subsequent mixing). Keep washed beads on ice.

9. Centrifuge cell lysates from step 7 at maximum speed (e.g. 14,000 g) at 4°C for 15 min.

10. This step is best performed in the cold room. Aspirate supernatants with 1-ml tip and load into chilled 10-ml syringes with 0.45 µm filters attached. Push all of the solution into fresh Eppendorf tubes on ice. Optional: save Before Binding (BB) analytical sample: mix 50 µL of lysate with 25 µL of 4x SDS sample buffer (see Note 10). Vortex and heat at 95°C for 5 minutes. Store at -20°C.

11. Binding: resuspend washed streptavidin beads by pipetting and add 100 µL of slurry (corresponding to 50 µL of packed beads) to each sample (see Note 11). Rotate for 2-3 hours at 4°C on a rotating wheel.

12. Remove the tubes from the rotating wheel and centrifuge at 500 g for 1 min at 4 °C.

Optional: save the Flow-through (FT) analytical sample: mix 50 µL of supernatant with 25 µL of 4x SDS sample buffer. Vortex and heat at 95°C for 5 minutes. Store at -20 °C. Aspirate and discard the rest of the supernatants, keeping the bead pellets.

13. Washes: add 1 mL of lysis buffer (see step 2) to the beads, mix by inversion 4-5 times and spin down at 500 g for 1 min at 4°C. Aspirate and discard the supernatant.

14. Repeat step 13 four more times for a total of 5 washes. After the last wash, take care to remove as much supernatant as possible, without dislodging the beads.

15. Elution: prepare 2 mM biotin working solution, 300 µL per sample, right before use, by diluting 200 mM biotin stock solution 1:10 with lysis buffer. Resuspend bead samples in 100 µL of 2 mM biotin working solution. Use a pipet tip with a large orifice to resuspend the beads gently but completely by pipetting. Incubate on ice for 5 min. Centrifuge at 500 g for 1 min at 4°C. Carefully collect 100 µL of supernatant, avoiding the beads, and place in a new Eppendorf tube on ice.

16. Repeat step 15 two more times, each time adding 100 µL of the supernatant to the same Eppendorf tube on ice, for a total of 300 µL of eluate after 3 elution steps. Optional: collect the Retentate (RT) sample: place the tubes with the beads into a rack at room temperature and let stand for 2 min. Add 50 µL of 4x SDS sample buffer to the beads,

mix by swirling with a tip without pipetting, heat at 95 °C for 5 min and store at -20°C (see Note 12).

17. Spin down pooled eluate at full speed for 30 sec at 4°C and transfer supernatant into a fresh Eppendorf tube, avoiding any beads that may remain at the bottom. Optional: collect the Eluate (EL) sample: combine 10 µL of eluate with 10 µL of 4x SDS sample buffer. Mix by flicking, heat at 95 °C for 5 min and store at -20°C.

18. TCA precipitation: the final eluate will be divided into two unequal parts to prepare samples for mass spectrometry and silver-stained gel analysis (see Fig. 1B). For the mass spectrometry sample, combine 180 µL of eluate with 20 µL of 100% TCA in a fresh Eppendorf tube labeled "MS." For the silver-stained gel sample, combine 90 µL of eluate with 10 µL of 100% TCA in a fresh Eppendorf tube labeled "SSG." Mix well and incubate on ice for 1 hr.

19. Centrifuge samples at maximum speed for 15 min at 4°C.

20. TCA wash: remove supernatant, add 500 µL of 10% TCA, mix by inversion, and centrifuge samples at maximum speed for 15 min at 4°C.

21. Acetone washes: remove TCA wash and add 500 µL of cold acetone. Mix by inversion. Centrifuge samples at maximum speed for 5 min at 4°C.

22. Remove supernatant and repeat acetone washes (step 21) three more times for a total of 4 washes. After the last wash, remove supernatant as completely as possible and allow the pellets to dry overnight in open tubes at room temperature. Loosely cover the rack

with the tubes with aluminum foil to prevent dust from falling into tubes. Store dried samples at -20°C until ready to analyze by gel electrophoresis.

3.3. Silver-stained gel

1. Prepare samples for analysis on a silver-stained gel. To the SSG dried pellet from step 3.2.18, add 20 μL of 2x SDS sample buffer and let stand at room temperature for 15 min, flicking the tube periodically. Heat at 95°C for 5 min.

2. Run the samples using your choice of SDS-PAGE setup. I have successfully used Novex NuPAGE 4-12% Bis-Tris gradient gels run with MOPS running buffer, as they offer excellent separation of most molecular weights. Other brands can be used for this purpose.

3. After the dye front reaches the bottom of the gel, open the cassette and place the gel in a staining dish. Perform silver staining of the gel using the SilverQuest Staining Kit following the Basic Staining Protocol, per manufacturer's instructions.

4. Capture the image of the stained gel using a scanner or another imaging device. An example of a silver-stained gel after ERK-SBP purification is shown in Fig. 2A (see Note 13).

3.4. Suggestions for preparation of samples for mass spectrometry and analysis of interacting proteins

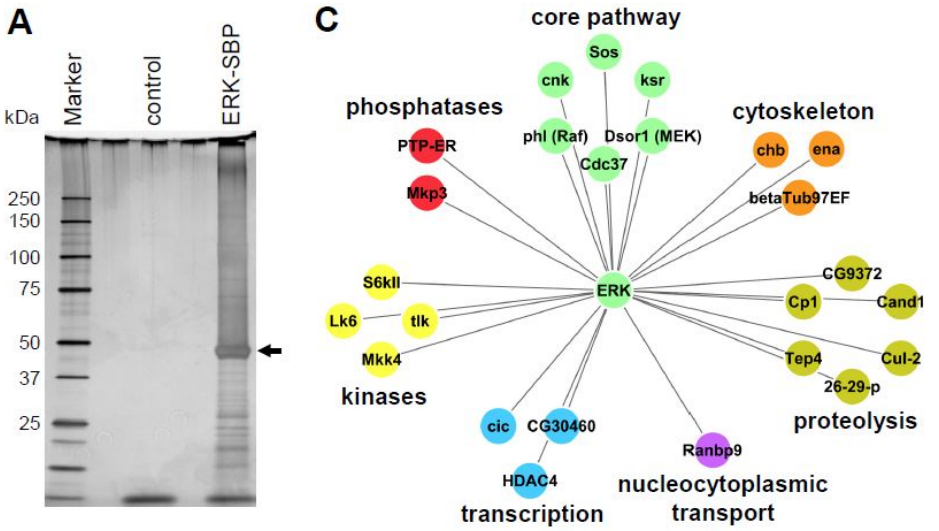

B

	A	B	C	D	E	F	G	H	I	J	K	L
1	Bait	Prey	PreyGene	IP	Spec	SpecSum	NumRep	Prob	iProb	ctrlCounts	AvgP	MaxP
2	ERKWT	FBgn0003256	rl (ERK)	ERKWT1|ERKWT2	51|46	97	2	1	1.00|1.00	3|0|0|0|0	1	1
3	ERKWT	FBgn0041180	Tep4	ERKWT1|ERKWT2	40|32	72	2	1	1.00|1.00	2|1|0|0|0	1	1
4	ERKWT	FBgn0260748	CG5004	ERKWT1|ERKWT2	46|34	80	2	1	1.00|1.00	0|0|0|0|0	1	1
5	ERKWT	FBgn0001225	Hsp26	ERKWT1|ERKWT2	7|7	14	2	1	1.00|1.00	0|0|0|0|0	1	1
6	ERKWT	FBgn0262582	cic	ERKWT1|ERKWT2	8|7	15	2	1	1.00|1.00	0|0|0|0|0	1	1
7	ERKWT	FBgn0016081	fry	ERKWT1|ERKWT2	75|21	96	2	1	1.00|1.00	0|0|0|0|0	1	1
8	ERKWT	FBgn0016641	PTP-ER	ERKWT1|ERKWT2	53|50	103	2	1	1.00|1.00	0|0|0|0|0	1	1
9	ERKWT	FBgn0017581	Lk6	ERKWT1|ERKWT2	48|44	92	2	1	1.00|1.00	0|0|0|0|0	1	1
10	ERKWT	FBgn0262866	S6kII	ERKWT1|ERKWT2	38|27	65	2	1	1.00|1.00	0|0|0|0|0	1	1
11	ERKWT	FBgn0036844	Mkp3	ERKWT1|ERKWT2	16|8	24	2	1	1.00|1.00	0|0|0|0|0	1	1
12	ERKWT	FBgn0013275	Hsp70Aa	ERKWT1|ERKWT2	15|9	24	2	1	1.00|1.00	4|1|1|0|0	0.9995	1
13	ERKWT	FBgn0000578	ena	ERKWT1|ERKWT2	6|3	9	2	1	1.00|1.00	0|0|0|0|0	0.9965	0.997
14	ERKWT	FBgn0250848	26-29-p	ERKWT1|ERKWT2	3|3	6	2	0.99	0.99|0.99	0|0|0|0|0	0.993	0.994
15	ERKWT	FBgn0013770	Cp1	ERKWT1|ERKWT2	5|3	8	2	0.99	1.00|0.98	1|0|0|0|0	0.9895	0.998
16	ERKWT	FBgn0052016	CG32016	ERKWT1|ERKWT2	4|38	42	2	0.98	0.96|1.00	0|0|0|0|0	0.9825	1
17	ERKWT	FBgn0001226	Hsp27	ERKWT1|ERKWT2	3|3	6	2	0.98	0.98|0.98	0|0|0|0|0	0.979	0.981
18	ERKWT	FBgn0003079	phl	ERKWT1|ERKWT2	6|2	8	2	0.97	0.99|0.95	0|0|0|0|0	0.972	0.993

Figure 2. Results of ERK-SBP purification from *Drosophila* S2 cells. (A) Silver-stained gel showing a typical result from SBP-based purifications. Arrow indicates position of the bait ERK-SBP protein. (B) Top portion of SAINT output. Proteins are sorted according to the average probability of interaction, AvgP (column K). (C) The ERK protein interactome in *Drosophila* S2 cells. The proteins shown were identified with the SAINT score of >0.6, and were grouped into functional classes.

After obtaining the final dried pellets of purified protein complexes, samples can be analyzed by a variety of methods, including mass spectrometry (MS). Generally, the user is advised to follow recommendations of their mass spectrometry facility of choice. Dried pellets can be used directly for trypsin digestion and liquid chromatography tandem mass spectrometry (nanoLC-MS/MS) analysis. In that case, care should be taken to purify the peptides away from biotin and detergent. I found that separating the samples on a short SDS-PAGE gel prior to submission for MS analysis improves protein identification. The dye front is allowed to migrate in the separating gel up to a distance of 1 cm, then the gel is stained using a standard Coomassie dye/methanol/acetic acid procedure, destained with 25% methanol/5% acetic acid and extensively washed in water, after which the lane is cut into two square 5 mm x 5 mm pieces which are submitted for MS analysis.

MS results can be analyzed in various ways. When applied to studying protein-protein interactions, often a goal is to identify genuine interacting components and eliminate contaminants. I found that one reliable and unbiased way to do it is using the program SAINT (significance analysis of interactome) (Choi et al., 2011). Our lab and others have validated SAINT in studies of various signaling complexes (Dent et al., 2014; Kwon et al., 2013). The user is advised to follow the procedure described in the original SAINT publication (Choi et al., 2011). I use the number of unique peptides identified for each protein in a given purification dataset as input values, and run SAINT using defaults. The most reliable results are obtained when two or more experimental purifications are compared to two or more controls, preferably (but not critically) run in

parallel with experimental samples. A higher number of controls further increases the reliability of identifying genuine interactions.

Using this approach, I analyzed data from two independent ERK-SBP purifications from *Drosophila* S2 cells and compared them to 5 control samples obtained from untransfected S2 cells. The top portion of the SAINT output for these experiments is shown in Fig. 2B. A key value to consider for evaluating protein interactions returned by SAINT is AvgP, which is an average probability of interaction for every identified protein (Fig. 2B). AvgP values above 0.8 are considered significant (Choi et al., 2011), however relevant proteins may be identified even with lower values. Using SAINT cutoff of 0.6, I was able to identify most of the known components of ERK signaling in our studies (such as the core kinases Phl (Raf) and Dsor1 (MEK) (6), scaffolds and adaptors Sos, Ksr, and Cnk (5), phosphatases Mkp3 and PTP-ER (Rintelen et al., 2003), and a transcriptional repressor Cic (Jimenez et al., 2012), as well as several novel putative ERK interactors (Fig. 2C).

4. Notes

1. There are different "flavors" of S2 cells grown in various laboratories. Our lab obtained our S2 cells from Dr. S. Artavanis-Tsakonas (Harvard medical school). Once a given line is selected for work, it should be consistently used for both control and experimental samples.

2. Our lab has developed these vectors based on our previously published pMK33-NTAP (GS) and pMK33-CTAP (SG) vectors *(15)*. pMK33-based vectors allow for inducible

expression of a gene of interest using induction with $CuSO_4$, and facilitate establishment of stable cell lines using hygromycin selection, because hygromycin resistance gene is carried in the same construct. These vectors are medium-copy plasmids.

3. I have found that a final phenol/chloroform extraction of plasmid DNA after Qiagen Maxiprep followed by precipitation with sodium acetate/ethanol further improves transfection efficiency.

4. Qiagen Effectene transfection reagent does not require incubation of either cells or DNA in serum-free media. It is always good to include a separate transfection control performed in parallel to the main experiment, e.g. a plasmid encoding actin-GFP. This way general success of transfection can be verified by assessing the number of GFP-positive cells in a small aliquot from that well, and also the same well can be used to verify successful selection using hygromycin, as control cells that do not have the pMK33 plasmid should all die during selection.

5. After establishment of a stable cell line, expression of the tagged protein can be verified after an overnight induction with 0.35 mM $CuSO_4$ followed by cell lysis and western blotting using anti-SBP antibody.

6. For holding Eppendorf tubes during the washes and solution changes, I use an aluminum block that is embedded in ice (e.g. from a dry bath). This makes it convenient to perform tube inversions by removing the whole block with the tubes, rather than doing it one by one for each tube, and keeps the samples at 0°C at all times. Care should be taken to make sure that the ice is well packed around the block and there is little water in the ice bucket, otherwise the block may sink.

7. While hygromycin-containing medium should be used for maintaining the main cell line at all times, hygromycin can be omitted from the medium for final cell amplification step, which can reduce the cost.

8. This concentration of $CuSO_4$ will result in a medium level of protein induction. This is recommended to avoid possible artefacts resulting from extreme overexpression of the tagged protein.

9. I am using 2x recommended concentration of cOmplete™ protease inhibitor for a stronger inhibition of proteases. Remaining buffer with cOmplete™ protease inhibitor can be stored in 1- mL single-use aliquots at -80°C.

10. Analytical samples can be collected throughout the procedure where indicated. These fractions can be analyzed by western blotting with anti-SBP antibody using approximately 10 µL from each of the collected samples.

11. Cut off the tip to obtain a larger orifice for bead resuspension.

12. The Retentate (RT) sample may contain a lot of protein, so further dilution (e.g. 1:5 with 2x SDS buffer) is recommended for western blot analysis.

13. Silver staining is used for a sensitive quality assessment of the sample. Some proteins may be visible in a control sample from untransfected S2 cells. The major band in the experimental lane will be the SBP-tagged bait protein, which should migrate at the expected molecular weight (taking into account 4 kDa added by the SBP tag). Additional bands of interacting proteins should be visible in the experimental lane.

REFERENCES

Ajuria, L., Nieva, C., Winkler, C., Kuo, D., Samper, N., José Andreu, M., Helman, A., González-Crespo, S., Paroush, Z., Courey, A.J*., et al.* (2011). Capicua DNA binding sites are general response elements for RTK signaling in Drosophila. Development *138*, 915-924.

Alentorn, A., Sanson, M., and Idbaih, A. (2012). Oligodendrogliomas: new insights from the genetics and perspectives. Curr Opin Oncol *24*, 687-693.

Altafaj, X., Dierssen, M., Baamonde, C., Marti, E., Visa, J., Guimera, J., Oset, M., Gonzalez, J.R., Florez, J., Fillat, C*., et al.* (2001). Neurodevelopmental delay, motor abnormalities and cognitive deficits in transgenic mice overexpressing Dyrk1A (minibrain), a murine model of Down's syndrome. Hum Mol Genet *10*, 1915-1923.

Altafaj, X., Martin, E.D., Ortiz-Abalia, J., Valderrama, A., Lao-Peregrin, C., Dierssen, M., and Fillat, C. (2013). Normalization of Dyrk1A expression by AAV2/1-shDyrk1A attenuates hippocampal-dependent defects in the Ts65Dn mouse model of Down syndrome. Neurobiol Dis *52*, 117-127.

Alvarez, M., Altafaj, X., Aranda, S., and de la Luna, S. (2007). DYRK1A autophosphorylation on serine residue 520 modulates its kinase activity via 14-3-3 binding. Mol Biol Cell *18*, 1167-1178.

Arque, G., Fotaki, V., Fernandez, D., Martinez de Lagran, M., Arbones, M.L., and Dierssen, M. (2008). Impaired spatial learning strategies and novel object recognition in mice haploinsufficient for the dual specificity tyrosine-regulated kinase-1A (Dyrk1A). PLoS One *3*, e2575.

Arvand, A., and Denny, C.T. (2001). Biology of EWS/ETS fusions in Ewing's family tumors. Oncogene *20*, 5747-5754.

Astigarraga, S., Grossman, R., Diaz-Delfin, J., Caelles, C., Paroush, Z., and Jimenez, G. (2007). A MAPK docking site is critical for downregulation of Capicua by Torso and EGFR RTK signaling. Embo Journal *26*, 668-677.

Atkey, M.R., Lachance, J.F., Walczak, M., Rebello, T., and Nilson, L.A. (2006). Capicua regulates follicle cell fate in the Drosophila ovary through repression of mirror. Development *133*, 2115-2123.

Baena-Lopez, L.A., Rodriguez, I., and Baonza, A. (2008). The tumor suppressor genes dachsous and fat modulate different signalling pathways by regulating dally and dally-like. Proc Natl Acad Sci U S A *105*, 9645-9650.

Bain, J., McLauchlan, H., Elliott, M., and Cohen, P. (2003). The specificities of protein kinase inhibitors: an update. Biochem J *371*, 199-204.

Baumgartner, R., Poernbacher, I., Buser, N., Hafen, E., and Stocker, H. (2010). The WW domain protein Kibra acts upstream of Hippo in Drosophila. Dev Cell *18*, 309-316.

Becker, W., and Sippl, W. (2011). Activation, regulation, and inhibition of DYRK1A. FEBS J *278*, 246-256.

Becker, W., Soppa, U., and Tejedor, F.J. (2014). DYRK1A: a potential drug target for multiple Down syndrome neuropathologies. CNS Neurol Disord Drug Targets *13*, 26-33.

Benavides-Piccione, R., Dierssen, M., Ballesteros-Yanez, I., Martinez de Lagran, M., Arbones, M.L., Fotaki, V., DeFelipe, J., and Elston, G.N. (2005). Alterations in the phenotype of neocortical pyramidal cells in the Dyrk1A+/- mouse. Neurobiol Dis *20*, 115-122.

Bennett, F.C., and Harvey, K.F. (2006). Fat cadherin modulates organ size in Drosophila via the Salvador/Warts/Hippo signaling pathway. Curr Biol *16*, 2101-2110.

Bettegowda, C., Agrawal, N., Jiao, Y., Sausen, M., Wood, L.D., Hruban, R.H., Rodriguez, F.J., Cahill, D.P., McLendon, R., Riggins, G.*, et al.* (2011). Mutations in CIC and FUBP1 contribute to human oligodendroglioma. Science *333*, 1453-1455.

Biggs, W.H., 3rd, Zavitz, K.H., Dickson, B., van der Straten, A., Brunner, D., Hafen, E., and Zipursky, S.L. (1994). The Drosophila rolled locus encodes a MAP kinase required in the sevenless signal transduction pathway. EMBO J *13*, 1628-1635.

Blair, S.S. (2007). Wing Vein Patterning in Drosophila and the Analysis of Intercellular Signaling. Annu Rev Cell Dev Biol.

Boggiano, J.C., Vanderzalm, P.J., and Fehon, R.G. (2011). Tao-1 phosphorylates Hippo/MST kinases to regulate the Hippo-Salvador-Warts tumor suppressor pathway. Dev Cell *21*, 888-895.

Bosch, J.A., Tran, N.H., and Hariharan, I.K. (2015). CoinFLP: a system for efficient mosaic screening and for visualizing clonal boundaries in Drosophila. Development *142*, 597-606.

Branchi, I., Bichler, Z., Minghetti, L., Delabar, J.M., Malchiodi-Albedi, F., Gonzalez, M.C., Chettouh, Z., Nicolini, A., Chabert, C., Smith, D.J.*, et al.* (2004). Transgenic mouse in vivo library of human Down syndrome critical region 1: association between DYRK1A overexpression, brain development abnormalities, and cell cycle protein alteration. J Neuropathol Exp Neurol *63*, 429-440.

Brand, A.H., and Perrimon, N. (1993). Targeted gene expression as a means of altering cell fates and generating dominant phenotypes. Development *118*, 401-415.

Bronicki, L.M., Redin, C., Drunat, S., Piton, A., Lyons, M., Passemard, S., Baumann, C., Faivre, L., Thevenon, J., Riviere, J.B.*, et al.* (2015). Ten new cases further delineate the syndromic intellectual disability phenotype caused by mutations in DYRK1A. Eur J Hum Genet *23*, 1482-1487.

Brunner, D., Oellers, N., Szabad, J., Biggs, W.H., 3rd, Zipursky, S.L., and Hafen, E. (1994). A gain-of-function mutation in Drosophila MAP kinase activates multiple receptor tyrosine kinase signaling pathways. Cell *76*, 875-888.

Bryant, P.J., and Levinson, P. (1985). Intrinsic growth control in the imaginal primordia of Drosophila, and the autonomous action of a lethal mutation causing overgrowth. Dev Biol *107*, 355-363.

Bryant, P.J., and Simpson, P. (1984). Intrinsic and extrinsic control of growth in developing organs. Q Rev Biol *59*, 387-415.

Buchon, N., Broderick, N.A., Kuraishi, T., and Lemaitre, B. (2010). Drosophila EGFR pathway coordinates stem cell proliferation and gut remodeling following infection. BMC Biol *8*, 152.

Burckstummer, T., Bennett, K.L., Preradovic, A., Schutze, G., Hantschel, O., Superti-Furga, G., and Bauch, A. (2006). An efficient tandem affinity purification procedure for interaction proteomics in mammalian cells. Nat Methods *3*, 1013-1019.

Cai, Z., Tao, C., Li, H., Ladher, R., Gotoh, N., Feng, G.S., Wang, F., and Zhang, X. (2013). Deficient FGF signaling causes optic nerve dysgenesis and ocular coloboma. Development *140*, 2711-2723.

Capdevila, J., and Guerrero, I. (1994). Targeted expression of the signaling molecule decapentaplegic induces pattern duplications and growth alterations in Drosophila wings. EMBO J *13*, 4459-4468.

Carver, B.S., Tran, J., Chen, Z., Carracedo-Perez, A., Alimonti, A., Nardella, C., Gopalan, A., Scardino, P.T., Cordon-Cardo, C., Gerald, W.*, et al.* (2009). ETS rearrangements and prostate cancer initiation. Nature *457*, E1; discussion E2-3.

Chan, A.K., Pang, J.C., Chung, N.Y., Li, K.K., Poon, W.S., Chan, D.T., Shi, Z., Chen, L., Zhou, L., and Ng, H.K. (2014). Loss of CIC and FUBP1 expressions are potential markers of shorter time to recurrence in oligodendroglial tumors. Mod Pathol *27*, 332-342.

Chen, C.L., Gajewski, K.M., Hamaratoglu, F., Bossuyt, W., Sansores-Garcia, L., Tao, C., and Halder, G. (2010). The apical-basal cell polarity determinant Crumbs regulates Hippo signaling in Drosophila. Proc Natl Acad Sci U S A *107*, 15810-15815.

Cho, E., Feng, Y., Rauskolb, C., Maitra, S., Fehon, R., and Irvine, K.D. (2006). Delineation of a Fat tumor suppressor pathway. Nat Genet *38*, 1142-1150.

Choi, H., Larsen, B., Lin, Z.Y., Breitkreutz, A., Mellacheruvu, D., Fermin, D., Qin, Z.S., Tyers, M., Gingras, A.C., and Nesvizhskii, A.I. (2011). SAINT: probabilistic scoring of affinity purification-mass spectrometry data. Nat Methods *8*, 70-73.

Choi, N., Park, J., Lee, J.S., Yoe, J., Park, G.Y., Kim, E., Jeon, H., Cho, Y.M., Roh, T.Y., and Lee, Y. (2015). miR-93/miR-106b/miR-375-CIC-CRABP1: a novel regulatory axis in prostate cancer progression. Oncotarget *6*, 23533-23547.

Cinnamon, E., Gur-Wahnon, D., Helman, A., St Johnston, D., Jimenez, G., and Paroush, Z. (2004). Capicua integrates input from two maternal systems in Drosophila terminal patterning. Embo Journal *23*, 4571-4582.

Cinnamon, E., Helman, A., Ben-Haroush, S.R., Orian, A., Jiménez, G., and Paroush, Z. (2008). Multiple RTK pathways downregulate Groucho-mediated repression in Drosophila embryogenesis. Development *135*, 829-837.

Coppey, M., Boettiger, A.N., Berezhkovskii, A.M., and Shvartsman, S.Y. (2008). Nuclear trapping shapes the terminal gradient in the Drosophila embryo. Curr Biol *18*, 915-919.

Crespo-Barreto, J., Fryer, J.D., Shaw, C.A., Orr, H.T., and Zoghbi, H.Y. (2010). Partial loss of ataxin-1 function contributes to transcriptional dysregulation in spinocerebellar ataxia type 1 pathogenesis. PLoS Genet *6*, e1001021.

De la Torre, R., De Sola, S., Pons, M., Duchon, A., de Lagran, M.M., Farre, M., Fito, M., Benejam, B., Langohr, K., Rodriguez, J.*, et al.* (2014). Epigallocatechin-3-gallate, a DYRK1A inhibitor, rescues cognitive deficits in Down syndrome mouse models and in humans. Mol Nutr Food Res *58*, 278-288.

de las Heras, J.M., and Casanova, J. (2006). Spatially distinct downregulation of Capicua repression and tailless activation by the Torso RTK pathway in the Drosophila embryo. Mech Dev *123*, 481-486.

Degoutin, J.L., Milton, C.C., Yu, E., Tipping, M., Bosveld, F., Yang, L., Bellaiche, Y., Veraksa, A., and Harvey, K.F. (2013). Riquiqui and minibrain are regulators of the hippo pathway downstream of Dachsous. Nat Cell Biol *15*, 1176-1185.

Deng, H., Wang, W., Yu, J., Zheng, Y., Qing, Y., and Pan, D. (2015). Spectrin regulates Hippo signaling by modulating cortical actomyosin activity. Elife *4*, e06567.

Dent, L.G., Poon, C.L., Zhang, X., Degoutin, J.L., Tipping, M., Veraksa, A., and Harvey, K.F. (2014). The GTPase Regulatory Proteins Pix and Git Control Tissue Growth via the Hippo Pathway. Curr Biol *in press*.

Dhillon, A.S., von Kriegsheim, A., Grindlay, J., and Kolch, W. (2007). Phosphatase and feedback regulation of Raf-1 signaling. Cell Cycle *6*, 3-7.

Dierssen, M. (2013). A commentary on: Overexpression of Dyrk1A inhibits choline acetyltransferase induction by oleic acid in cellular models of Down syndrome. Exp Neurol *247*, 110-112.

Dierssen, M., and de Lagran, M.M. (2006). DYRK1A (dual-specificity tyrosine-phosphorylated and -regulated kinase 1A): a gene with dosage effect during development and neurogenesis. ScientificWorldJournal *6*, 1911-1922.

Dierssen, M., Gratacos, M., Sahun, I., Martin, M., Gallego, X., Amador-Arjona, A., Martinez de Lagran, M., Murtra, P., Marti, E., Pujana, M.A.*, et al.* (2006). Transgenic mice overexpressing the full-length neurotrophin receptor TrkC exhibit increased catecholaminergic neuron density in specific brain areas and increased anxiety-like behavior and panic reaction. Neurobiol Dis *24*, 403-418.

Dierssen, M., Herault, Y., and Estivill, X. (2009). Aneuploidy: from a physiological mechanism of variance to Down syndrome. Physiol Rev *89*, 887-920.

Dissanayake, K., Toth, R., Blakey, J., Olsson, O., Campbell, D.G., Prescott, A., and Mackintosh, C. (2011). Erk/p90RSK/14-3-3 signalling impacts on expression of PEA3 Ets transcription factors via the transcriptional repressor capicúa. Biochem J *433*, 515-525.

Duchon, A., and Herault, Y. (2016). DYRK1A, a Dosage-Sensitive Gene Involved in Neurodevelopmental Disorders, Is a Target for Drug Development in Down Syndrome. Front Behav Neurosci *10*, 104.

Fernandez-Martinez, P., Zahonero, C., and Sanchez-Gomez, P. (2015). DYRK1A: the double-edged kinase as a protagonist in cell growth and tumorigenesis. Mol Cell Oncol *2*, e970048.

Fernandez, B.G., Gaspar, P., Bras-Pereira, C., Jezowska, B., Rebelo, S.R., and Janody, F. (2011). Actin-Capping Protein and the Hippo pathway regulate F-actin and tissue growth in Drosophila. Development *138*, 2337-2346.

Ferrer, I., Barrachina, M., Puig, B., Martinez de Lagran, M., Marti, E., Avila, J., and Dierssen, M. (2005). Constitutive Dyrk1A is abnormally expressed in Alzheimer disease, Down syndrome, Pick disease, and related transgenic models. Neurobiol Dis *20*, 392-400.

Fletcher, G.C., Elbediwy, A., Khanal, I., Ribeiro, P.S., Tapon, N., and Thompson, B.J. (2015). The Spectrin cytoskeleton regulates the Hippo signalling pathway. EMBO J *34*, 940-954.

Fores, M., Ajuria, L., Samper, N., Astigarraga, S., Nieva, C., Grossman, R., Gonzalez-Crespo, S., Paroush, Z., and Jimenez, G. (2015). Origins of context-dependent gene repression by capicua. PLoS Genet *11*, e1004902.

Fotaki, V., Dierssen, M., Alcantara, S., Martinez, S., Marti, E., Casas, C., Visa, J., Soriano, E., Estivill, X., and Arbones, M.L. (2002). Dyrk1A haploinsufficiency affects viability and causes developmental delay and abnormal brain morphology in mice. Mol Cell Biol *22*, 6636-6647.

Fotaki, V., Martinez De Lagran, M., Estivill, X., Arbones, M., and Dierssen, M. (2004). Haploinsufficiency of Dyrk1A in mice leads to specific alterations in the development and regulation of motor activity. Behav Neurosci *118*, 815-821.

Freeman, M., and Gurdon, J.B. (2002). Regulatory principles of developmental signaling. Annu Rev Cell Dev Biol *18*, 515-539.

Friedman, A.A., Tucker, G., Singh, R., Yan, D., Vinayagam, A., Hu, Y., Binari, R., Hong, P., Sun, X., Porto, M.*, et al.* (2011). Proteomic and functional genomic landscape of receptor tyrosine kinase and ras to extracellular signal-regulated kinase signaling. Sci Signal *4*, rs10.

Frolov, M.V., Huen, D.S., Stevaux, O., Dimova, D., Balczarek-Strang, K., Elsdon, M., and Dyson, N.J. (2001). Functional antagonism between E2F family members. Genes Dev *15*, 2146-2160.

Fryer, J.D., Yu, P., Kang, H., Mandel-Brehm, C., Carter, A.N., Crespo-Barreto, J., Gao, Y., Flora, A., Shaw, C., Orr, H.T.*, et al.* (2011). Exercise and genetic rescue of SCA1 via the transcriptional repressor Capicua. Science *334*, 690-693.

Furriols, M., and Casanova, J. (2003). In and out of Torso RTK signalling. Embo Journal *22*, 1947-1952.

Futran, A.S., Kyin, S., Shvartsman, S.Y., and Link, A.J. (2015). Mapping the binding interface of ERK and transcriptional repressor Capicua using photocrosslinking. Proc Natl Acad Sci U S A *112*, 8590-8595.

Gabay, L., Scholz, H., Golembo, M., Klaes, A., Shilo, B.Z., and Klambt, C. (1996). EGF receptor signaling induces pointed P1 transcription and inactivates Yan protein in the Drosophila embryonic ventral ectoderm. Development *122*, 3355-3362.

Gavin, A.C., Maeda, K., and Kuhner, S. (2011). Recent advances in charting protein-protein interaction: mass spectrometry-based approaches. Curr Opin Biotechnol *22*, 42-49.

Genevet, A., Polesello, C., Blight, K., Robertson, F., Collinson, L.M., Pichaud, F., and Tapon, N. (2009). The Hippo pathway regulates apical-domain size independently of its growth-control function. J Cell Sci *122*, 2360-2370.

Genevet, A., Wehr, M.C., Brain, R., Thompson, B.J., and Tapon, N. (2010). Kibra is a regulator of the Salvador/Warts/Hippo signaling network. Dev Cell *18*, 300-308.

Gilbert, M.M., Tipping, M., Veraksa, A., and Moberg, K.H. (2011). A Screen for Conditional Growth Suppressor Genes Identifies the Drosophila Homolog of HD-PTP as a Regulator of the Oncoprotein Yorkie. Dev Cell *20*, 700-712.

Gleize, V., Alentorn, A., Connen de Kerillis, L., Labussiere, M., Nadaradjane, A.A., Mundwiller, E., Ottolenghi, C., Mangesius, S., Rahimian, A., Ducray, F.*, et al.* (2015). CIC inactivating mutations identify aggressive subset of 1p19q codeleted gliomas. Ann Neurol *78*, 355-374.

Gockler, N., Jofre, G., Papadopoulos, C., Soppa, U., Tejedor, F.J., and Becker, W. (2009). Harmine specifically inhibits protein kinase DYRK1A and interferes with neurite formation. FEBS J *276*, 6324-6337.

Goff, D.J., Nilson, L.A., and Morisato, D. (2001). Establishment of dorsal-ventral polarity of the Drosophila egg requires capicua action in ovarian follicle cells. Development *128*, 4553-4562.

Goulev, Y., Fauny, J.D., Gonzalez-Marti, B., Flagiello, D., Silber, J., and Zider, A. (2008). SCALLOPED interacts with YORKIE, the nuclear effector of the hippo tumor-suppressor pathway in Drosophila. Curr Biol *18*, 435-441.

Grimm, O., Sanchez Zini, V., Kim, Y., Casanova, J., Shvartsman, S.Y., and Wieschaus, E. (2012). Torso RTK controls Capicua degradation by changing its subcellular localization. Development *139*, 3962-3968.

Guedj, F., Pereira, P.L., Najas, S., Barallobre, M.J., Chabert, C., Souchet, B., Sebrie, C., Verney, C., Herault, Y., Arbones, M.*, et al.* (2012). DYRK1A: a master regulatory protein controlling brain growth. Neurobiol Dis *46*, 190-203.

Guimera, J., Casas, C., Pucharcos, C., Solans, A., Domenech, A., Planas, A.M., Ashley, J., Lovett, M., Estivill, X., and Pritchard, M.A. (1996). A human homologue of Drosophila minibrain (MNB) is expressed in the neuronal regions affected in Down syndrome and maps to the critical region. Hum Mol Genet *5*, 1305-1310.

Guimera, J., Pritchard, M., Nadal, M., and Estivill, X. (1997). Minibrain (MNBH) is a single copy gene mapping to human chromosome 21q22.2. Cytogenet Cell Genet *77*, 182-184.

Hamaratoglu, F., Willecke, M., Kango-Singh, M., Nolo, R., Hyun, E., Tao, C., Jafar-Nejad, H., and Halder, G. (2006). The tumour-suppressor genes NF2/Merlin and Expanded act through Hippo signalling to regulate cell proliferation and apoptosis. Nat Cell Biol *8*, 27-36.

Hammerle, B., Elizalde, C., Galceran, J., Becker, W., and Tejedor, F.J. (2003). The MNB/DYRK1A protein kinase: neurobiological functions and Down syndrome implications. J Neural Transm Suppl, 129-137.

Hariharan, I.K. (2015). Organ Size Control: Lessons from Drosophila. Dev Cell *34*, 255-265.

Hariharan, I.K., and Bilder, D. (2006). Regulation of imaginal disc growth by tumor-suppressor genes in Drosophila. Annu Rev Genet *40*, 335-361.

Harvey, K.F., Pfleger, C.M., and Hariharan, I.K. (2003). The Drosophila Mst ortholog, hippo, restricts growth and cell proliferation and promotes apoptosis. Cell *114*, 457-467.

Helms, W., Lee, H., Ammerman, M., Parks, A.L., Muskavitch, M.A., and Yedvobnick, B. (1999). Engineered truncations in the Drosophila mastermind protein disrupt Notch pathway function. Dev Biol *215*, 358-374.

Hermans, K.G., van der Korput, H.A., van Marion, R., van de Wijngaart, D.J., Ziel-van der Made, A., Dits, N.F., Boormans, J.L., van der Kwast, T.H., van Dekken, H., Bangma, C.H.*, et al.* (2008). Truncated ETV1, fused to novel tissue-specific genes, and full-length ETV1 in prostate cancer. Cancer Res *68*, 7541-7549.

Herranz, H., Hong, X., and Cohen, S.M. (2012). Mutual repression by bantam miRNA and Capicua links the EGFR/MAPK and Hippo pathways in growth control. Curr Biol *22*, 651-657.

Himpel, S., Tegge, W., Frank, R., Leder, S., Joost, H.G., and Becker, W. (2000). Specificity determinants of substrate recognition by the protein kinase DYRK1A. J Biol Chem *275*, 2431-2438.

Hollenhorst, P.C., Ferris, M.W., Hull, M.A., Chae, H., Kim, S., and Graves, B.J. (2011). Oncogenic ETS proteins mimic activated RAS/MAPK signaling in prostate cells. Genes Dev *25*, 2147-2157.

Hong, S.H., Lee, K.S., Kwak, S.J., Kim, A.K., Bai, H., Jung, M.S., Kwon, O.Y., Song, W.J., Tatar, M., and Yu, K. (2012). Minibrain/Dyrk1a regulates food intake through the Sir2-FOXO-sNPF/NPY pathway in Drosophila and mammals. PLoS Genet *8*, e1002857.

Huang, J., Wu, S., Barrera, J., Matthews, K., and Pan, D. (2005). The Hippo signaling pathway coordinately regulates cell proliferation and apoptosis by inactivating Yorkie, the Drosophila Homolog of YAP. Cell *122*, 421-434.

Irvine, K.D., and Harvey, K.F. (2015). Control of organ growth by patterning and hippo signaling in Drosophila. Cold Spring Harb Perspect Biol *7*.

Ishikawa, H.O., Takeuchi, H., Haltiwanger, R.S., and Irvine, K.D. (2008). Four-jointed is a Golgi kinase that phosphorylates a subset of cadherin domains. Science *321*, 401-404.

Jacobs, D., Beitel, G.J., Clark, S.G., Horvitz, H.R., and Kornfeld, K. (1998). Gain-of-function mutations in the Caenorhabditis elegans lin-1 ETS gene identify a C-terminal regulatory domain phosphorylated by ERK MAP kinase. Genetics *149*, 1809-1822.

Jane-Valbuena, J., Widlund, H.R., Perner, S., Johnson, L.A., Dibner, A.C., Lin, W.M., Baker, A.C., Nazarian, R.M., Vijayendran, K.G., Sellers, W.R.*, et al.* (2010). An oncogenic role for ETV1 in melanoma. Cancer Res *70*, 2075-2084.

Jiang, H., and Edgar, B.A. (2009). EGFR signaling regulates the proliferation of Drosophila adult midgut progenitors. Development *136*, 483-493.

Jiang, H., Grenley, M.O., Bravo, M.J., Blumhagen, R.Z., and Edgar, B.A. (2011). EGFR/Ras/MAPK signaling mediates adult midgut epithelial homeostasis and regeneration in Drosophila. Cell Stem Cell *8*, 84-95.

Jiao, Y., Killela, P.J., Reitman, Z.J., Rasheed, A.B., Heaphy, C.M., de Wilde, R.F., Rodriguez, F.J., Rosemberg, S., Oba-Shinjo, S.M., Nagahashi Marie, S.K.*, et al.* (2012). Frequent ATRX, CIC, FUBP1 and IDH1 mutations refine the classification of malignant gliomas. Oncotarget *3*, 709-722.

Jimenez, G., Guichet, A., Ephrussi, A., and Casanova, J. (2000). Relief of gene repression by Torso RTK signaling: role of capicua in Drosophila terminal and dorsoventral patterning. Genes & Development *14*, 224-231.

Jimenez, G., Shvartsman, S.Y., and Paroush, Z. (2012). The Capicua repressor--a general sensor of RTK signaling in development and disease. J Cell Sci *125*, 1383-1391.

Jin, Y., Ha, N., Fores, M., Xiang, J., Glasser, C., Maldera, J., Jimenez, G., and Edgar, B.A. (2015). EGFR/Ras Signaling Controls Drosophila Intestinal Stem Cell Proliferation via Capicua-Regulated Genes. PLoS Genet *11*, e1005634.

Jindal, G.A., Goyal, Y., Burdine, R.D., Rauen, K.A., and Shvartsman, S.Y. (2015). RASopathies: unraveling mechanisms with animal models. Dis Model Mech *8*, 769-782.

Justice, R.W., Zilian, O., Woods, D.F., Noll, M., and Bryant, P.J. (1995). The Drosophila tumor suppressor gene warts encodes a homolog of human myotonic dystrophy kinase and is required for the control of cell shape and proliferation. Genes Dev *9*, 534-546.

Kango-Singh, M., Nolo, R., Tao, C., Verstreken, P., Hiesinger, P.R., Bellen, H.J., and Halder, G. (2002). Shar-pei mediates cell proliferation arrest during imaginal disc growth in Drosophila. Development *129*, 5719-5730.

Karim, F.D., and Rubin, G.M. (1998). Ectopic expression of activated Ras1 induces hyperplastic growth and increased cell death in Drosophila imaginal tissues. Development *125*, 1-9.

Kawamura-Saito, M., Yamazaki, Y., Kaneko, K., Kawaguchi, N., Kanda, H., Mukai, H., Gotoh, T., Motoi, T., Fukayama, M., Aburatani, H*., et al.* (2006). Fusion between CIC and DUX4 up-regulates PEA3 family genes in Ewing-like sarcomas with t(4;19)(q35;q13) translocation. Hum Mol Genet *15*, 2125-2137.

Keefe, A.D., Wilson, D.S., Seelig, B., and Szostak, J.W. (2001). One-step purification of recombinant proteins using a nanomolar-affinity streptavidin-binding peptide, the SBP-Tag. Protein Expr Purif *23*, 440-446.

Kim, J.H., Chang, T.M., Graham, A.N., Choo, K.H., Kalitsis, P., and Hudson, D.F. (2010a). Streptavidin-Binding Peptide (SBP)-tagged SMC2 allows single-step affinity fluorescence, blotting or purification of the condensin complex. BMC Biochem *11*, 50.

Kim, Y., Coppey, M., Grossman, R., Ajuria, L., Jimenez, G., Paroush, Z., and Shvartsman, S.Y. (2010b). MAPK substrate competition integrates patterning signals in the Drosophila embryo Curr Biol *20*, 446-451.

Kimura, R., Kamino, K., Yamamoto, M., Nuripa, A., Kida, T., Kazui, H., Hashimoto, R., Tanaka, T., Kudo, T., Yamagata, H.*, et al.* (2007). The DYRK1A gene, encoded in chromosome 21 Down syndrome critical region, bridges between beta-amyloid production and tau phosphorylation in Alzheimer disease. Hum Mol Genet *16*, 15-23.

Kratchmarova, I., Blagoev, B., Haack-Sorensen, M., Kassem, M., and Mann, M. (2005). Mechanism of divergent growth factor effects in mesenchymal stem cell differentiation. Science *308*, 1472-1477.

Kwon, Y., Vinayagam, A., Sun, X., Dephoure, N., Gygi, S.P., Hong, P., and Perrimon, N. (2013). The Hippo signaling pathway interactome. Science *342*, 737-740.

Kyriakakis, P., Tipping, M., Abed, L., and Veraksa, A. (2008). Tandem affinity purification in Drosophila: The advantages of the GS-TAP system. Fly (Austin) *2*, 229-235.

Laguna, A., Aranda, S., Barallobre, M.J., Barhoum, R., Fernandez, E., Fotaki, V., Delabar, J.M., de la Luna, S., de la Villa, P., and Arbones, M.L. (2008). The protein kinase DYRK1A regulates caspase-9-mediated apoptosis during retina development. Dev Cell *15*, 841-853.

Lai, Z.C., Wei, X., Shimizu, T., Ramos, E., Rohrbaugh, M., Nikolaidis, N., Ho, L.L., and Li, Y. (2005). Control of cell proliferation and apoptosis by mob as tumor suppressor, mats. Cell *120*, 675-685.

Lam, Y.C., Bowman, A.B., Jafar-Nejad, P., Lim, J., Richman, R., Fryer, J.D., Hyun, E.D., Duvick, L.A., Orr, H.T., Botas, J.*, et al.* (2006). ATAXIN-1 interacts with the repressor Capicua in its native complex to cause SCA1 neuropathology. Cell *127*, 1335-1347.

Laplante, M., and Sabatini, D.M. (2012). mTOR signaling in growth control and disease. Cell *149*, 274-293.

Lasagna-Reeves, C.A., Rousseaux, M.W., Guerrero-Munoz, M.J., Park, J., Jafar-Nejad, P., Richman, R., Lu, N., Sengupta, U., Litvinchuk, A., Orr, H.T.*, et al.* (2015). A native interactor scaffolds and stabilizes toxic ATAXIN-1 oligomers in SCA1. Elife *4*.

Lemmon, M.A., and Schlessinger, J. (2010). Cell signaling by receptor tyrosine kinases. Cell *141*, 1117-1134.

Li, E., and Hristova, K. (2006). Role of receptor tyrosine kinase transmembrane domains in cell signaling and human pathologies. Biochemistry *45*, 6241-6251.

Li, Q., Li, S., Mana-Capelli, S., Roth Flach, R.J., Danai, L.V., Amcheslavsky, A., Nie, Y., Kaneko, S., Yao, X., Chen, X.*, et al.* (2014). The conserved misshapen-warts-Yorkie pathway acts in enteroblasts to regulate intestinal stem cells in Drosophila. Dev Cell *31*, 291-304.

Li, W.X. (2005). Functions and mechanisms of receptor tyrosine kinase Torso signaling: lessons from Drosophila embryonic terminal development. Dev Dyn *232*, 656-672.

Lim, B., Samper, N., Lu, H., Rushlow, C., Jimenez, G., and Shvartsman, S.Y. (2013). Kinetics of gene derepression by ERK signaling. Proc Natl Acad Sci U S A *110*, 10330-10335.

Lim, J., Crespo-Barreto, J., Jafar-Nejad, P., Bowman, A.B., Richman, R., Hill, D.E., Orr, H.T., and Zoghbi, H.Y. (2008). Opposing effects of polyglutamine expansion on native protein complexes contribute to SCA1. Nature *452*, 713-718.

Lim, J., Hao, T., Shaw, C., Patel, A.J., Szabo, G., Rual, J.F., Fisk, C.J., Li, N., Smolyar, A., Hill, D.E.*, et al.* (2006). A protein-protein interaction network for human inherited ataxias and disorders of Purkinje cell degeneration. Cell *125*, 801-814.

Ling, C., Zheng, Y., Yin, F., Yu, J., Huang, J., Hong, Y., Wu, S., and Pan, D. (2010). The apical transmembrane protein Crumbs functions as a tumor suppressor that regulates Hippo signaling by binding to Expanded. Proc Natl Acad Sci U S A *107*, 10532-10537.

Lloyd, A.C. (2013). The regulation of cell size. Cell *154*, 1194-1205.

Lochhead, P.A., Sibbet, G., Morrice, N., and Cleghon, V. (2005). Activation-loop autophosphorylation is mediated by a novel transitional intermediate form of DYRKs. Cell *121*, 925-936.

Ma, D., Yang, C.H., McNeill, H., Simon, M.A., and Axelrod, J.D. (2003). Fidelity in planar cell polarity signalling. Nature *421*, 543-547.

Markow, T.A. (2015). The secret lives of Drosophila flies. Elife *4*.

Marshall, C.J. (1995). Specificity of receptor tyrosine kinase signaling: transient versus sustained extracellular signal-regulated kinase activation. Cell *80*, 179-185.

Martin, F.A., Herrera, S.C., and Morata, G. (2009). Cell competition, growth and size control in the Drosophila wing imaginal disc. Development *136*, 3747-3756.

Martinez de Lagran, M., Altafaj, X., Gallego, X., Marti, E., Estivill, X., Sahun, I., Fillat, C., and Dierssen, M. (2004). Motor phenotypic alterations in TgDyrk1a transgenic mice implicate DYRK1A in Down syndrome motor dysfunction. Neurobiol Dis *15*, 132-142.

Massague, J., Blain, S.W., and Lo, R.S. (2000). TGFbeta signaling in growth control, cancer, and heritable disorders. Cell *103*, 295-309.

Matakatsu, H., and Blair, S.S. (2006). Separating the adhesive and signaling functions of the Fat and Dachsous protocadherins. Development *133*, 2315-2324.

Meloche, S., and Pouyssegur, J. (2007). The ERK1/2 mitogen-activated protein kinase pathway as a master regulator of the G1- to S-phase transition. Oncogene *26*, 3227-3239.

Moller, R.S., Kubart, S., Hoeltzenbein, M., Heye, B., Vogel, I., Hansen, C.P., Menzel, C., Ullmann, R., Tommerup, N., Ropers, H.H.*, et al.* (2008). Truncation of the Down syndrome candidate gene DYRK1A in two unrelated patients with microcephaly. Am J Hum Genet *82*, 1165-1170.

Morriss, G.R., Jaramillo, C.T., Mikolajczak, C.M., Duong, S., Jaramillo, M.S., and Cripps, R.M. (2013). The Drosophila wings apart gene anchors a novel, evolutionarily conserved pathway of neuromuscular development. Genetics *195*, 927-940.

Murphy, L.O., Smith, S., Chen, R.H., Fingar, D.C., and Blenis, J. (2002). Molecular interpretation of ERK signal duration by immediate early gene products. Nat Cell Biol *4*, 556-564.

Neumuller, R.A., Wirtz-Peitz, F., Lee, S., Kwon, Y., Buckner, M., Hoskins, R.A., Venken, K.J., Bellen, H.J., Mohr, S.E., and Perrimon, N. (2012). Stringent analysis of gene function and protein-protein interactions using fluorescently tagged genes. Genetics *190*, 931-940.

Newbern, J., Zhong, J., Wickramasinghe, R.S., Li, X., Wu, Y., Samuels, I., Cherosky, N., Karlo, J.C., O'Loughlin, B., Wikenheiser, J.*, et al.* (2008). Mouse and human phenotypes indicate a critical conserved role for ERK2 signaling in neural crest development. Proc Natl Acad Sci U S A *105*, 17115-17120.

Nishida, Y., Hata, M., Ayaki, T., Ryo, H., Yamagata, M., Shimizu, K., and Nishizuka, Y. (1988). Proliferation of both somatic and germ cells is affected in the Drosophila mutants of raf proto-oncogene. EMBO J *7*, 775-781.

Noll, C., Tlili, A., Ripoll, C., Mallet, L., Paul, J.L., Delabar, J.M., and Janel, N. (2012). Dyrk1a activates antioxidant NQO1 expression through an ERK1/2-Nrf2 dependent mechanism. Mol Genet Metab *105*, 484-488.

Nolo, R., Morrison, C.M., Tao, C., Zhang, X., and Halder, G. (2006). The bantam microRNA is a target of the hippo tumor-suppressor pathway. Curr Biol *16*, 1895-1904.

O'Roak, B.J., Stessman, H.A., Boyle, E.A., Witherspoon, K.T., Martin, B., Lee, C., Vives, L., Baker, C., Hiatt, J.B., Nickerson, D.A.*, et al.* (2014). Recurrent de novo mutations implicate novel genes underlying simplex autism risk. Nat Commun *5*, 5595.

Oh, H., and Irvine, K.D. (2008). In vivo regulation of Yorkie phosphorylation and localization. Development *135*, 1081-1088.

Oldham, S., and Hafen, E. (2003). Insulin/IGF and target of rapamycin signaling: a TOR de force in growth control. Trends Cell Biol *13*, 79-85.

Olsen, J.V., Blagoev, B., Gnad, F., Macek, B., Kumar, C., Mortensen, P., and Mann, M. (2006). Global, in vivo, and site-specific phosphorylation dynamics in signaling networks. Cell *127*, 635-648.

Ortiz-Abalia, J., Sahun, I., Altafaj, X., Andreu, N., Estivill, X., Dierssen, M., and Fillat, C. (2008). Targeting Dyrk1A with AAVshRNA attenuates motor alterations in TgDyrk1A, a mouse model of Down syndrome. Am J Hum Genet *83*, 479-488.

Pan, D. (2010). The hippo signaling pathway in development and cancer. Dev Cell *19*, 491-505.

Pantalacci, S., Tapon, N., and Leopold, P. (2003). The Salvador partner Hippo promotes apoptosis and cell-cycle exit in Drosophila. Nat Cell Biol *5*, 921-927.

Poon, C.L., Lin, J.I., Zhang, X., and Harvey, K.F. (2011). The sterile 20-like kinase Tao-1 controls tissue growth by regulating the Salvador-Warts-Hippo pathway. Dev Cell *21*, 896-906.

Poon, C.L., Mitchell, K.A., Kondo, S., Cheng, L.Y., and Harvey, K.F. (2016). The Hippo Pathway Regulates Neuroblasts and Brain Size in Drosophila melanogaster. Curr Biol *26*, 1034-1042.

Port, F., Chen, H.M., Lee, T., and Bullock, S.L. (2014). Optimized CRISPR/Cas tools for efficient germline and somatic genome engineering in Drosophila. Proc Natl Acad Sci U S A *111*, E2967-2976.

Postlethwait, J.H., and Schneiderman, H.A. (1973). Developmental genetics of Drosophila imaginal discs. Annu Rev Genet *7*, 381-433.

Pozo, N., Zahonero, C., Fernandez, P., Linares, J.M., Ayuso, A., Hagiwara, M., Perez, A., Ricoy, J.R., Hernandez-Lain, A., Sepulveda, J.M.*, et al.* (2013). Inhibition of DYRK1A destabilizes EGFR and reduces EGFR-dependent glioblastoma growth. J Clin Invest *123*, 2475-2487.

Prober, D.A., and Edgar, B.A. (2000). Ras1 promotes cellular growth in the Drosophila wing. Cell *100*, 435-446.

Rauen, K.A. (2013). The RASopathies. Annu Rev Genomics Hum Genet *14*, 355-369.

Rauen, K.A., Banerjee, A., Bishop, W.R., Lauchle, J.O., McCormick, F., McMahon, M., Melese, T., Munster, P.N., Nadaf, S., Packer, R.J.*, et al.* (2011). Costello and cardio-facio-cutaneous syndromes: Moving toward clinical trials in RASopathies. Am J Med Genet C Semin Med Genet *157C*, 136-146.

Rauskolb, C., Sun, S., Sun, G., Pan, Y., and Irvine, K.D. (2014). Cytoskeletal tension inhibits Hippo signaling through an Ajuba-Warts complex. Cell *158*, 143-156.

Rebay, I., and Rubin, G.M. (1995). Yan functions as a general inhibitor of differentiation and is negatively regulated by activation of the Ras1/MAPK pathway. Cell *81*, 857-866.

Reddy, B.V., Rauskolb, C., and Irvine, K.D. (2010). Influence of fat-hippo and notch signaling on the proliferation and differentiation of Drosophila optic neuroepithelia. Development *137*, 2397-2408.

Rigaut, G., Shevchenko, A., Rutz, B., Wilm, M., Mann, M., and Seraphin, B. (1999). A generic protein purification method for protein complex characterization and proteome exploration. Nat Biotechnol *17*, 1030-1032.

Rintelen, F., Hafen, E., and Nairz, K. (2003). The Drosophila dual-specificity ERK phosphatase DMKP3 cooperates with the ERK tyrosine phosphatase PTP-ER. Development *130*, 3479-3490.

Robertson, S.C., Tynan, J., and Donoghue, D.J. (2000). RTK mutations and human syndromes: when good receptors turn bad. Trends Genet *16*, 368.

Robinson, B.S., Huang, J., Hong, Y., and Moberg, K.H. (2010). Crumbs regulates Salvador/Warts/Hippo signaling in Drosophila via the FERM-domain protein Expanded. Curr Biol *20*, 582-590.

Roch, F., Jiménez, G., and Casanova, J. (2002). EGFR signalling inhibits Capicua-dependent repression during specification of Drosophila wing veins. Development *129*, 993-1002.

Rocha-Lima, C.M., Soares, H.P., Raez, L.E., and Singal, R. (2007). EGFR targeting of solid tumors. Cancer Control *14*, 295-304.

Ruaud, L., Mignot, C., Guet, A., Ohl, C., Nava, C., Heron, D., Keren, B., Depienne, C., Benoit, V., Maystadt, I.*, et al.* (2015). DYRK1A mutations in two unrelated patients. Eur J Med Genet *58*, 168-174.

Sahm, F., Koelsche, C., Meyer, J., Pusch, S., Lindenberg, K., Mueller, W., Herold-Mende, C., von Deimling, A., and Hartmann, C. (2012). CIC and FUBP1 mutations in oligodendrogliomas, oligoastrocytomas and astrocytomas. Acta Neuropathol *123*, 853-860.

Sansores-Garcia, L., Bossuyt, W., Wada, K., Yonemura, S., Tao, C., Sasaki, H., and Halder, G. (2011). Modulating F-actin organization induces organ growth by affecting the Hippo pathway. EMBO J *30*, 2325-2335.

Schlessinger, J. (2000). Cell signaling by receptor tyrosine kinases. Cell *103*, 211-225.

Seshagiri, S., Stawiski, E.W., Durinck, S., Modrusan, Z., Storm, E.E., Conboy, C.B., Chaudhuri, S., Guan, Y., Janakiraman, V., Jaiswal, B.S.*, et al.* (2012). Recurrent R-spondin fusions in colon cancer. Nature *488*, 660-664.

Shaner, N.C., Lin, M.Z., McKeown, M.R., Steinbach, P.A., Hazelwood, K.L., Davidson, M.W., and Tsien, R.Y. (2008). Improving the photostability of bright monomeric orange and red fluorescent proteins. Nat Methods *5*, 545-551.

Shilo, B.Z. (2014). The regulation and functions of MAPK pathways in Drosophila. Methods *68*, 151-159.

Silva, E., Tsatskis, Y., Gardano, L., Tapon, N., and McNeill, H. (2006). The tumor-suppressor gene fat controls tissue growth upstream of expanded in the hippo signaling pathway. Curr Biol *16*, 2081-2089.

Simon, M. (2000). Receptor tyrosine kinases: specific outcomes from general signals. Cell *103*, 13-15.

Sjoblom, T., Jones, S., Wood, L.D., Parsons, D.W., Lin, J., Barber, T.D., Mandelker, D., Leary, R.J., Ptak, J., Silliman, N.*, et al.* (2006). The consensus coding sequences of human breast and colorectal cancers. Science *314*, 268-274.

Skurat, A.V., and Dietrich, A.D. (2004). Phosphorylation of Ser640 in muscle glycogen synthase by DYRK family protein kinases. J Biol Chem *279*, 2490-2498.

Slamon, D.J., Leyland-Jones, B., Shak, S., Fuchs, H., Paton, V., Bajamonde, A., Fleming, T., Eiermann, W., Wolter, J., Pegram, M.*, et al.* (2001). Use of chemotherapy plus a monoclonal antibody against HER2 for metastatic breast cancer that overexpresses HER2. N Engl J Med *344*, 783-792.

Smith, D.J., Stevens, M.E., Sudanagunta, S.P., Bronson, R.T., Makhinson, M., Watabe, A.M., O'Dell, T.J., Fung, J., Weier, H.U., Cheng, J.F.*, et al.* (1997). Functional screening of 2 Mb of human chromosome 21q22.2 in transgenic mice implicates minibrain in learning defects associated with Down syndrome. Nat Genet *16*, 28-36.

Sopko, R., and Perrimon, N. (2013). Receptor tyrosine kinases in Drosophila development. Cold Spring Harb Perspect Biol *5*.

Sousa-Nunes, R., Cheng, L.Y., and Gould, A.P. (2010). Regulating neural proliferation in the Drosophila CNS. Curr Opin Neurobiol *20*, 50-57.

Sun, S., and Irvine, K.D. (2016). Cellular Organization and Cytoskeletal Regulation of the Hippo Signaling Network. Trends Cell Biol *26*, 694-704.

Tapon, N., Harvey, K.F., Bell, D.W., Wahrer, D.C., Schiripo, T.A., Haber, D., and Hariharan, I.K. (2002). salvador Promotes both cell cycle exit and apoptosis in Drosophila and is mutated in human cancer cell lines. Cell *110*, 467-478.

Tejedor, F., Zhu, X.R., Kaltenbach, E., Ackermann, A., Baumann, A., Canal, I., Heisenberg, M., Fischbach, K.F., and Pongs, O. (1995). minibrain: a new protein kinase family involved in postembryonic neurogenesis in Drosophila. Neuron *14*, 287-301.

Tejedor, F.J., and Hammerle, B. (2011). MNB/DYRK1A as a multiple regulator of neuronal development. FEBS J *278*, 223-235.

Theodosiou, N.A., and Xu, T. (1998). Use of FLP/FRT system to study Drosophila development. Methods *14*, 355-365.

Thompson, B.J., and Cohen, S.M. (2006). The Hippo pathway regulates the bantam microRNA to control cell proliferation and apoptosis in Drosophila. Cell *126*, 767-774.

Tidyman, W.E., and Rauen, K.A. (2009). The RASopathies: developmental syndromes of Ras/MAPK pathway dysregulation. Curr Opin Genet Dev *19*, 230-236.

Tseng, A.S., Tapon, N., Kanda, H., Cigizoglu, S., Edelmann, L., Pellock, B., White, K., and Hariharan, I.K. (2007). Capicua regulates cell proliferation downstream of the receptor tyrosine kinase/ras signaling pathway. Curr Biol *17*, 728-733.

Udan, R.S., Kango-Singh, M., Nolo, R., Tao, C., and Halder, G. (2003). Hippo promotes proliferation arrest and apoptosis in the Salvador/Warts pathway. Nat Cell Biol *5*, 914-920.

van Bon, B.W., Coe, B.P., Bernier, R., Green, C., Gerdts, J., Witherspoon, K., Kleefstra, T., Willemsen, M.H., Kumar, R., Bosco, P.*, et al.* (2016). Disruptive de novo mutations of DYRK1A lead to a syndromic form of autism and ID. Mol Psychiatry *21*, 126-132.

Veraksa, A. (2013). Regulation of developmental processes: insights from mass spectrometry-based proteomics. Wiley Interdiscip Rev Dev Biol *2*, 723-734.

Veraksa, A., Bauer, A., and Artavanis-Tsakonas, S. (2005). Analyzing protein complexes in Drosophila with tandem affinity purification-mass spectrometry. Dev Dyn *232*, 827-834.

von Kriegsheim, A., Baiocchi, D., Birtwistle, M., Sumpton, D., Bienvenut, W., Morrice, N., Yamada, K., Lamond, A., Kalna, G., Orton, R.*, et al.* (2009). Cell fate decisions are specified by the dynamic ERK interactome. Nat Cell Biol *11*, 1458-1464.

Vrabioiu, A.M., and Struhl, G. (2015). Fat/Dachsous Signaling Promotes Drosophila Wing Growth by Regulating the Conformational State of the NDR Kinase Warts. Dev Cell *35*, 737-749.

Watase, K., Weeber, E.J., Xu, B., Antalffy, B., Yuva-Paylor, L., Hashimoto, K., Kano, M., Atkinson, R., Sun, Y., Armstrong, D.L.*, et al.* (2002). A long CAG repeat in the mouse Sca1 locus replicates SCA1 features and reveals the impact of protein solubility on selective neurodegeneration. Neuron *34*, 905-919.

Wesseling, P., van den Bent, M., and Perry, A. (2015). Oligodendroglioma: pathology, molecular mechanisms and markers. Acta Neuropathol *129*, 809-827.

Willecke, M., Hamaratoglu, F., Kango-Singh, M., Udan, R., Chen, C.L., Tao, C., Zhang, X., and Halder, G. (2006). The fat cadherin acts through the hippo tumor-suppressor pathway to regulate tissue size. Curr Biol *16*, 2090-2100.

Willsey, A.J., and State, M.W. (2015). Autism spectrum disorders: from genes to neurobiology. Curr Opin Neurobiol *30*, 92-99.

Wodarz, A., Hinz, U., Engelbert, M., and Knust, E. (1995). Expression of crumbs confers apical character on plasma membrane domains of ectodermal epithelia of Drosophila. Cell *82*, 67-76.

Worley, M.I., Setiawan, L., and Hariharan, I.K. (2013). TIE-DYE: a combinatorial marking system to visualize and genetically manipulate clones during development in Drosophila melanogaster. Development *140*, 3275-3284.

Wu, S., Huang, J., Dong, J., and Pan, D. (2003). hippo encodes a Ste-20 family protein kinase that restricts cell proliferation and promotes apoptosis in conjunction with salvador and warts. Cell *114*, 445-456.

Wu, S., Liu, Y., Zheng, Y., Dong, J., and Pan, D. (2008). The TEAD/TEF family protein Scalloped mediates transcriptional output of the Hippo growth-regulatory pathway. Dev Cell *14*, 388-398.

Xu, T., Wang, W., Zhang, S., Stewart, R.A., and Yu, W. (1995). Identifying tumor suppressors in genetic mosaics: the Drosophila lats gene encodes a putative protein kinase. Development *121*, 1053-1063.

Yeh, E., Gustafson, K., and Boulianne, G.L. (1995). Green fluorescent protein as a vital marker and reporter of gene expression in Drosophila. Proc Natl Acad Sci U S A *92*, 7036-7040.

Yip, S., Butterfield, Y.S., Morozova, O., Chittaranjan, S., Blough, M.D., An, J., Birol, I., Chesnelong, C., Chiu, R., Chuah, E.*, et al.* (2012). Concurrent CIC mutations, IDH mutations, and 1p/19q loss distinguish oligodendrogliomas from other cancers. J Pathol *226*, 7-16.

Yu, F.X., and Guan, K.L. (2013). The Hippo pathway: regulators and regulations. Genes Dev *27*, 355-371.

Yu, J., Zheng, Y., Dong, J., Klusza, S., Deng, W.M., and Pan, D. (2010). Kibra functions as a tumor suppressor protein that regulates Hippo signaling in conjunction with Merlin and Expanded. Dev Cell *18*, 288-299.

Yue, T., Tian, A., and Jiang, J. (2012). The cell adhesion molecule echinoid functions as a tumor suppressor and upstream regulator of the Hippo signaling pathway. Dev Cell *22*, 255-267.

Zhai, B., Villen, J., Beausoleil, S.A., Mintseris, J., and Gygi, S.P. (2008). Phosphoproteome analysis of Drosophila melanogaster embryos. J Proteome Res *7*, 1675-1682.

Zhang, C., Robinson, B.S., Xu, W., Yang, L., Yao, B., Zhao, H., Byun, P.K., Jin, P., Veraksa, A., and Moberg, K.H. (2015). The ecdysone receptor coactivator Taiman links Yorkie to transcriptional control of germline stem cell factors in somatic tissue. Dev Cell *34*, 168-180.

Zhang, L., Ren, F., Zhang, Q., Chen, Y., Wang, B., and Jiang, J. (2008). The TEAD/TEF family of transcription factor Scalloped mediates Hippo signaling in organ size control. Dev Cell *14*, 377-387.

Zhang, X., Milton, C.C., Humbert, P.O., and Harvey, K.F. (2009). Transcriptional output of the Salvador/warts/hippo pathway is controlled in distinct fashions in Drosophila melanogaster and mammalian cell lines. Cancer Res *69*, 6033-6041.

Zhao, B., Lei, Q.Y., and Guan, K.L. (2008a). The Hippo-YAP pathway: new connections between regulation of organ size and cancer. Curr Opin Cell Biol *20*, 638-646.

Zhao, B., Ye, X., Yu, J., Li, L., Li, W., Li, S., Lin, J.D., Wang, C.Y., Chinnaiyan, A.M., Lai, Z.C.*, et al.* (2008b). TEAD mediates YAP-dependent gene induction and growth control. Genes Dev *22*, 1962-1971.

Zoghbi, H.Y., and Orr, H.T. (2009). Pathogenic mechanisms of a polyglutamine-mediated neurodegenerative disease, spinocerebellar ataxia type 1. J Biol Chem *284*, 7425-7429.

Zwick, E., Bange, J., and Ullrich, A. (2002). Receptor tyrosine kinases as targets for anticancer drugs. Trends Mol Med *8*, 17-23.